

**Neurodegeneration and the *m*-AAA protease:
pathogenic cascades in neurons and myelinating cells**

Inaugural-Dissertation

zur

Erlangung des Doktorgrades
der Mathematisch-Naturwissenschaftlichen Fakultät
der Universität zu Köln



vorgelegt von
Shuaiyu Wang
aus Hunan, China

Köln, 2016

Berichterstatter:

Prof. Dr. Elena I. Rugarli

Prof. Dr. Aleksandra Trifunovic

Tag der Mündlichen Prüfung:

01.07.2016

To my dear family, teachers and friends

Table of contents

Table of contents	1
Abstract.....	4
Abbreviations.....	5
1 Introduction	7
1.1 Mitochondria	8
1.1.1 Mitochondrial function.....	8
1.1.2 Mitochondrial quality control.....	8
1.2 The <i>m</i> -AAA protease.....	9
1.2.1 The <i>m</i> -AAA protease subunits and function	9
1.2.2 Human diseases causes by the <i>m</i> -AAA protease mutations.....	12
1.2.3 Available murine models of the <i>m</i> -AAA protease	14
1.3 Myelinating cells	18
1.3.1 Oligodendrocytes.....	20
1.3.2 Schwann cells	22
1.3.3 Pathology of myelin-forming cells.....	24
1.3.4 The role of mitochondria in myelinating cells.....	26
2 Aim of the thesis.....	28
3 Material and methods	30
3.1 Animal experiments.....	31
3.1.1 Mouse breedings.....	31
3.1.2 Genotyping	33
3.1.3 Tamoxifen administration.....	34
3.1.4 Behavioral tests.....	34
3.1.5 Fat content measurement.....	35
3.2 Tissue Collection	35
3.3 Histology and immunohistochemistry.....	35
3.3.1 Slice preparation.....	35
3.3.2 Immunostaining on vibratome sections.....	36
3.3.3 Immunostaining on paraffin sections	36
3.3.4 Nissl staining	37
3.3.5 Gallyas staining	37
3.3.6 Haematoxylin and eosin staining.....	38

3.3.7 TUNEL assay	38
3.4 Microscopy	39
3.4.1 Light microscopy	39
3.4.2 Electron microscopy	39
3.5 Cell counting and axon morphometry	40
3.5.1 Cell counting	40
3.5.2 g ratio and myelinated axon counting	40
3.6 Oligodendrocytes preparation	40
3.7 Biochemistry	41
3.7.1 Isolation of crude mitochondria	41
3.7.2 Myelin isolation	41
3.7.3 Protein extraction	41
3.7.4 Western blot	42
3.7.5 Oxyblot	44
3.8 Statistical analysis	45
3.8.1 <i>Chi-square</i> test	45
3.8.2 Unpaired Student's <i>t</i> test	45
3.8.3 Two-way ANOVA test	45
4 Results	46
4.1 <i>Afg3l2</i> full-body knockout mice show severe developmental phenotype	47
4.1.1 Phenotypic complexity of L2 KO mice	47
4.1.2 Loss of <i>Afg3l2</i> unbalances mitochondrial fission and fusion	49
4.1.3 Lack of <i>Afg3l2</i> triggers tauopathy	51
4.1.4 Investigation of possible kinases involved in tau hyperphosphorylation	51
4.2 <i>Afg3l2</i> forebrain-neuron specific knockout mice show early-onset neurodegeneration	54
4.2.1 Signs of neurodegeneration in AFG3L2 ^{NKO} mice	54
4.2.2 Mitochondrial morphology aberration in AFG3L2 ^{NKO} mice	56
4.2.3 Tau hyperphosphorylation in AFG3L2 ^{NKO} mice	56
4.3 <i>Afg3l2</i> oligodendrocytes-specific knockouts display late-onset myelin abnormalities	60
4.3.1 AFG3L2 is abundantly expressed in oligodendrocytes	60
4.3.2 The <i>PLP1</i> promoter is efficiently and specifically expressed in oligodendrocytes in the adult mice	62

4.3.3 Deletion of <i>Afg3l2</i> induces mitochondrial abnormalities in oligodendrocytes	65
4.3.4 Lack of AFG3L2 does not affect the survival of oligodendrocytes	65
4.3.5 Late-onset motor impairment and axonal dysmyelination in AFG3L2 ^{MC-KO} mice	66
4.4 <i>Afg3l1</i> full-body knockout mice show no evident sign of neurodegeneration	70
4.4.1 Normal growth curve of <i>Afg3l1</i> KO mice	70
4.4.2 Preserved axonal myelination and integrity in <i>Afg3l1</i> KO mice	72
4.5 Ablation of the <i>m</i> -AAA protease in myelinating cells causes axonal demyelination and hair greying	74
4.5.1 DKO mice showed progressive motor impairment and hair greying	74
4.5.2 Genetic tracing of targeted cells in the skin	74
4.5.3 Loss of melanocytes and melanoblasts in the skin of DKO mice	78
4.5.4 Peripheral neuropathy in the DKO mice	80
4.5.5 Axonal demyelination and neuroinflammation in the DKO mice	82
4.5.6 Rapid loss of targeted cells in the DKO mice	88
5 Discussion	95
5.1 Mitochondrial morphology alteration upon loss of the <i>m</i> -AAA protease	96
5.2 Tau hyperphosphorylation evoked by AFG3L2 deficiency in neurons	99
5.3 Physiological role of AFG3L1 in the mouse	101
5.4 AFG3L2 is required for oligodendrocyte maturation but is dispensable for the survival of adult oligodendrocytes	102
5.5 Lack of the <i>m</i> -AAA protease causes death of myelinating cells	103
5.5.1 Oligodendrocyte death and axonal demyelination in the central nervous system	103
5.5.2 Peripheral neuropathy	105
5.5.3 Melanocytes reduction and hair greying in the skin	106
5.6 Conclusions	109
Zusammenfassung	110
References	112
Acknowledgements	127
Eidesstattliche Erklärung	129
Curriculum Vitae	130

Abstract

The *m*-AAA protease is a hexameric complex involved in processing of specific substrates and turnover of misfolded polypeptides in the mitochondrial inner membrane. In humans, the *m*-AAA protease is composed of AFG3L2 and paraplegin. Mutations in *AFG3L2* have been implicated in dominant spinocerebellar ataxia (SCA28) and recessive spastic ataxia-neuropathy syndrome (SPAX5). Mutations of *SPG7*, encoding paraplegin, are linked to hereditary spastic paraplegia. In the mouse, a third subunit AFG3L1 is expressed. Various mouse models recapitulate the phenotype of these neurodegenerative disorders, however, the pathogenic mechanism of neurodegeneration is not completely understood.

Here, we studied several mouse models and focused on cell-autonomous role of the *m*-AAA protease in neurons and myelinating cells. We show that lack of *Afg3l2* triggers mitochondrial fragmentation and swelling, tau hyperphosphorylation and pathology in *Afg3l2* full-body and forebrain neuron-specific knockout mice. Moreover, deletion of *Afg3l2* in adult myelinating cells causes early-onset mitochondrial abnormalities as in the neurons, but the survival of these cells is not affected, which is a contrast to early neuronal death. Despite the fact that myelinating cells have been previously shown to survive respiratory deficiency by glycolysis, total ablation of the *m*-AAA protease by deleting *Afg3l2* in an *Afg3l1* null background (DKO), leads to myelinating cell demise and subsequently progressive axonal demyelination. Interestingly, DKO mice show premature hair greying due to loss of melanoblasts. Together, our data demonstrate cell-autonomous survival thresholds to *m*-AAA protease deficiency, and an essential role of the *m*-AAA protease to prevent cell death independent from mitochondrial dynamics and the oxidative capacity of the cell. Thus, our findings provide novel insights to the pathogenesis of diseases linked to *m*-AAA protease deficiency, and also establish valuable mitochondrial dysfunctional mouse models to study other neurodegenerative diseases, such as tauopathies and demyelinating diseases.

Abbreviations

ABCD1	ABC binding cassette family D member 1
AD	Alzheimer's diseases
AFG3L1	AFG-like protein 1
AFG3L2	AFG-like protein 2
APC	Adenomatous Polyposis Coli
APS	Ammoniumpersulfate
ASA	Aryl Sulphatase A
BSA	Bovine Serum Albumin
CECAD	Cologne Cluster of Excellence in Cellular Stress Responses in Aging-associated Diseases
CMT	Charcot-Marie-Tooth disease
CNP	2', 3'-cyclic nucleotide 3'-phosphodiesterase
CNS	Central Nervous System
CNX	Calnexin
COX	Cytochrome c oxidase
CTRL	Control
DKO	Double knockout
DNPH	2,4-dinitrophenylhydrazine
EAE	Experimental Autoimmune Encephalomyelitis
ECL	Enhanced chemiluminescent
GFAP	Glial Fibrillary Acidic Protein
GJB1	Gap Junction Protein β 1
GJC2	Gap Junction Protein γ 2
h	hour (s)
HBSS	Hanks' Balanced Salt Solution
HSP	Hereditary Spastic Paraplegia
HET	Heterozygous
IBA1	Ionized calcium Binding Adaptor molecule 1
KO (ko)	Knockout
LHON	Leber's Hereditary Optic Neuropathy
<i>m</i> -AAA	matrix ATPases Associated with diverse cellular Activities

MAG	Myelin Associated Glycoprotein
MBP	Myelin Basic Protein
MC	Melanocytes
min	minute (s)
MPTP	Mitochondrial Permeability Transition Pore
MOG	Myelin Oligodendrocyte Glycoprotein
MS	Multiple Sclerosis
mt	Mitochondrial
Ndufs4	NADH dehydrogenase-ubiquinone-FeS 4
NRG1	Neuregulin-1
OXPPOS	Oxidative phosphorylation
OPA1	Optic atrophy type 1
OPC	Oligodendrocyte Precursor Cells
PBS	Phosphate Buffered Saline
PLP 1	Proteolipid protein 1
PNS	Peripheral Nervous System
PDGF α	Platelet-Derived Growth Factor receptor alpha
PFA	Paraformaldehyde
PMD	Pelizaeus–Merzbacher disease
PMLD	Pelizaeus–Merzbacher-like disease
RIPA	RadioImmunoPrecipitation Assay
ROS	Reactive Oxygen Species
SCA28	Spinocerebellar ataxia type 28
SCP	Schwann Cell Precursors
SDHA	Succinate dehydrogenase A
SDS	Sodium Dodecyl Sulfate
SPAX5	Spastic ataxia type 5
SPG	Spastic paraplegia
Surf1	Surfeit locus protein 1
TE	Tris-EDTA
TEMED	N,N,N',N'-Tetramethylethylenediamine
UPR ^{mt}	Mitochondrial unfolded protein response
WT (wt)	Wildtype

1 Introduction

1.1 Mitochondria

About 2 billion years ago, ancient bacteria entered primordial eukaryotic cells with a symbiotic relationship and evolved into mitochondria, which are semi-autonomous and essential organelles in modern eukaryotic cells (Gerdes et al., 2012; Wallace, 2005). In humans, although 99% of mitochondrial proteins are encoded by the nuclear genome, synthesized in the cytosol and imported into mitochondria, mitochondria maintain a genome encoding 13 proteins that are core subunits of respiratory chain complexes I, III, IV, and V, but not complex II, which is exclusively composed of proteins encoded by nuclear genes (Chan, 2006; Gerdes et al., 2012; Wallace, 2005). The mitochondrial DNA (mtDNA) genome also encodes 2 rRNAs and 22 tRNAs that are required for translation of mtDNA transcripts (Chan, 2006; Wallace, 2005).

1.1.1 Mitochondrial function

The well-known function of mitochondria is ATP production through the process of oxidative phosphorylation (OXPHOS). Moreover, mitochondria participate in diverse cellular processes, such as lipid biosynthesis, Ca^{2+} and iron homeostasis, autophagy and apoptosis (Chan, 2006; Rugarli and Langer, 2012). Endoplasmic reticulum (ER) regulate mitochondrial morphology and function through the ER-mitochondria contact sites (Friedman and Nunnari, 2014). Proper mitochondrial morphology and function are extremely required for neurons, which are polarized cells, need high amount of ATP and rely on OXPHOS to produce energy (Rugarli and Langer, 2012). However, OXPHOS generates reactive oxygen species (ROS) as a by-product, which may in turn impair mitochondrial function (Wallace, 2005).

1.1.2 Mitochondrial quality control

Cells have a hierarchical system of surveillance mechanisms to prevent mitochondrial damage or selectively remove dysfunctional mitochondrial proteins or entire organelles under stress (Rugarli and Langer, 2012). At molecular levels, the first line of defense is conducted by mitochondrial chaperones and proteases, which promote folding of newly imported polypeptides and degrade irreversibly misfolded or damaged proteins (Rugarli and Langer, 2012; Tatsuta and Langer, 2008). During protein homeostasis and mitochondrial stress, mitochondria communicate with nucleus to activate the expression of mitochondrial unfolded protein response (UPR^{mt}) genes, such as chaperones and

proteases, to perform intramitochondrial quality control (Quiros et al., 2016; Rugarli and Langer, 2012). The UPR^{mt} has been characterized extensively in *C. elegans* and also has been reported in mammals (Dogan et al., 2014; Quiros et al., 2016). In addition, at organellar levels, sustained mitochondrial stress and damage, lead to mitochondrial morphological alterations, including hyperfusion and fragmentation, to alleviate mild stress or segregate severe damaged mitochondria, which might be eliminated by selective autophagy namely mitophagy (Rugarli and Langer, 2012). Recently, a novel mitochondrial quality control pathway has been identified, in which mitochondria selectively degrade impaired proteins and lipids by generating small vesicular carriers that transport mitochondrial proteins and lipids to intracellular organelles, such as late endosome and peroxisomes (Sugiura et al., 2014).

Failure of mitochondrial quality control leads to cell death, and mitochondrial dysfunction has been implicated in various neurodegenerative diseases, metabolic disorders, ageing, and cancer (Burte et al., 2015; Chan, 2006; Rugarli and Langer, 2012; Wallace, 2005).

1.2 The *m*-AAA protease

Mitochondrial proteases, termed mitoproteases, act as key regulators for mitochondrial biogenesis, protein quality control, dynamics, mitophagy and apoptosis (Figure 1.1) (Martinelli and Rugarli, 2010; Quiros et al., 2015; Rugarli and Langer, 2012; Tatsuta and Langer, 2008). Numerous mitoproteases have been identified, and they are classified into three categories- intrinsic, transient and pseudo mitoproteases, according to their location, function, and structural and proteolytic characteristics (Quiros et al., 2015). The mitochondrial matrix ATPases associated with diverse cellular activities (*m*-AAA) protease is an intrinsic metalloprotease in the inner membrane with the catalytic domain facing the matrix (Gerdes et al., 2012; Koppen and Langer, 2007; Martinelli and Rugarli, 2010; Quiros et al., 2015).

1.2.1 The *m*-AAA protease subunits and function

In the mouse, the *m*-AAA protease is a hexameric complex formed by AFG3L1, AFG3L2 and paraplegin (Koppen et al., 2007). Whereas in humans, *AFG3L1* is pseudogene (Kremmidiotis et al., 2001) and the *m*-AAA protease is composed by AFG3L2 and paraplegin. All subunits of the *m*-AAA protease have similar domains

including a mitochondrial targeting sequence, two transmembrane domains, an AAA domain and a metal-dependant proteolytic domain (Martinelli and Rugarli, 2010). AFG3L1 and AFG3L2 form homo- and hetero-oligomeric complexes, but paraplegin can only assemble into hetero-hexamers (Koppen and Langer, 2007; Koppen et al., 2007) (Figure 1.2).

In the last decade, the function of *m*-AAA protease has been broadly explored in yeast, cell lines, murine models and human patients. These studies have shown that the *m*-AAA protease processes specific substrates and also regulates the turnover of misfolded mitochondrial respiratory chain complex subunits. The best-characterized substrate of the *m*-AAA protease is the mitochondrial ribosomal protein MrpL32, which mediates ribosome assembly and mitochondrial translation (Almajan et al., 2012; Bonn et al., 2011; Nolden et al., 2005). The *m*-AAA protease degrades a truncated form of cytochrome c oxidase subunit I (COX1) to maintain mitochondrial protein quality control (Hornig-Do et al., 2012). Depletion or mutations of the *m*-AAA protease harms mitochondrial function in multiple aspects, including mitochondrial respiratory chain complex deficiency, dynamic disturbance, Ca²⁺ handling defect, and anterograde transport impairment (Atorino et al., 2003; Ehses et al., 2009; Kondadi et al., 2014; Maltecca et al., 2015; Maltecca et al., 2012).

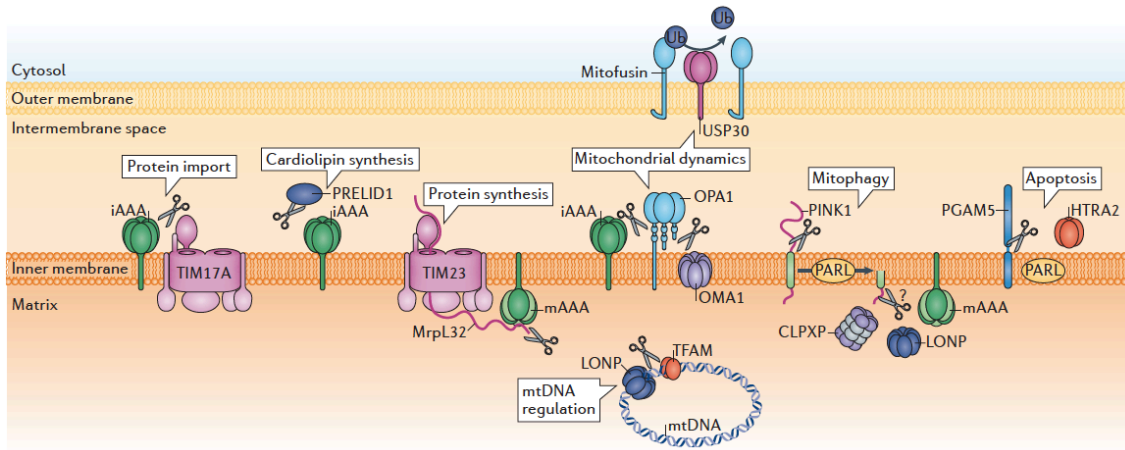


Figure 1.1 Proteolytic regulation of mitochondrial functions by mitoproteases

Mitoproteases perform proteolytic reactions to regulate mitochondrial protein import, cardiolipin synthesis, protein synthesis, dynamics, mitophagy, apoptosis and mitochondrial DNA (mtDNA) (Quiros et al., 2015).

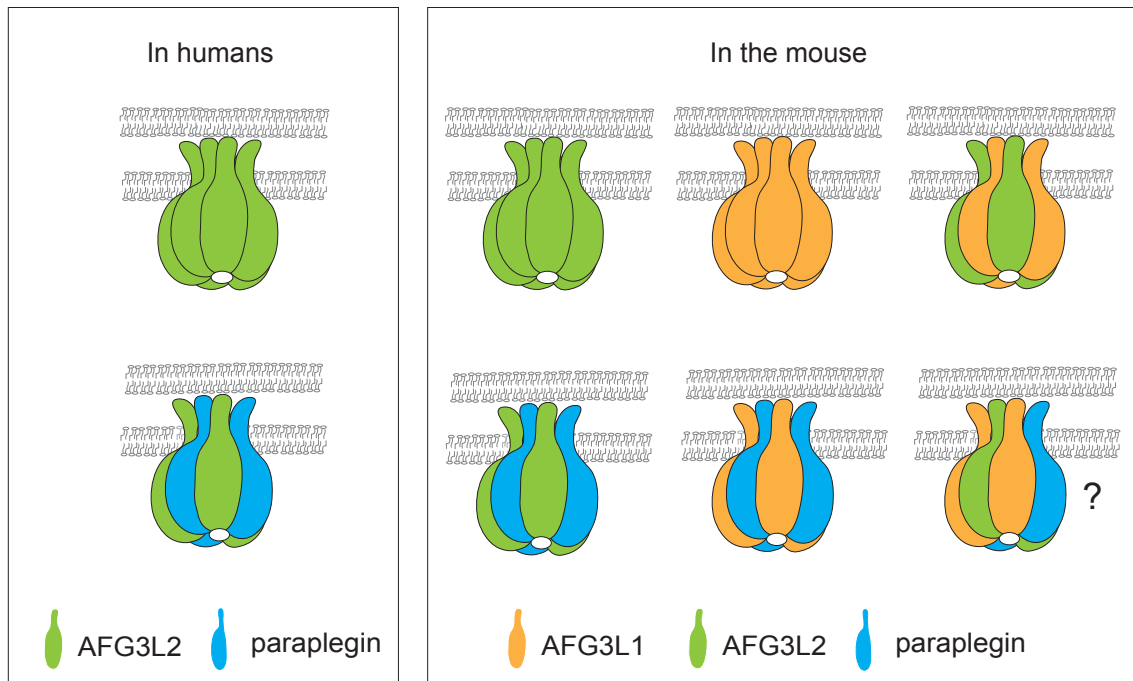


Figure 1.2 Isoenzymes of the *m*-AAA protease

In humans, AFG3L2 and paraplegin assemble into homo-oligomeric AFG3L2 and hetero-oligomeric AFG3L2/paraplegin complexes. In the mouse, a third subunit AFG3L1 is present. Therefore, five isoenzymes of the *m*-AAA protease have been identified, and the hetero-oligomeric complex composed by AFG3L1, AFG3L2 and paraplegin is speculative (indicated by a question mark) (Koppen and Langer, 2007).

1.2.2 Human diseases causes by the *m*-AAA protease mutations

Mutations of the *m*-AAA protease subunits have been linked to three rare inherited neurodegenerative disorders. In general, these diseases are clinically heterogeneous, and the phenotype is variable among affected individuals even within the same family.

SPG7 gene, maps on chromosome 16q24.3 and encodes for paraplegin, which mutation causes autosomal recessive hereditary spastic paraplegia (HSP) characterized by lower limb weakness and spasticity due to retrograde degeneration of corticospinal axons (Arnoldi et al., 2008; Brugman et al., 2008; Casari et al., 1998; De Michele et al., 1998; Elleuch et al., 2006; McDermott et al., 2001; Warnecke et al., 2007; Wilkinson et al., 2004). So far, more than 30 mutations in *SPG7* gene have been found, accounting for approximately 5% of autosomal recessive HSP (Salinas et al., 2008; Sánchez-Ferrero et al., 2013). Recently, familial analysis from a large cohort of Spanish HSP patients suggests a dominant inheritance of *SPG7* mutations (Sánchez-Ferrero et al., 2013). The onset of HSP patients carrying *SPG7* mutations is mostly in the adulthood (mean age, 30 years), and the range is from 1 year to 77 years (Arnoldi et al., 2008; Brugman et al., 2008; Casari et al., 1998; De Michele et al., 1998; Elleuch et al., 2006; McDermott et al., 2001; Sánchez-Ferrero et al., 2013; Warnecke et al., 2007; Wilkinson et al., 2004). *SPG7* affected individuals may show variable clinical features with both pure and complicated HSP (Casari and Marconi, 2006, updated 2010; Harding, 1983). The phenotype of pure HSP includes gait disturbance, hyperreflexia, extensor plantar responses, and decreased vibratory sense in the distal limbs (Casari et al., 1998; Casari and Marconi, 2006, updated 2010; Harding, 1983). Some patients show complicated form of HSP, which is characterized by additionally symptoms, such as mental retardation, optic atrophy, peripheral neuropathy, ptosis, decreased hearing, amyotrophy and ataxia (Casari et al., 1998; Casari and Marconi, 2006, updated 2010). Mitochondrial DNA deletion and mitochondrial respiratory chain defects in *SPG7* patient muscles imply mitochondria dysfunction in the pathogenesis of HSP (Atorino et al., 2003; Casari et al., 1998; McDermott et al., 2001; Wedding et al., 2014; Wilkinson et al., 2004).

Mutations in *AFG3L2* on chromosome 18p11.21 (Banfi et al., 1999; Cagnoli et al., 2006; Di Bella et al., 2010), cause two neurological diseases, autosomal dominant spinocerebellar ataxia type 28 (SCA28) (Cagnoli et al., 2006; Cagnoli et al., 2010; Di

Bella et al., 2010; Edener et al., 2010; Mariotti et al., 2008; Smets et al., 2014; Svenstrup et al., 2016; Zuhlke et al., 2015) and recessive spastic ataxia 5 (SPAX5) (Pierson et al., 2011). Additionally, two unrelated subjects carrying homozygous missense mutation of *AFG3L2*, have been identified from a cohort of progressive myoclonus epilepsy by exome sequencing (Muona et al., 2015). Spinocerebellar ataxia (SCA), characterized by progressive gait, stance and limb ataxia, oculomotor disturbances, dysarthria, is mostly owing to degeneration of Purkinje cells in the cerebellum (Brussino et al., 2011, updated 2013; Di Bella et al., 2010; Schols et al., 2004). SCA28, one of the most recently characterized forms of SCA, is the first autosomal dominant spinocerebellar ataxia shown to be caused by mitochondrial gene mutations (Mariotti et al., 2012). The general onset of SCA28 is in young adulthood (24.4 ± 14.9 years) with the range from 3 years to 60 years (Brussino et al., 2011, updated 2013). Patients show slowly progressive gait disorder, upper limb ataxia, lower limb hyperreflexia, dysarthria, nystagmus and ophthalmoparesis (Brussino et al., 2011, updated 2013; Edener et al., 2010; Mariotti et al., 2012; Zuhlke et al., 2015). To date, 15 missense mutations of *AFG3L2* have been identified (Cagnoli et al., 2006; Cagnoli et al., 2010; Di Bella et al., 2010; Lobbe et al., 2014; Svenstrup et al., 2016; Zuhlke et al., 2015), which represent around 3% of all SCAs and 1.5% of autosomal dominant cerebellar ataxias in Europe (Cagnoli et al., 2010). Recently, one partial deletion and one frameshift mutations of *AFG3L2* also have been shown to cause SCA28 (Musova et al., 2014; Smets et al., 2014). Most mutations in the exon 15-16 of *AFG3L2* corresponding the highly conserved proteolytic domain indicate specific substrates processing might be critical in the molecular pathology of SCA28 (Cagnoli et al., 2010; Di Bella et al., 2010; Lobbe et al., 2014; Svenstrup et al., 2016; Zuhlke et al., 2015). Likewise, two reported homozygous mutations of *AFG3L2* are also in this mutational hotspot exon 15-16 (Muona et al., 2015; Pierson et al., 2011). The two brothers identified with *AFG3L2* homozygous mutations from a consanguineous family, showed early onset SPAX5, which is characterized clinically by lower extremity spasticity, progressive myoclonic epilepsy, peripheral neuropathy, dysarthria, ptosis, oculomotor apraxia and cerebellar atrophy (Pierson et al., 2011). This phenotype is reminiscent of a combined syndrome of HSP and SCA28. The disease course of these two brothers was similar, and the younger sibling was more severe and died at the age of 13 years due to pneumonia-related complications (Pierson et al., 2011). The newly reported two cases carrying homozygous mutations of *AFG3L2*, known to be unrelated, also displayed

severe progressive myoclonus, ataxia and mild cognitive decline (Muona et al., 2015). Notably, their phenotype is not as severe as the two brothers', suggesting clinical variability in SPAX5. Loss-of-function mutations in AFG3L2 cause proteolytic impairment and mitochondrial respiratory chain deficiency have been implicated in the pathogenesis of SCA28 and SPAX5 (Di Bella et al., 2010; Pierson et al., 2011).

1.2.3 Available murine models of the *m*-AAA protease

In order to better unravel the pathogenesis of human diseases associated with mutations of *SPG7* and *AFG3L2*, multiple murine models of the *m*-AAA protease have been established. These models show dosage-dependant phenotype, probably owing to the fact that AFG3L2 forms both homo- and hetero-hexameric complexes and paraplegin only forms hetero-hexameric complex (Koppen et al., 2007).

Two murine models of SPAX5 have been reported: *Afg3l2* null (*Afg3l2*^{EMV66/EMV66}) generated by integrating ecotropic murine leukemia virus insertion 66 (EMV66) within intron 14, and a spontaneous mutant carrying a missense mutation in exon 10 (Maltecca et al., 2008). Both *Afg3l2* null and spontaneous missense mutant mice display a very severe neuromuscular syndrome with hindlimb paraparesis one week after birth and general die at P16 (Maltecca et al., 2008). *Afg3l2* deletion or loss-of-function causes mitochondrial morphological alternation and respiratory chain complexes deficit, leading to an impairment of axonal development with myelination delay and radial growth defect (Kondadi et al., 2014; Maltecca et al., 2008). Notably, in these *Afg3l2* mutant mice, non-neuronal tissues, such as muscle and liver, are not significantly affected, indicating that nervous system are solely affected by *Afg3l2* deletion or mutation (Maltecca et al., 2008). Interestingly, studies from our group provided novel insights into pathogenic mechanism of neurodegeneration. We have shown that an impairment of mitochondrial ribosome assembly and a decrease of mitochondrial translation in the *Afg3l2* null mice (Almajan et al., 2012). More recently, in these *Afg3l2* null mice, we have found microtubular network disruption and accumulation of hypersphosphorylated tau in the neurons (Kondadi et al., 2014).

The murine model haploinsufficient for *Afg3l2* (*Afg3l2*^{+EMV66}), which represents model of SCA28, shows progressive impairment in motor balance and coordination owing to Purkinje cell dark degeneration (Martinelli et al., 2009). Mitochondrial respiratory chain dysfunction and increased ROS level were previously implicated in the pathology

(Martinelli et al., 2009). Moreover, recent data have shown that the ataxic phenotype of *Afg3l2*^{+/*EMV66*} mice can be partial restored by reducing Ca²⁺ influx in Purkinje cells by either genetic silencing of the metabotropic glutamate receptor or administration of the β -lactam antibiotic ceftriaxone (Maltecca et al., 2015). Thus, mitochondrial Ca²⁺ handling inefficiency is also involved in the pathogenesis of SCA28 and might be a potential therapeutic target (Maltecca et al., 2015).

In comparison with severe developmental phenotype of *Afg3l2* null and missense mutant mice, *Spg7* knockout mice (*Spg7*^{-/-}) grow normally and show progressive axonal degeneration and motor impairment starting from 4 months of age (Ferreirinha et al., 2004), which models the disease of HSP with loss-of-function mutations in *SPG7*. Interestingly, in the *Spg7*^{-/-} mice, abnormal mitochondrial morphology occurs before initial signs of axonopathy, and followed by axonal swelling with organelle and neurofilament accumulation, together, suggesting that primary mitochondrial dysfunction and secondary axonal transport defect may lead to corticospinal and peripheral axonal swelling and degeneration (Ferreirinha et al., 2004). Interestingly, alternative splicing of *Spg7* produces a variant of paraplegin in the mouse, which localizes to the endoplasmic reticulum, still presents in the *Spg7*^{-/-} mice. The *Spg7*^{-/-} murine model is therefore an isoform-specific knockout (Mancuso et al., 2012).

Spg7^{-/-} *Afg3l2*^{+/*EMV66*} double mutant mice display an early-onset severe neurologic phenotype characterized by loss of balance, tremor, and ataxia (Martinelli et al., 2009). These mice show an acceleration of the axonopathy observed in *Spg7*^{-/-} mice, and prominent Purkinje cell degeneration at earlier age comparing to *Afg3l2*^{+/*EMV66*} mice (Martinelli et al., 2009), revealing a genetic interaction between the *m*-AAA protease isoenzymes homo-oligomeric AFG3L2 complex and hetero-oligomeric complex composed of paraplegin and AFG3L2 (Martinelli et al., 2009).

Studies of *Afg3l2* conditional murine models provide more insights into the pathogenic mechanism. Deletion of *Afg3l2* in Purkinje cells in the cerebellum causes mitochondrial fragmentation and COX deficiency prior to neurodegeneration, suggesting that mitochondrial morphological alternation and respiratory chain complex defect are early events in the pathogenic cascades (Almajan et al., 2012). Notably, the number of COX-deficient cells does not increase with time suggesting that Purkinje cells die shortly after displaying this phenotype (Almajan et al., 2012). Similarly, postnatal ablation of *Afg3l2*

in forebrain neurons causes rapidly neuronal death (Kondadi et al., 2014). Interestingly, we have identified ERK1/2 and PKA activation and tau hyperphosphorylation in *Afg3l2*-deficient neurons (Kondadi et al., 2014). Thus, together with the finding of tau hyperphosphorylation in *Afg3l2* null mice, a novel pathogenic mechanism in which tau pathology caused by AFG3L2 depletion leads to neurodegeneration is proposed (Kondadi et al., 2014).

In summary, aforementioned murine models recapitulate the important pathophysiological features of related human diseases. Mechanistically, these mouse models show that AFG3L2 influences mitochondrial dynamics, respiration, ROS levels and Ca²⁺ handling, it is therefore essential for neuronal survival (Figure 1.3). Besides, different neuronal populations have variable thresholds of susceptibility to the *m*-AAA protease deficiency (Martinelli et al., 2009) and Purkinje cells seem to be the most vulnerable cells upon loss of the *m*-AAA protease. However, the cell-autonomous role of the *m*-AAA protease in other cell types, such as glial cells, has not been extensively investigated. Moreover, these studies have not considered that an additional subunit of the *m*-AAA protease, AFG3L1, which is a high homologous to AFG3L2, is present in the mouse.

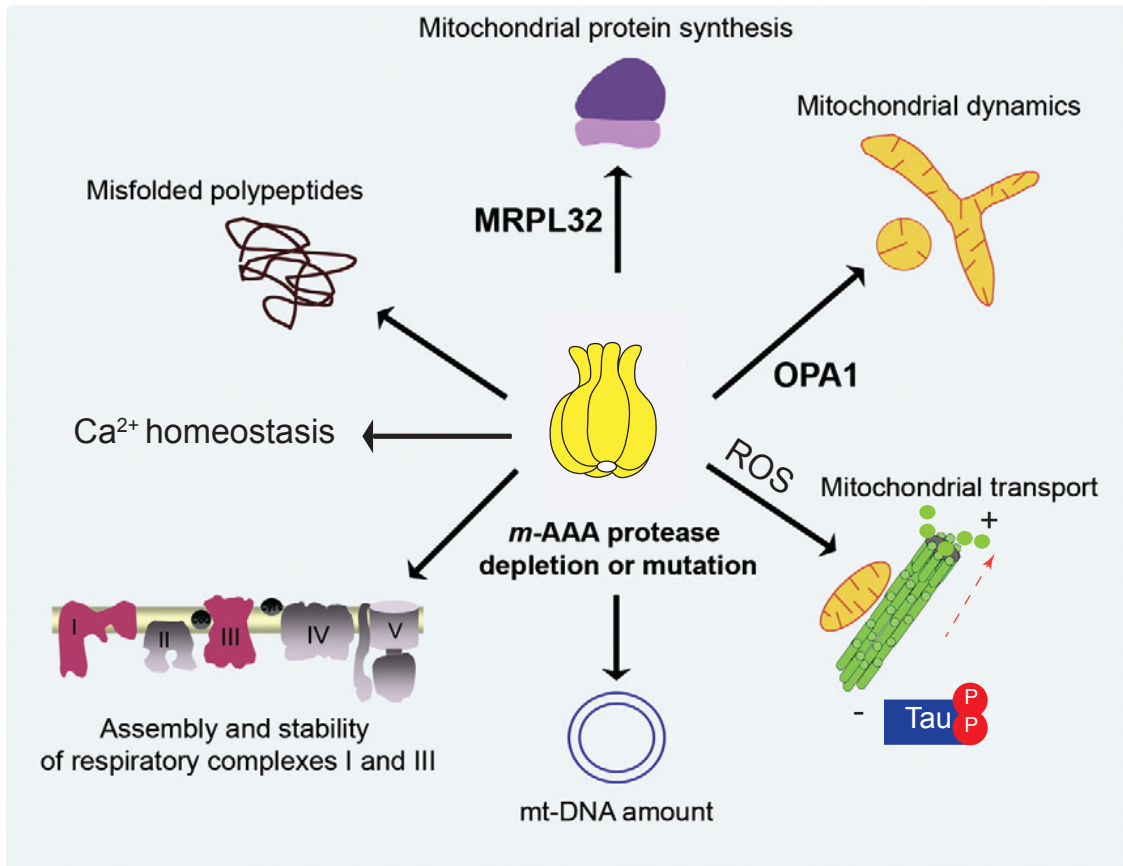


Figure 1.3 Pathogenic mechanisms of neurodegeneration caused by *m*-AAA protease deficiency

Depletion or mutations of the *m*-AAA protease subunits cause several pathogenic pathways including impaired mitochondrial protein synthesis, accumulation of misfolded proteins, inefficient Ca^{2+} handling, decreased assembly and stability of respiratory chain complexes I and III, reduced mt-DNA, defective anterograde transport and disturbed mitochondrial dynamics. Adapted from (Martinelli and Rugarli, 2010).

1.3 Myelinating cells

In vertebrates, myelinating cells are highly specialized glial cells that wrap axons with multi-layered myelin for rapid impulse propagation and axonal integrity (Nave and Trapp, 2008; Simons and Trotter, 2007). The myelin sheath, a specialized cell membrane, is formed by oligodendrocytes in the central nervous system (CNS) and Schwann cells in the peripheral nervous system (PNS) (Nave and Trapp, 2008; Simons and Trotter, 2007). The myelin membrane is composed of unique lipids and proteins that have to be assembled temporally and spatially (Figure 1.4) (Aggarwal et al., 2011; Baumann and Pham-Dinh, 2001; Simons and Trotter, 2007). A recent study has shown that myelin growth occurs by consecutive wrapping of the inner tongue around the axon and simultaneous lateral extension of newly formed myelin layers (Snaidero et al., 2014). Neuronal signals regulate myelinating cell development and myelin assembly (Nave and Trapp, 2008; Simons and Trajkovic, 2006); in turn, deficiency of myelin proteins or myelinating cells causes axonal demyelination and/or degeneration (Dewar et al., 2003; Lee et al., 2012; Nave et al., 2007; Nave and Trapp, 2008; Olmos-Serrano et al., 2016; Trapp and Nave, 2008; Viader et al., 2011).

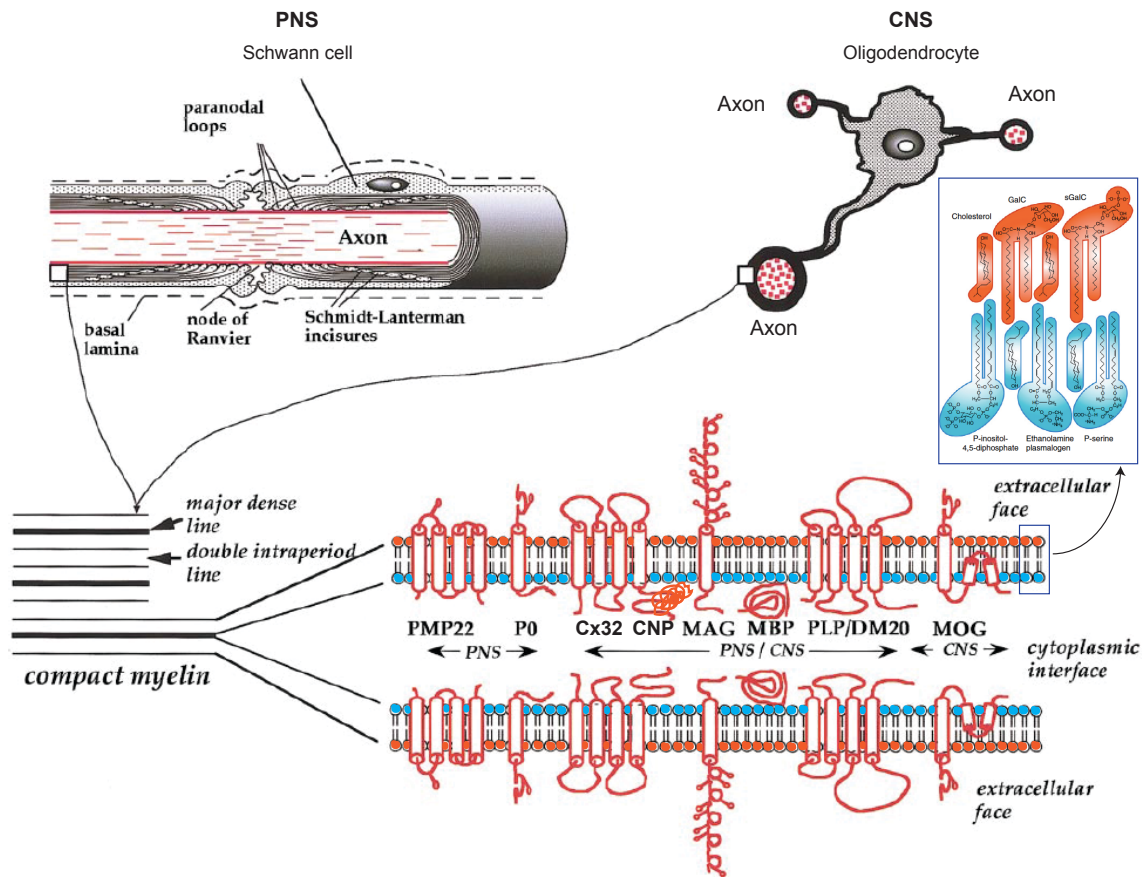


Figure 1.4 Schematic representation of myelinating cells, myelin structure and components.

While Schwann cells in the PNS only myelinate one axon, oligodendrocytes in the CNS are able to wrap several axons. The compact myelin is formed by the apposition of the external surfaces of the myelinating cell membrane, forming the “double intraperiod line”; the apposition of the internal surfaces followed by the extrusion of the cytoplasm, forming the “major dense line.” The lipid composition of myelin bilayer is asymmetric. Some major myelin proteins are indicated and classified according to the expression region. Adapted from (Aggarwal et al., 2011; Baumann and Pham-Dinh, 2001).

1.3.1 Oligodendrocytes

During the development of CNS, oligodendrogenesis takes place in multiple foci. In the spinal cord, most oligodendrocyte precursor cells (OPC) arise from the ventral progenitor domain starting from E12.5, then migrate laterally and dorsally to occupy the whole spinal cord after specification (Fancy et al., 2011). Besides, commencing ~E15.5, dorsal-derived OPC contribute to 20-30% of total OPC (Fancy et al., 2011; Vallstedt et al., 2005). In the forebrain, multiple waves of OPC production and migration occur from embryonic to postnatal stages (El Waly et al., 2014; Fancy et al., 2011). At E12.5, the first wave of OPC production originates in the medial ganglionic eminence and anterior entopeduncular area in the ventral brain (Kessaris et al., 2006). However, the majority of adult oligodendrocytes in mouse arise from the second and third wave of OPCs emanating from the lateral and/or caudal ganglionic eminences at E15.5 and from the cortex after birth, respectively (El Waly et al., 2014; Kessaris et al., 2006). Interestingly, genetical ablation of one population of oligodendrocytes in restricted areas in the CNS, triggers adjacent populations rapid migration and proliferation to maintain their normal density in adult mouse (Hughes et al., 2013; Kessaris et al., 2006).

While some OPC are reserved for myelin regeneration, others are specified and differentiate to myelinating oligodendrocytes (Figure 1.5) (Fancy et al., 2011). Oligodendrocytes are capable to myelinate several axons selectively with diameter above 0.2 μm (Simons and Trajkovic, 2006; Waxman and Sims, 1984). The process of oligodendrocyte maturation and myelination is very complicated, because it is highly coordinated with neurons/axons, and numerous signal pathways and regulatory factors are involved (Bradl and Lassmann, 2010; Fancy et al., 2011) (Figure 1.5).

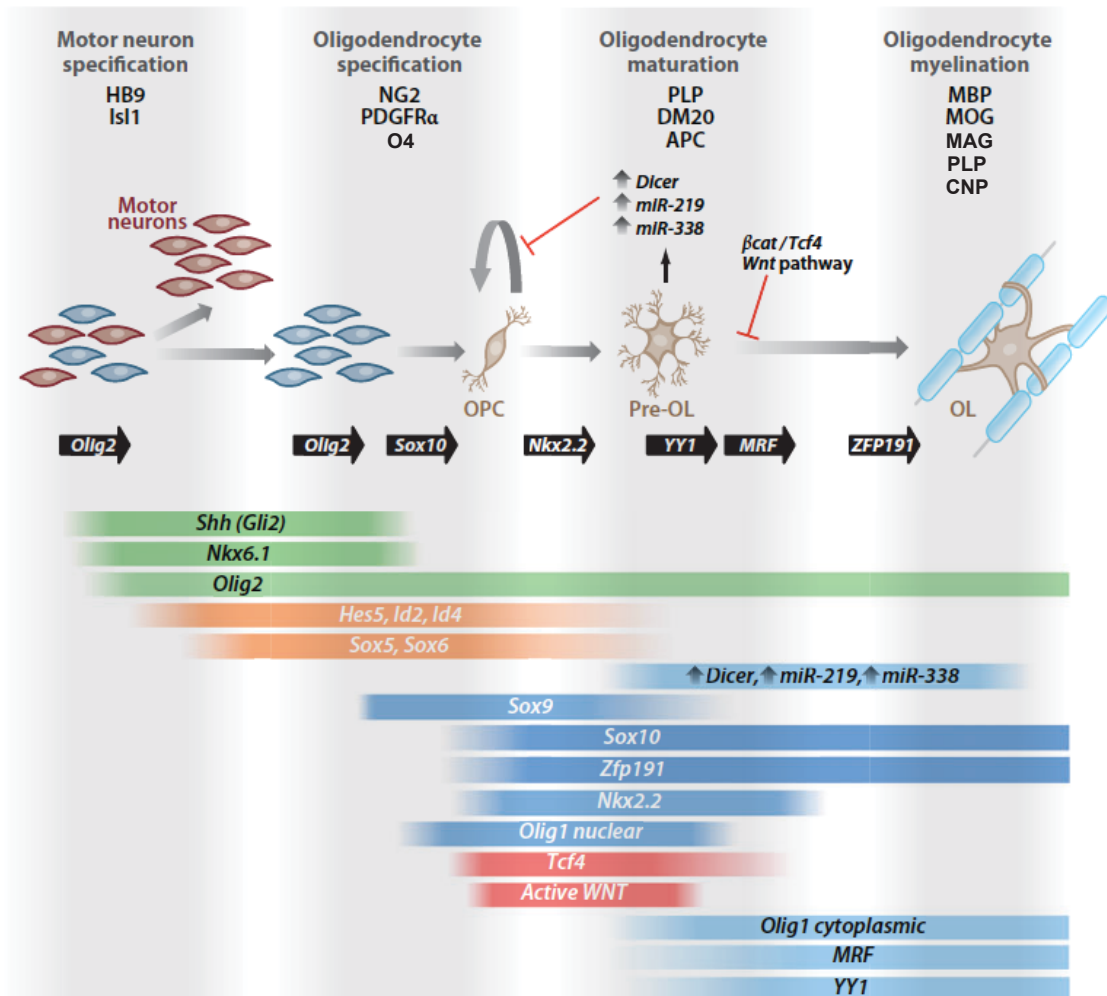


Figure 1.5 Schematic illustrating oligodendrocyte development and differentiation

In the spinal cord, oligodendrocyte precursor cells (OPC) are derived from the ventral progenitor domain, which also produces motor neurons. Oligodendrocytes express specific antigenic markers and follow a stepwise morphological transformation during development and differentiation. Solid black arrows indicate oligodendrocyte-lineage transitions that are dependent on specific transcription factors, and coloured gradient bars represent predicted temporal expression pattern of essential factors or regulators (Fancy et al., 2011).

1.3.2 Schwann cells

At early embryonic developmental stage of peripheral nerves, neural crest cells give rise to Schwann cell precursors (SCP) that are found among the axons of nascent nerves, and SCP develop into immature Schwann cells before birth (Jessen and Mirsky, 2005). Postnatal immature Schwann cells differentiate into either myelinating Schwann cells or non-myelinating Schwann cells (Figure 1.6) (Jessen and Mirsky, 2005; Woodhoo and Sommer, 2008). Schwann cells produce basal lamina and start radial sorting of 1:1 relationship (one myelinating Schwann cell ensheaths one axon) with large-calibre axons (diameter $> \sim 1 \mu\text{m}$) (Jessen and Mirsky, 2005; Simons and Trotter, 2007). Unmyelinated smaller axons (also known as C-fibre axons) forming Remak bundles are wrapped and segregated by non-myelinating Schwann cells. Multiple molecules and factors have been implicated in the regulation of Schwann cell development and myelination (Jessen and Mirsky, 2005). For instance, axon-derived signaling molecule Neuregulin-1 (NRG1), a EGF-like ligand for the ErbB family of tyrosine kinase receptors (Garratt et al., 2000; Van Raamsdonk and Deo, 2013), promotes Schwann cell lineage survival and development, and regulates myelin sheath thickness (Brinkmann et al., 2008; Garratt et al., 2000; Grinspan et al., 1996; Michailov et al., 2004; Taveggia et al., 2005).

One fascinating aspect of SCP is bipotentiality, not only having glial fate, but also giving rise to melanocytes that originate from neural crest cells as SCP. In the mouse at E10.5, shortly after neural crest delamination, the first wave of melanocyte precursor-melanoblasts migrate dorsolaterally between the dermamyotome and eventually reach the destination of the basal layer of the epidermis and the hair follicles (Adameyko et al., 2009; Erickson, 1993). At around E12.5, a second pathway, melanoblasts differentiated from SCP migrate ventrally along the nerves and contribute to a large number of melanocytes in the limbs, in the dorsal and lateral body wall (Adameyko et al., 2009; Van Raamsdonk and Deo, 2013). However, the role of SCP in formation of melanocytes in the adult or age-related hair greying remains elusive (Adameyko et al., 2009).

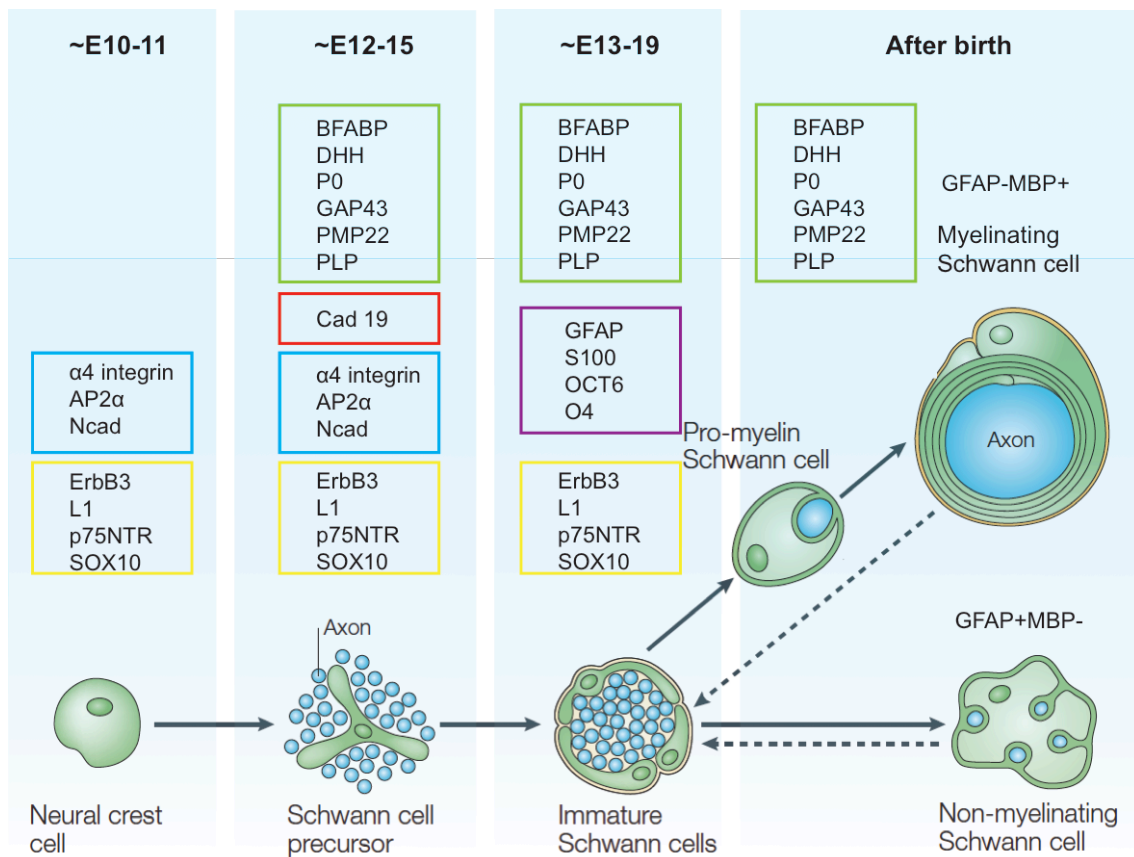


Figure 1.6 Development of Schwann cell lineage in mouse.

Schwann cells originate from the neural crest cells at early embryonic development. Markers of different developmental Schwann cell lineages are in coloured frames. The same colour means shared antigen expression. Dashed arrows indicate the reversible transformation of mature myelinating and nonmyelinating Schwann cells to immature Schwann cells. Adapted from (Jessen and Mirsky, 2005).

1.3.3 Pathology of myelin-forming cells

One of the main functions of myelinating cells is to produce multi-layered membrane structure of myelin, which insulates the axon and clusters sodium channels into the nodes of Ranvier, thus enables the action potential to conduct from one node to the other (Aggarwal et al., 2011). During the peak of myelination, oligodendrocytes elaborate several times the cell weight in membrane per day and ultimately produce membranes up to 100 times the weight of the cell body (Bradl and Lassmann, 2010), and the process of myelin synthesis and assembly requires a great amount of energy. Assuming that all basic components for lipid and proteins were available locally, the minimum energetic cost of myelin synthesis would be 3.30×10^{23} ATP molecules per gram myelin in the CNS (Harris and Attwell, 2012). Oligodendrocytes have very high metabolic rates to produce ATP, and this process also generates toxic by-product ROS (Bradl and Lassmann, 2010). Additionally, oligodendrocytes contain high amount of myelin synthetic enzyme cofactor-iron (Thorburne and Juurlink, 1996), which can provoke free radical formation and lipid peroxidation under adverse conditions (Bradl and Lassmann, 2010; Braughler et al., 1986; Juurlink, 1997). Given the fact that oligodendrocytes have low concentration of ROS scavenger glutathione and the susceptibility to inflammatory cytokines exposure, hypoxia, ischemia and pathogenic autoimmune, these cells are particularly vulnerable under pathological conditions (Bradl and Lassmann, 2010; Dewar et al., 2003; Thorburne and Juurlink, 1996).

In addition to myelin sheath formation, myelinating cells also metabolically support axonal survival (Funfschilling et al., 2012; Lee et al., 2012). Oligodendrocytes highly express monocarboxylate transporter 1 (MCT1) to transport glycolysis product lactate to axons (Funfschilling et al., 2012; Lee et al., 2012; Rinholm et al., 2011), and MCT1 deficiency leads to axonal degeneration (Lee et al., 2012). Importantly, several human neurodegenerative disorders, for instance, Multiple Sclerosis (MS), inherited leukodystrophies and Charcot-Marie-Tooth disease (CMT), have been implicated with myelinating cell pathology and myelin defects (Nave, 2010). Primary axonal degeneration occurs in some forms of demyelinating diseases, but secondary axonal degeneration is believed be the major cause of persistent neurological impairments (Table 1.1) (Nave, 2010).

Table 1.1 Human diseases associated with myelin defects and secondary axonal degeneration

Diseases	Frequency and causes	Glia and myelin pathology	Secondary axonal loss	Animal models
Multiple Sclerosis (MS)	<ul style="list-style-type: none"> • Relatively common autoimmune disease • Primary cause unknown • Viral origin and genetic risk factors suggested 	<ul style="list-style-type: none"> • CNS-specific disease • Inflammatory lesions in white-matter tracts cause oligodendrocyte death, extensive demyelination and macroscopic plaques 	<ul style="list-style-type: none"> • Axonal swellings and transections in white- and grey-matter lesions • Axon loss associated with permanent disability at later disease stages 	<ul style="list-style-type: none"> • EAE for modelling autoimmunity against myelin epitopes and the inflammatory phase of MS
Inherited leukodystrophies	<ul style="list-style-type: none"> • Very rare genetic disorders • Several single-gene defects identified, such as in <i>PLP1</i> (for PMD), <i>GJC2</i> (for PMLD), <i>ABCD1</i> (for adrenoleukodystrophy) and <i>ASA</i> (for metachromatic leukodystrophy) 	<ul style="list-style-type: none"> • Defects of terminal oligodendrocyte differentiation and myelin formation • Defects of myelin maintenance with demyelination (also secondary inflammation in adrenoleukodystrophy) 	<ul style="list-style-type: none"> • Perturbation of axonal transport followed by Wallerian degeneration • Purely axonal forms of leukodystrophies : SPG2 (associated with PLP1 defects) and adrenomyeloneuropathy (associated with ABCD1 defects) 	<ul style="list-style-type: none"> • Rodents with mutations corresponding to the human disease gene, such as a <i>Plp1</i> point mutation or <i>Plp1</i> overexpression (for PMD), <i>Plp1</i> knockout (for SPG2) and <i>Abcd1</i> knockout (for adrenomyeloneuropathy)
Inherited demyelinating neuropathies	<ul style="list-style-type: none"> • Rare genetic disorders, such as CMT • Many disease genes identified, such as <i>PMP22</i> (for CMT1A), <i>P0</i> (for CMT1B) and <i>GJB1</i> (for X-linked CMT) 	<ul style="list-style-type: none"> • Defects of Schwann cell differentiation and peripheral myelination, or myelin maintenance • Segmental demyelination with formation of ‘onion bulbs’ 	<ul style="list-style-type: none"> • Slowly progressive and length-dependent axon loss causing denervation, sensory deficits and muscle weakness — the clinical hallmarks of CMT 	<ul style="list-style-type: none"> • Rodents with mutations in or overexpression of genes corresponding to human disease genes, such as <i>Pmp22</i> (for CMT1A), <i>Mpz</i> (for CMT1B) and <i>Gjb1</i> (for X-linked CMT)

ABCD1, ABC binding cassette family D member 1; *ASA*, aryl sulphatase A; EAE, Experimental allergic encephalomyelitis; *GJB1*, gap junction protein $\beta 1$; *GJC2*, gap junction protein $\gamma 2$ (also known as *GJA12* and *CX47*); *PLP1*, proteolipid protein 1; PMD, Pelizaeus–Merzbacher disease; PMLD, Pelizaeus–Merzbacher-like disease. This table is from (Nave, 2010).

1.3.4 The role of mitochondria in myelinating cells

Mitochondrial dysfunction has been implicated in inflammatory demyelinating diseases (Mahad et al., 2008; Mahad et al., 2015; Popescu and Lucchinetti, 2012; Witte et al., 2014), and axonal demyelination is associated with several mitochondrial diseases, such as autosomal dominant optic atrophy, caused by OPA1 mutations (Alexander et al., 2000; Johnston et al., 1979); dominant CMT type 2 disease, caused by MFN2 mutations (Niemann et al., 2006; Zuchner et al., 2004); inherited Leber's hereditary optic neuropathy (LHON), caused by mitochondrial DNA mutations (Kovacs et al., 2005). Therefore, more insights into the function of mitochondria in myelinating cells may be beneficial to understand the pathogenic cascades of axonal demyelination and neurodegeneration.

The roles of mitochondria in myelinating cells are distinct and depend on the developmental stages. *In vitro* studies have demonstrated that oligodendrocyte precursors are more resistant to mitochondrial respiratory chain complex inhibitors; in contrast, differentiated and mature oligodendrocytes are much more sensitive to mitochondrial respiratory defects (Schoenfeld et al., 2010; Ziabreva et al., 2010). Inhibition of mitochondrial complex I or complex IV impairs differentiated oligodendrocyte process formation and myelin protein expression (Schoenfeld et al., 2010; Ziabreva et al., 2010), despite the fact that the viability of oligodendrocytes under these circumstances needs further investigation. Moreover, differentiated oligodendrocytes upregulate globally the transcripts of mitochondrial genes to provide energy and metabolites for myelin synthesis (Schoenfeld et al., 2010). Nevertheless, limited *in vivo* studies have shown that mitochondrial respiratory deficiency does not affect the survival of Schwann cells nor oligodendrocytes, and an energy metabolism adaptation is proposed (Funfschilling et al., 2012; Viader et al., 2011). Interestingly, Schwann cell-specific deletion of mitochondrial transcription factor A (*Tfam*), which is essential for mitochondrial DNA maintenance and biogenesis (Larsson et al., 1998), activates heme-regulated inhibitor kinase and induces an integrated stress response maladaptation, thereby causing a lipid metabolism shift from fatty acid synthesis toward oxidation and subsequently leading to progressive demyelination (Viader et al., 2011; Viader et al., 2013). *Cox10*, which encodes a heme A farnesyl transferase and is an assembly factor of COX (Antonicka et al., 2003; Nobrega et al., 1990), depletion of which using mice constitutively expressing Cre recombinase in Schwann cells or in both Schwann cells

and oligodendrocytes leads to severe neuropathy (Funfschilling et al., 2012). By contrast, using an inducible PLP1-CreERT2 line to delete *Cox10* in oligodendrocytes in adult mice does not cause any phenotype. This is because when myelination is complete, mature oligodendrocytes utilize glycolysis to supply lactate for the maintenance of myelin and axonal integrity (Funfschilling et al., 2012). Thus, mitochondria play crucial roles for myelinating cell differentiation and myelination, but these glial cells do not rely on mitochondria to produce ATP for the survival of these cells or axonal energy requirement in the adulthood.

2 Aim of the thesis

Mitochondria are pivotal organelles to support cellular energy requirement, Ca^{2+} homeostasis, metabolism, and apoptosis regulation, especially in polarized and aerobic neurons. Mitoproteases degrade misfolded, non-assembled or damaged proteins as part of quality control surveillance system (Martinelli and Rugarli, 2010; Quiros et al., 2015; Rugarli and Langer, 2012). Moreover, mitoproteases perform highly regulated proteolytic reactions, such as processing specific substrates that are crucial for mitochondrial biogenesis, translation, dynamics, mitophagy and apoptosis. Mitoproteases therefore emerge as essential regulators of mitochondrial function and quality control at molecular, organellar and cellular levels (Anand et al., 2013; Quiros et al., 2015).

One of the known mitoproteases is the *m*-AAA protease, localized in the mitochondrial inner membrane, and composed of hexameric complexes formed by AFG3L2 and paraplegin in humans (Koppen et al., 2007). Mutations of AFG3L2 and paraplegin have been associated with three neurodegenerative diseases SCA28, SPAX5 and HSP (Rugarli and Langer, 2012). Previous studies have shown that *m*-AAA protease deficiency causes mitochondrial respiratory deficits, morphological alterations, anterograde transport impairment, and calcium handling failure (Almajan et al., 2012; Atorino et al., 2003; Ehses et al., 2009; Ferreirinha et al., 2004; Kondadi et al., 2014; Maltecca et al., 2008; Maltecca et al., 2015; Maltecca et al., 2012; Martinelli et al., 2009). However, the pathogenic cascades of neurodegenerative diseases linked to *m*-AAA protease mutations remain elusive. In addition, the cell-autonomous role of the *m*-AAA protease is poorly understood. Therefore, in this study, we have these two aims:

1. Investigation the pathogenic cascades of AFG3L2 deficiency in neurodegeneration

Lack of AFG3L2 leads to mitochondrial fragmentation and dysfunction, and subsequently neuronal death, however, the pathogenic mechanism is not very clear. Since *Afg3l2* full-body knockout mice show phenotypic complexity and early death, we generated forebrain neuron-specific mice in which *Afg3l2* is depleted postnatally. We studied these two murine models to investigate the molecular alterations or signaling pathways triggered by *Afg3l2* deletion.

2. Elucidation the role of the *m*-AAA protease in myelinating cells.

Oligodendrocytes and Schwann cells produce myelin sheaths to wrap axons, thus facilitating the efficient and rapid propagation of nerve impulse (Nave and Trapp, 2008), and metabolically support axonal long-term survival (Funfschilling et al., 2012). How mitochondrial dysfunction in glial cells contributes to neurodegenerative diseases is largely unknown. Moreover, the *m*-AAA protease plays key roles in multiple aspects of mitochondria, but all published *m*-AAA protease related mouse studies have either used constitutive mutant models or focused on the role of AFG3L2 in neurons. Whether AFG3L2 deficiency in glial cells leads to mitochondrial dysfunction and contributes to neurodegenerative phenotype has not been explored. To this end, we deleted *Afg3l2* in myelinating cells by crossing tamoxifen inducible PLP1-CreERT mice (Doerflinger et al., 2003) with conditional *Afg3l2*^{fl/fl} mice (Almajan et al., 2012). Moreover, considering potential compensatory effect of AFG3L1 that is also expressed in the mouse, we depleted the whole *m*-AAA protease in myelinating cells by crossing PLP1-CreERT/*Afg3l2*^{fl/fl} mice with unpublished *Afg3l1* full-body knockout mice, which do not show evident neurological phenotype. In addition, a reporter ROSA26^{+SmY} line (Sterky et al., 2011) was used to examine mitochondrial morphology and the fate of targeted cells. With these murine models, we explored possible OXPHOS-independent function of the *m*-AAA protease in myelinating cells, which in comparison with neurons, may survive by glycolysis.

3 Material and methods

3.1 Animal experiments

All animals procedures were conducted in accordance with European, national and institutional guidelines and were approved by local authorities. Unless stated otherwise, animals were hosted in the CECAD in vivo research facility with 12:12 light/dark cycle. Daily care of animals was performed by qualified caretakers in compliance with institutional animal welfare protocols. Mice of both female and male were used in this study.

3.1.1 Mouse breedings

Single transgenic mouse strains:

1. *Afg3l2*^{+/*EMV66*} mice were generated originally in FVB genetic background (Maltecca et al., 2008). *Afg3l2*^{*EMV66/EMV66*} (L2 KO) mice were produced by mating *Afg3l2*^{+/*EMV66*} (pure FVB background) mice with *Afg3l2*^{+/*EMV66*} (50% FVB + 50% C57BL/6) mice (Figure 3.1).

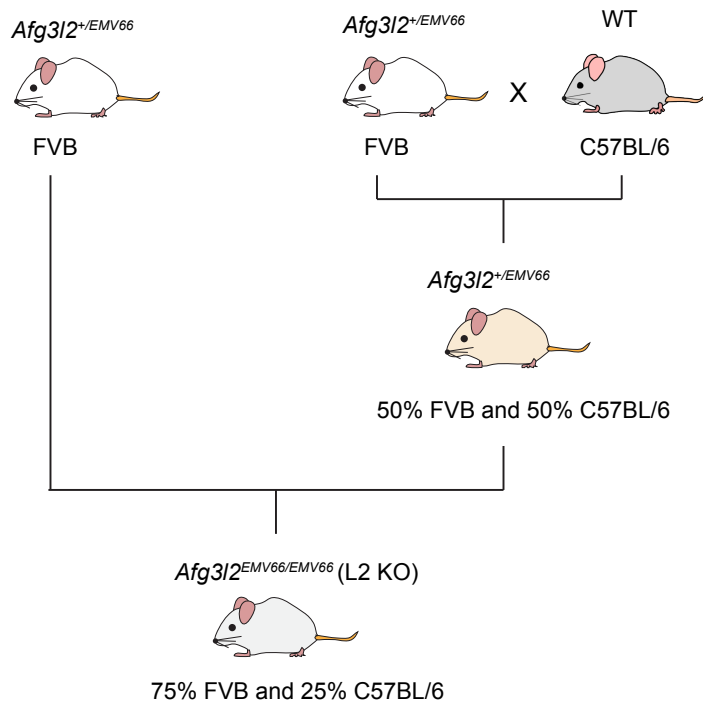


Figure 3.1 L2 KO mice were obtained on a mixed FVB-C57BL/6 background.

2. The generation of CamkII α -Cre mice was as previously described (Minichiello et al., 1999). Starting from P20, Cre recombinase is expressed in neurons in the forebrain including the neocortex, the hippocampus, and the striatum, but it is not expressed in the cerebellum (Merkwirth et al., 2012; Minichiello et al., 1999).

3. PLP1-CreERT, a tamoxifen inducible mouse line, in which the expression of Cre recombinase and a mutated ligand-binding domain of the human estrogen receptor (CreERT) is under the transcriptional control of the regulatory sequences of the gene encoding myelin proteolipid protein 1 (PLP1) (Doerflinger et al., 2003). PLP1-CreERT mice were purchased from Jackson Laboratory.
4. Conditional *Afg3l2*^{loxed/floxed} (*Afg3l2*^{fl/fl}) mice carrying two LoxP sites flanking exons 4 and 5 of *Afg3l2* gene were previously described (Almajan et al., 2012).
5. ROSA26^{+SmY} mice carrying a lox-flanked stop cassette placed upstream of the mitochondrial targeting sequence and YFP transgene were previously reported (Sterky et al., 2011).
6. *Afg3l1*^{-/-} mice were commercially generated by deletion of exon 2 and 3 in C57BL/6 background by TaconicArtemis GmbH.

Generation of mixed lines:

1. CamkII α -Cre/ *Afg3l2*^{fl/fl}

Mice from CamkII α -Cre line were crossed to *Afg3l2*^{fl/fl} mice to produce conditional forebrain neuron-specific *Afg3l2* knockout mice (*CamkII α -Cre*^{wt/tg}/*Afg3l2*^{fl/fl}, referred to as L2^{NKO}). Littermates with the genotype *CamkII α -Cre*^{wt/wt}/*Afg3l2*^{fl/fl} or *CamkII α -Cre*^{wt/wt}/*Afg3l2*^{wt/fl} were used as controls. This line was maintained by Anne Korwitz (Thomas Langer group) in the animal facility in institute for Genetics, University of Cologne.

2. PLP1-CreERT/ROSA26^{+SmY}

PLP1-CreERT mice were mated with ROSA26^{+SmY} mice to examine recombination efficiency and the fate of targeted cells.

3. PLP1-CreERT/*Afg3l2*^{fl/fl}

PLP1-CreERT mice were crossed with *Afg3l2*^{fl/fl} mice to produce myelinating cells-specific *Afg3l2* knockout mice (*PLP1-Cre*^{wt/tg}/*Afg3l2*^{fl/fl}, referred to as L2^{MC-KO}) upon tamoxifen administration. The littermates with the genotype *PLP1-Cre*^{wt/wt}/*Afg3l2*^{fl/fl} referred to as L2^{fl/fl} were also injected with tamoxifen and employed as controls.

4. PLP1-CreERT/*Afg3l2*^{fl/fl}/ROSA26^{+SmY}

PLP1-CreERT/*Afg3l2*^{fl/fl} mice were mated with ROSA26^{+SmY} mice (Sterky et al., 2011) to visualize mitochondrial morphology in *Afg3l2* deficient myelinating cells.

5. PLP1-CreERT/*Afg3l2*^{fl/fl}/*Afg3l1*^{-/-}

PLP1-CreERT/*Afg3l2*^{fl/fl} mice were bred with *Afg3l1*^{-/-} mice to completely delete the *m*-AAA protease in myelinating cells. Mice with genotype of *PLP1-Cre*^{wt/tg}/*Afg3l2*^{fl/fl}/*Afg3l1*^{-/-} were referred to as DKO. The control littermates with genotype *PLP1-Cre*^{wt/wt}/*Afg3l2*^{fl/fl}/*Afg3l1*^{-/-} were referred to as CTRL. All experimental CTRL and DKO were injected with tamoxifen.

6. PLP1-CreERT/*Afg3l2*^{fl/fl}/*Afg3l1*^{-/-}/ROSA26^{+SmY}

PLP1-CreERT/*Afg3l2*^{fl/fl}/*Afg3l1*^{-/-} mice were further crossed to ROSA26^{+SmY} line to visualize mitochondrial morphology in myelinating cells upon deletion of the whole *m*-AAA protease.

3.1.2 Genotyping

Tails were incubated in lysis buffer (50 mM Tris-HCl pH 8, 100 mM NaCl, 100 mM EDTA pH 8, 0.5% SDS, and 0.9 mg/ml proteinase K) at 55°C overnight. After centrifugation at 10,000 g for 10 minutes at room temperature, the supernatant was collected in a new tube, and the DNA was precipitated with 100% ethanol, and washed with 70% ethanol. The DNA was resuspended in TE buffer (10 mM Tris-HCl, 1 mM EDTA, pH 8). EmeraldAmp MAX PCR Master Mix (TaKaRa) was applied to set up polymerase chain reaction (PCR) according to the user guide with minor modification that the volume of each reaction was reduced to 15 µl. The primers for PCR are listed below (Table 3.1). Final PCR products were loaded onto 1% or 1.5% agarose gels.

Table 3.1 Primers for genotyping

Locus	Primer name	Sequence (5'-3')	Amplicon Size
<i>Afg3l2</i>	wt FW	GGAAGTACCATATCTGGTTGTCTG	wt 258 bp ko 390 bp
	ko FW	CCAGAAACTGTCTCAAGGTTCC	
	wt/ko RV	TGGATTCTGCACATCTCTTAACCC	
Cre	FW	TCCAATTTACTGACCGTACAC	tg 750 bp
	RV	GTTATTCGGATCATCAGCTAC	
<i>Afg3l2</i>	wt/fl FW	TTGGTTTTGTATGTGTTAGGTCAG	wt 387 bp
	wt/fl RV	GCCTGCACAGCTCCATGAT	fl 506 bp
<i>Afg3l1</i>	wt/ko FW	GCATTGCACAGTCATTTTCAGG	wt 272 bp ko 509 bp
	wt RV	GCCGTGGGTAATGTTTGTCC	
	ko RV	TGGACAGGGCATTATGATGC	
<i>ROSA26</i>	mt-YFP1	AAAGTCGCTCTGAGTTGTTAT	tg 250 bp wt 583 bp
	mt-YFP2	GCGAAGAGTTTGTCTCAACC	
	mt-YFP3	GGAGCGGGAGAAATGGATATG	

Abbreviation: FW, forward primer; RV, reverse primer; tg, transgene band.

3.1.3 Tamoxifen administration

Tamoxifen (T5648, Sigma) was dissolved in a corn oil/ethanol (9:1) mixture at a final concentration of 10 mg/ml. For pregnant female (~E15.5), 1 mg tamoxifen per 10 g body weight was administered by gavage once. For 4-week-old (P28-30) mice, 1 mg tamoxifen was administered by intraperitoneal injection once a day for 5 consecutive days.

3.1.4 Behavioral tests

In order to test motor ability and coordination of mice, rotarod test and beam-walking test were performed. For the rotarod test, mice were placed on an accelerating rotating (TSE systems) rod with a starting speed of 4 rpm and a constant acceleration of 7.2 rpm/min and the latency time to fall was recorded for each mouse up to a maximum of 300 seconds. Three tests were performed each day for 3 consecutive days, and mice were allowed to rest for 15 minutes after each test. Steffen Hermans assisted with the rotarod test.

In the beam-walking test, mice have to stay upright and walk through an elevated narrow beam to reach a safety dark box, and it is more sensitive to detect subtle motor impairment in comparison with the rotarod test (Luong et al., 2011; Stanley et al., 2005). In this test, 2 days of training and 1 day of testing were performed. In all 3 consecutive days, mice were trained to walk sequentially across a 3 cm beam and a 1 cm beam, which were elevated by a 30 cm metal support. On the third day, the performance of each mouse while acrossing the 1 cm beam was filmed and the number of foot slips was quantified.

In both behavioral tests, all available aged-matched mice were employed during the testing period, and no mouse was discriminated.

3.1.5 Fat content measurement

The body composition of mice was examined with quantitative magnetic resonance analyser (Bruker Minispec, MQ10).

3.2 Tissue Collection

Mice were anaesthetized with ketamine/xylazine (10 mg/100 mg per kg of body weight), and perfused transcardially first with PBS followed by 4% paraformaldehyde (PFA) in PBS (pH 7.4). Brain, spinal cord, and the peripheral nerves were then dissected and post fixed in 4% PFA for histology and immunofluorescence or in 2% glutaraldehyde in 0.12 M phosphate buffer for electron microscopy. The skin was collected before perfusion and immersed in 4% PFA for 2-4 h at 4°C, then cryo-protected in 15% sucrose for 2 h followed by incubation in 30% sucrose overnight. For western blot analyses and TUNEL assay, mice were sacrificed by cervical dislocation and respective tissues were collected for analysis.

3.3 Histology and immunohistochemistry

3.3.1 Slice preparation

Vibratome sectioning:

Postfixed brain and spinal cord were embedded in 6% agar, and cut at a thickness of 30 µm with a vibratome (VS1000, Leica). Free-floating sections were stored in 0.12 M phosphate buffer supplemented with 0.01% sodium azide at 4°C.

Paraffin sectioning:

Following dehydration in gradient ethanol (70% to 100%) and xylene, the skin was embedded in paraffin and 5 μm thick sections were cut with a microtome (RM2255, Leica).

Frozen sectioning:

Fresh brain or PFA post-fixed skin were embedded in OCT (Tissue-Tek), frozen on dry ice and stored at -80°C till use. Samples were equilibrated to cutting temperature (-20°C to -25°C) 20 min in advance, and 7 or 10 μm thick sections were cut using a cryostat (CM1850, Leica).

3.3.2 Immunostaining on vibratome sections

Free-floating sections were post-fixed in 4% PFA or in methanol for 30 min, and rinsed in PBS. Alternatively, sections were washed in 1% Triton X-100 for 30 min at room temperature. Sections were then blocked in 0.4% Triton X-100 in 10% goat serum for 1 h at room temperature, and incubated with primary antibodies (Table 3.2) diluted in 5% goat serum overnight at 4°C . After washing with PBS, sections were incubated with the appropriate secondary antibodies (Table 3.3) for 2 h at room temperature. Sections were washed 3 times with PBS (if necessary, to counterstain the nuclei, DAPI (1:2000, stock 1 mg/ml, Sigma) was added in PBS during the second wash), and mounted with Flurosav medium (345789, Calbiochem).

3.3.3 Immunostaining on paraffin sections

Following deparaffinization with xylene and gradient ethanol (100% to 50%), slices were rinsed with water and boiled in 0.1 M citrate buffer (pH 6) to unmask epitopes. Slices were quickly washed in PBS, and then permeabilized and blocked in 0.4% Triton X-100 in 10% goat serum for 1 h at room temperature. Slices were incubated with primary antibody (Table 3.2) overnight at 4°C . After washing, slices were incubated with secondary antibody (Table 3.3) for 2 h at room temperature, were washed in PBS, and mounted with Flurosav medium. When it was required, DAPI was used for counterstaining.

Table 3.2 Primary antibodies for immunostaining

Antibody	Section preparation	Company	Dilution
APC*	Vibratome	#OP80, Calbiochem	1:400
COX1	Vibratome	#459600, Invitrogen	1:1000
Cytochrome c	Vibratome	#556432, BD Pharmingen	1:1000
GFAP	Vibratome	#3670, Cell signaling	1:500
GFAP	Vibratome	#Z0334, Dako	1:2000
GFP	Vibratome	#ab6556, Abcam	1:1000
IBA1	Vibratome	#019-19741, Wako	1:2000
c-KIT	Paraffin	#553352, BD Pharmingen	1:1000
MBP	Vibratome	#SMI-94R, Covance	1:1000
Olig2	Vibratome	#AB9610, Millipore	1:500
S100	Vibratome	#Z0311, Dako	1:1000

* APC antibody worked better when the sections were washed in 1% triton X-100, without methanol fixation. For other antibodies for vibratome sections, both treatments worked similarly.

Table 3.3 Secondary antibodies for immunostaining

Antibody	Company	Dilution
Anti-mouse Alexa Fluor 488	A-11029, Molecular Probes	1:1000
Anti-mouse Alexa Fluor 546	A-21143, Molecular Probes	1:1000
Anti-rabbit Alexa Fluor 488	A-11034, Molecular Probes	1:1000
Anti-rabbit Alexa Fluor 546	A-11035, Molecular Probes	1:1000
Anti-rabbit Alexa Fluor 594	A-21207, Molecular Probes	1:1000
Anti-rat Alexa Fluor 488	A-11001, Molecular Probes	1:1000

3.3.4 Nissl staining

Vibratome sections were cleaned by removing surrounding agar, and mounted onto slides in Cromalin solution (0.1% gelatine, 0.02% potassium chromium sulphate). The slides were allowed to air-dry for 10-20 min at room temperature, then they were immersed in Nissl solution (36 mM Sodium hydroxide, 0.24% acetic acid, 0.25% thionine acetate) for 30-45 sec. The slides were washed in water several times, dehydrated in gradient ethanol (50% to 100%) and xylene, and mounted with Eukitt mounting medium.

3.3.5 Gallyas staining

Gallyas staining was carried out as previously described (Pistorio et al., 2006). Briefly, free-floating sections were fixed in 10% formalin for 1 day up to several weeks, then immersed in 2:1 pyridine/acetic anhydride for 30 min. After washing in gradient pyridine (80% to 20%) and water, sections were immersed in freshly prepared ammoniacal silver nitrate solution (10 mg ammonium nitrate, 10 mg silver nitrate and 30 μ l 4% NaOH in 10 ml Millipore H₂O) for 45 min. Afterwards, sections were washed 3 times in 0.5% acetic acid for total of 10 min, and transferred into fresh 10% formalin. After at least one day of fixation, sections were washed 2 times in 0.5% acetic acid, and developed in fresh developer (2.5% sodium carbonate, 0.1% ammonium nitrate, 0.1% silver nitrate, 0.01% PFA) for 30-60 min. Finally, sections were washed with 1% acetic acid and water. In case of over exposure or strong background, sections were immersed in 0.1% potassium ferricyanide to increase contrast.

3.3.6 Haematoxylin and eosin staining

Paraffin slices were deparaffinized and rehydrated, and stained with Mayer's Haematoxylin solution (MHS32, Sigma) for 4 min. After washing in water, slices were stained in Eosin Y-solution 0.5% aqueous (1098441000, Millipore) for 20 sec, washed in water, dehydrated in gradient (75% to 100%) ethanol and xylene, and mounted with Eukitt medium.

3.3.7 TUNEL assay

To detect TUNEL positive (⁺) cells, the *In Situ* Apoptosis assay (S7101, Millipore) was applied on cryostat sections according to the manufacturer's manual. Briefly, frozen sections were fixed in 1% PFA for 10 min at room temperature. After washing in PBS, sections were post-fixed and permeabilized in 2:1 ethanol/acetic acid for 10 min at -20°C. Sections were washed in PBS, and endogenous peroxidase was quenched by 3% H₂O₂ in PBS for 5 min. Sections were incubated shortly with equilibration buffer, and then incubated with working strength TdT enzyme in a humidified chamber for 1 hour at 37°C. Afterwards, stop/wash buffer was applied for 10 min at room temperature. Sections were washed in PBS, and then incubated with anti-digoxigenin conjugate for 30 min at room temperature. After washing with PBS, sections were developed with peroxidase substrate for 5-10 min. Sections were washed in water, and dehydrated in ethanol and xylene, and then mounted with Eukitt mounting medium. Positive control sample was treated with 0.1-1 μ g/mL Deoxyribonuclease I (DNase I, D7291, Sigma) in

DNase buffer (30 mM Tris-HCl pH 7.2, 4 mM MgCl₂, 0.1 mM DTT) for 10 min at room temperature. For negative control, water or equilibration buffer was used to substitute working strength TdT enzyme.

The number of TUNEL⁺ cells within the corpus callosum was quantified manually. 2-3 sections from each mouse and 4 mice per group were used for quantification.

3.4 Microscopy

3.4.1 Light microscopy

If not stated otherwise, fluorescent images or bright-field images were acquired with an Axio-Imager M2 microscope equipped with Apotome 2 (Zeiss). When specified, confocal images were captured with a gSTED super-resolution and confocal microscope with HyD detector (TCS SP 8, Leica), and Huygens deconvolution software was applied. For Gallyas staining, Hematoxylin and eosin staining, entire sections were scanned with a slide scanner (SCN400, Leica), and regions of interest are shown in related figures.

3.4.2 Electron microscopy

The corpus callosum and the lumbar spinal cord were post-fixed in 2% glutaraldehyde (Sigma) in 0.12 M phosphate buffer at 4°C, and a small piece from each sample was prepared and immersed in fresh 2% glutaraldehyde one day before embedding. Small pieces of tissues were treated in 1% osmium tetroxide (Sigma) for 1-4 h. After dehydration with gradient ethanol (50%-100%) and propylene oxide, tissues were embedded in Epon (Fluka). Tissue in Epon-block was further trimmed with an ultramicrotome (EM UC7, Leica). 1 µm semithin sections were cut and stained with 1% toluidine blue for light microscopy. For electron microscopy, 70 nm ultrathin sections were cut and stained with 2% uranyl acetate (Plano GMBH) and Reynolds solution containing 3.52% sodium citrate (Electron Microscopy Sciences), 2.66% lead nitrate (Electron Microscopy Sciences) and 160 mM Sodium hydroxide. Images were acquired with a transmission electron microscope (CM10, Phillips) equipped with Orius SC200W camera.

3.5 Cell counting and axon morphometry

3.5.1 Cell counting

At least 3 mice per genotype at each time point were used for quantification. Quantification was performed on forebrain coronal sections, cerebellum sagittal sections at comparable levels, and spinal cord at lumbar levels. Low-magnification photographs of non-overlapping fields covering the lateral part of the corpus callosum, the most medial part of the internal capsule of one hemisphere and ventral grey matter of the spinal cord were taken and used for quantification. For the quantitative analysis of dark cells in the ventral white matter of spinal cords, at least 3 semithin micrographs of each mouse were used. One section per mouse was employed. APC⁺, Olig2⁺, mt-YFP⁺, or dark cells were counted manually. The cell size of APC⁺ cells was quantified on images acquired using the same exposure time by the measure function of Axiovision software (Zeiss).

3.5.2 g ratio and myelinated axon counting

The number of myelinated axons in the lumbar part of the spinal cord was quantified from micrographs of semithin sections using ImageJ particle analyzer with the setting of size 50-infinity and circularity 0.3-1.0. The g ratio was determined by measuring the diameter of inner axon and total outer on electron micrographs using Photoshop. 3 mice per genotype were analysed.

3.6 Oligodendrocytes preparation

Brains from P5 pups were removed and manually dissociated with the Neuronal Tissue Dissociation Kit (130-092-628, Miltenyi Biotec). Briefly, the weight of brain was determined in ice-cold HBSS without Ca²⁺ and Mg²⁺ (55021C, Sigma). Afterwards, the brain was cut into small pieces and mechanically dissociated in pre-warmed enzyme mix (as specified in the manufacturer's instruction) at 37°C. The cell suspension was applied to a 40 µm cell strainer (BD Falcon) and washed with HBSS with Ca²⁺ and Mg²⁺ (55037C, Sigma). After centrifugation, cells pellets were resuspended in 0.5% BSA in PBS. To purify oligodendrocytes, the cell suspension was further incubated with anti-O4 magnetic beads (130-094-543, Miltenyi Biotec) for 15 min at 4°C. Next, the cell suspension was washed and applied onto MACS column (130-042-201, Miltenyi Biotec), which was placed in a magnetic field of the MACS separator (130-

042-302, Miltenyi Biotec). The magnetic labelled O4⁺ cells were retained within the columns, while flow-through was collected. MACS column was removed from the magnetic MACS separator, after adding 1 ml buffer containing 0.5% BSA in PBS, O4⁺ cells were flushed out by pushing the plunger into the column. After centrifugation, cell pellet was stored at -80°C till use.

3.7 Biochemistry

3.7.1 Isolation of crude mitochondria

Mitochondrial preparation was performed as previously described (Wieckowski et al., 2009). Tissues were homogenized in ice-cold isolation buffer (225 mM Mannitol, 75 mM Sucrose, 30 mM Tris-HCl, 1mM EGTA, 0.5% BSA) using Potter S (Sartorius). The homogenate was centrifuged at 800 g for 5 min at 4°C, and the supernatant was collected and centrifuged at 10,000 g for 10 min at 4°C. The pellet was resuspended in mitochondrial resuspending buffer (225 mM Mannitol, 5 mM HEPES, 0.5 mM EGTA). After centrifugation at 10,000 g for 10 min at 4°C, the pellet was finally resuspended in mitochondrial resuspending buffer, and stored at -80°C till use.

3.7.2 Myelin isolation

Sucrose gradient centrifugation was used to purify myelin from mouse brain (Norton and Poduslo, 1973; Uschkureit et al., 2000). Briefly, half a brain was homogenized in 10 ml 0.32 M sucrose with Potter S homogenizer (Sartorius). The homogenate was layered over 20 ml of 0.85 M sucrose, and centrifuged at 20,000 g for 30 min at 4°C. The interphase of crude myelin was collected with a pipette, and resuspended in 30 ml Millipore water. Following centrifugation at 20,000 g for 15 min at 4°C, the crude myelin pellets were resuspended again in 30 ml Millipore water and centrifuged at 12,000 g for 10 min at 4°C. The myelin pellet was washed in water again, and was stored at -80°C till use.

3.7.3 Protein extraction

Mouse tissue was homogenized in RIPA buffer containing 50 mM Tris-HCl pH7.4, 150 mM NaCl, 5 mM EDTA, 1% Triton X-100, 1% sodium deoxycholate, 0.1% SDS, and fresh protease cocktail inhibitor (P2714, Sigma) on ice. The homogenate was centrifuged at 20 000 g for 30 min at 4°C. The supernatant was harvested, and protein

concentration was determined with Bio-Rad protein assay based on Bradford method (500-0006, Bio-Rad). Protein extraction from cells was similarly performed. Briefly, cells were lysed in RIPA on ice for 30 min, and the protein concentration was measured after high-speed centrifugation. The lysates from mouse tissues or cells were diluted into equal concentration, then were mixed with SDS sample loading buffer with a final concentration of 50 mM Tris-Cl pH 6.8, 2 % SDS, 10 % glycerol, 0.004 % bromophenol blue and 1 % of β -mercaptoethanol. After boiling 5 min on heating block (95°C), samples were subjected to immunoblot, or stored as aliquots at -80°C till use.

3.7.4 Western blot

Proteins were separated by 10% or 12% sodium dodecyl sulfate polyacrylamide gel electrophoresis (SDS-PAGE) at constant 10-30 mA till the ladder was resolved ideally.

Next, proteins were transferred onto 0.45 μ m PVDF membrane (GE Healthcare) in a buffer containing 25 mM Tris, 192 mM glycine and 20% methanol. The blotting was conducted at constant 300 mA for 90 min at 4°C.

Afterwards, the membrane was stained with in Ponceau solution (0.1% Ponceau S in 5% acetic acid) to visualize protein bands. The membrane was blocked in 5% milk or in 1 % western blot reagent (11921673001, Roche) in 0.1 % Tween 20 in TBS (TBST) and incubated with primary antibodies (Table 3.4) at 4°C overnight. After washing in TBST, the membrane was incubated with the secondary antibodies (Table 3.5), followed by washing in TBST. The membrane was then incubated with enhanced chemiluminescent (ECL) detection reagents (RPN2106, GE Healthcare) or ECL prime (RPN2232, GE Healthcare), exposed to X-ray films (4741019236, FUJIFILM), and developed in dark.

Table 3.4 Primary antibodies for western blot

Antibody	Company or source	Dilution
AFG3L1	Home-made, Rugarli lab (Koppen et al., 2007)	1:1000
AFG3L2	Home-made, Rugarli lab (Koppen et al., 2007)	1:1000
AFG3L2	Home-made, Langer lab (Koppen et al., 2007)	1:12500
AMPK	#2532, Cell signaling	1:1000
Phospho-AMPK (Thr172)	#2535, Cell signaling	1:1000

ATP5 a	#ab14748, Abcam	1:1000
CDK 5	#ab63550, Abcam	1:1000
CNP	#5922, Sigma	1:500
CNX	#ADI-SPA-860, Enzo	1:4000
DRP1 (DLP1)	#611112, BD Biosciences	1:1000
Phospho-DRP1 (Ser616)	#3455, Cell signaling	1:1000
ERK1/2	#9102, Cell signaling	1:1000
Phospho-ERK1/2	#4370, Cell signaling	1:1000
GAPDH	#MAB374, Chemicon	1:2000
GFAP	#Z0334, Dako	1:2000
GSK3 β	#9315, Cell signaling	1:1000
Phospho-GSK3 α/β (Ser21/9)	#9331, Cell signaling	1:1000
JNK	#9252, Cell signaling	1:1000
Phospho-JNK	#9255, Cell signaling	1:1000
Phospho-MARK	#4836, Cell signaling	1:1000
MBP	#SMI-94R, Covance	1:2000
NDUFA9	#459100, Molecular Probes	1:1000
OPA1	#612606, BD Biosciences	1:1000
P35/25	#2680, Cell signaling	1:1000
P38	#8690, Cell signaling	1:1000
Paraplegin	Home-made, Rugarli lab (Ferreirinha et al., 2004)	1:500
PHB	#MS-261-P1, Thermo Scientific	1:1000
PKA C- α	#4782, Cell signaling	1:1000
Phospho-PKA C (Thr197)	#4781, Cell signaling	1:1000
SDHA	#A-11142, Molecular probes	1:4000
SOD2 (Mn-SOD)	06-984, Upstate	1:1000
Tau (Tau-1)	#MAB3420, Chemicon	1:1000
Phospho-Tau (S202/T205)	#MN1050, Pierce	1:1000
Phospho-Tau (T181)	#701530, Pierce	1:2000
Phospho-Tau (S199)	#710124, Pierce	1:2000
Phospho-Tau (S396)	#710298, Pierce	1:2000
Tom20	#sc-11415, Santa Cruz	1:1000
β -III tubulin	#T8660, Sigma	1:1000

Table 3.5 Secondary antibodies for western blot

Antibody	Company	Dilution
Anti-mouse IgG	#A9044, Sigma	1:10000-1:30000
Anti-rabbit IgG	#A0545, Sigma	1:5000-1:10000

3.7.5 Oxyblot

To detect oxidative proteins modified by oxygen free radicals and other reactive species, Oxyblot protein oxidation detection kit (S7150, Millipore) was applied. Briefly, 10-20 µg proteins per sample were denatured in SDS and then treated with DNPH solution for 15 min at room temperature. For the negative control, derivatization-control solution was employed instead of DNPH solution. The reaction was stopped by adding neutralization solution. Afterwards, standard western blot was conducted with the primary antibody (dilution 1:150) and secondary antibody (dilution 1:300) provided in the Oxyblot kit.

If not stated specifically, all chemicals used in this study were purchased from Sigma.

3.8 Statistical analysis

3.8.1 *Chi-square* test

χ^2 was calculated with the formula below, and cumulative probability was calculated with an online calculator (<http://www.danielsoper.com/statcalc/calculator.aspx?id=11>).

$$\chi^2 = \sum \frac{(\text{observed} - \text{expected})^2}{\text{expected}}$$

3.8.2 Unpaired Student's *t* test

Unless stated otherwise, two-tailed unpaired *t* test was performed using GraphPad Prism 6 software, presenting the data as mean \pm standard error of the mean (S.E.M.).

3.8.3 Two-way ANOVA test

Two-way ANOVA test was performed using GraphPad Prism 6 software, presenting the data as mean \pm standard error of the mean (S.E.M.).

All statistical significance is defined as **p* < 0.05, ***p* < 0.01, ****p* < 0.001 and *****p* < 0.0001.

4 Results

4.1 *Afg3l2* full-body knockout mice show severe developmental phenotype

It has been previously shown that mouse models carrying null or missense homozygous mutations of *Afg3l2* display axonal development defects and die generally at P16 (Maltecca et al., 2008), however the pathogenesis was not completely understood. To gain new insights into the pathogenic mechanism, I further analyzed the *Afg3l2* null mutant mice, which was generated in FVB strain by integration of ecotropic murine leukemia virus insertion 66 (EMV66) within intron 14 of the *Afg3l2* gene (Maltecca et al., 2008). Western blot analysis confirmed that neither full-length nor truncated form of AFG3L2 was present in *Afg3l2*^{EMV66/EMV66} mice (Maltecca et al., 2008). Therefore, *Afg3l2*^{EMV66/EMV66} mice are *bona-fide* knockouts, hereafter referred to as L2 KO.

4.1.1 Phenotypic complexity of L2 KO mice

When *Afg3l2*^{+ /EMV66} line was hosted in our animal facility, we were not able to obtain L2 KO mice in a pure FVB background. To increase the birth rate of L2 KO mice, we decided to set up the breedings in a mixed FVB-C57BL/6 genetic background (Figure 3.1 in material and methods). Nonetheless, the percentage of L2 KO mice was 8.8% at P12 (Figure 4.1 A), and the mutants died before 3 weeks of age. We analyzed the mice at P12, in the middle-late stage of disease progression. As expected, L2 KO mice showed a severe muscle weakness and body weight reduction at P12 (Figure 4.1 B, C). Consistent with myelination defects in the spinal cord of AFG3L2 mutants (Maltecca et al., 2008), both immunofluorescence staining and western blot analysis to detect specific myelin proteins showed a reduction of MBP (Kondadi et al., 2014) and CNP in the brain (Figure 4.1 D, E), suggesting a global myelination defect throughout the CNS of L2 KO mice.

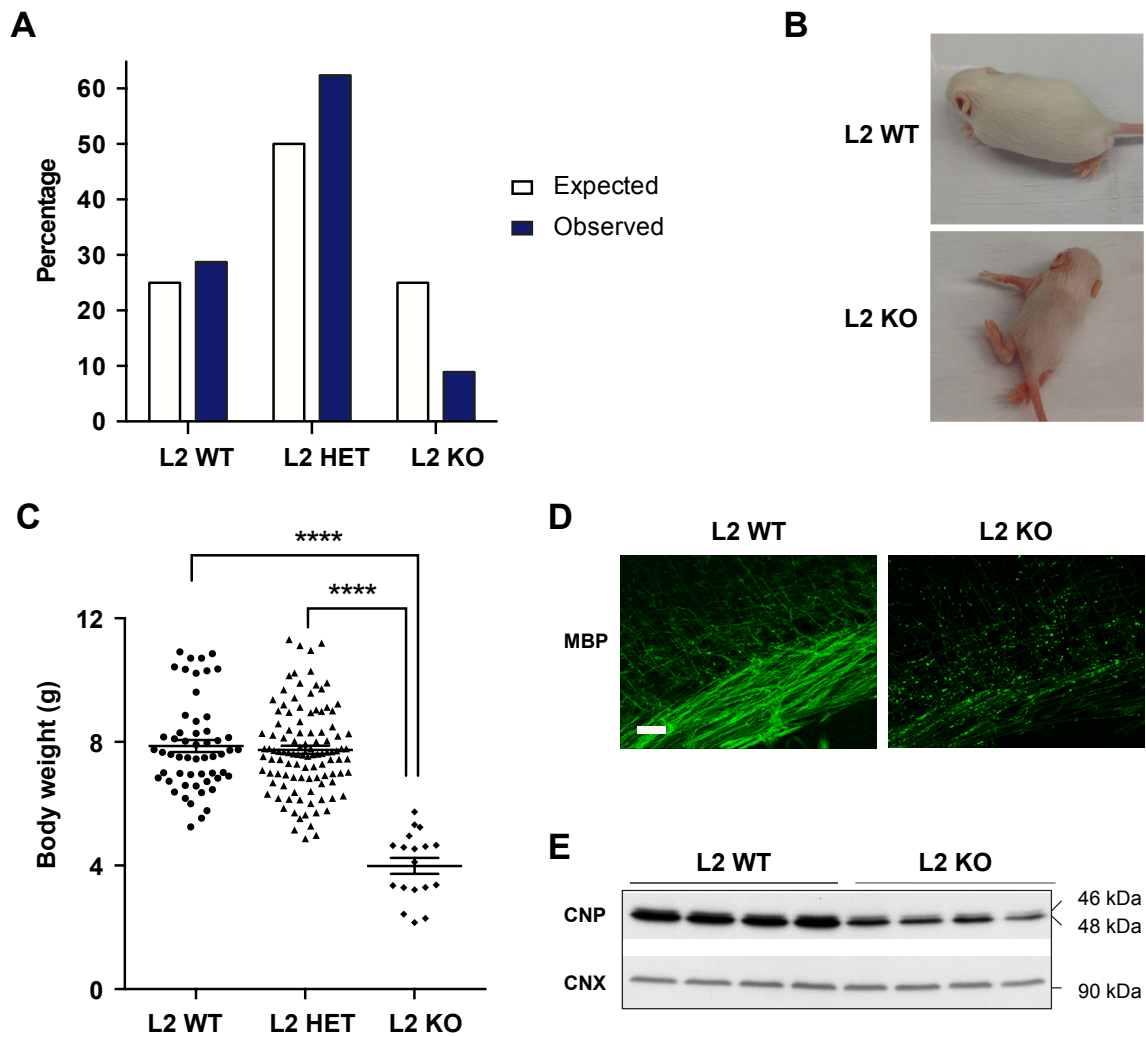


Figure 4.1 Characterization of *Afg3l2* full-body knockout mice.

(A) Distribution of different genotypes of animals at P12. *Chi-square* test, $\chi^2 = 27.91$, probability 8.7×10^{-7} . Observed *Afg3l2*^{+/+} (L2 WT) n = 58, *Afg3l2*^{+/*EMV66*} (L2 HET) n = 126, *Afg3l2*^{*EMV66/EMV66*} (L2 KO) n = 18. (B) Representative picture of one L2 KO mouse compared to a wild type littermate at P12. (C) Body weight reduction of L2 KO at P12. L2 WT n = 58, L2 HET n = 126, L2 KO n = 18. (D) Immunofluorescence staining of myelin protein MBP on coronal brain sections reveals myelin defect in the L2 KO mice. n = 3 per genotype. Scale bar, 50 μ m. (E) Western blot shows myelin protein CNP reduction in the brain lysates of L2 KO mice at P12.

4.1.2 Loss of *Afg3l2* unbalances mitochondrial fission and fusion

Since mitochondria are dynamic organelles undergoing fusion and fission constantly, perturbation of the balance between fusion and fission could change the fate of mitochondria and consequently affects neuronal survival (Chen and Chan, 2009; Itoh et al., 2013). Increased fission or fusion defects could result in mitochondrial fragmentation, while the opposite leads to mitochondrial elongation. Previous studies have shown that knockdown of *Afg3l2* leads to mitochondrial fragmentation via increased OPA1 processing (Ehse et al., 2009). Consistently, in *Afg3l2* full-body knockout mice, mitochondria were fragmented and swollen (Figure. 4.2 A). The fragmentation may be explained by the enhanced cleavage of OPA1 long isoforms that are required for mitochondrial fusion (Figure. 4.2 B), whereas it is unknown if mitochondrial fission protein DRP1 is also affected. To assess this possibility, I checked the levels of the mitochondrial fission protein DRP1 (Smirnova et al., 2001) in the brain of mice at P12. Notably, the total DRP1 level was significantly decreased in the L2 KO mice (Figure. 4.2 B). DRP1 promotes mitochondrial fission when Ser 616 is phosphorylated (DRP1 pS616) (Taguchi et al., 2007). Interestingly, DRP1 pS616 was also reduced in the L2 KO mice (Figure. 4.2 B). Cytosolic DRP1 is recruited to mitochondria to mediate mitochondrial division (De Vos et al., 2005; Korobova et al., 2013), thus I also examined DRP1 level in isolated mitochondrial fraction. The level of DRP1 in mitochondrial fraction was significantly diminished in the absence of AFG3L2 (Figure. 4.2 C), suggesting less mitochondrial fission events occur in L2 KO mice. Taken together, our data suggest that AFG3L2 deficiency leading to mitochondrial fragmentation and is caused by OPA1 regulated fusion impairment rather than increased fission.

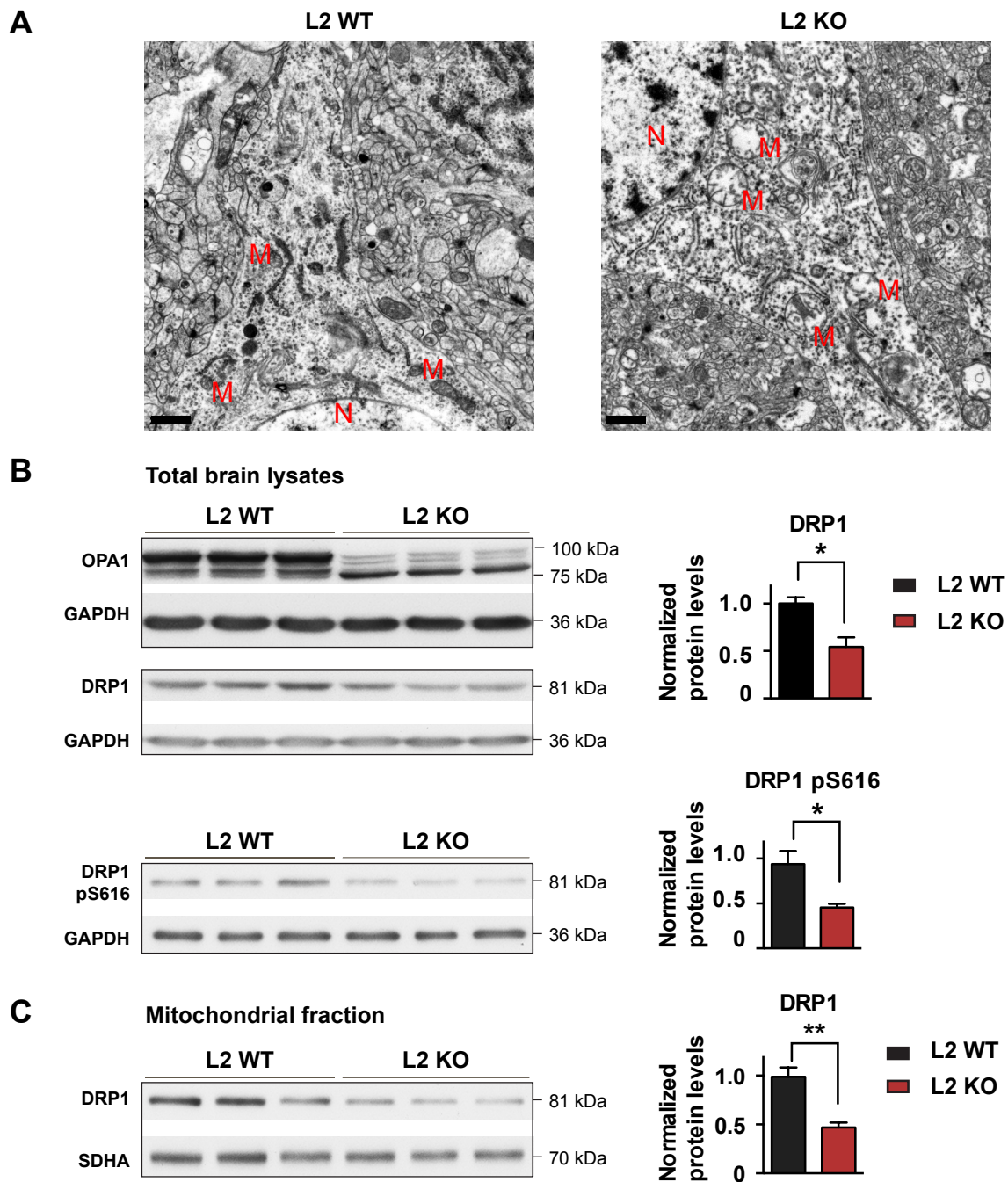


Figure 4.2 Disturbed mitochondrial dynamics in L2 KO mice.

(A) Ultrastructural analysis of mitochondrial morphology in neurons of the brain. M: mitochondria; N: nucleus. Scale bar, 1 μ m. (B) Immunoblot analysis of mitochondrial fusion/fission proteins OPA1 and DRP1 in total brain lysates from P12 pups. Quantification of the intensity of DRP1 and active form of DRP1 phosphorylated at Ser 616 (DRP1 pS616) normalized to loading control GAPDH is shown on the right. (C) Immunoblot analysis of DRP1 in crude mitochondrial fraction from the brain of P12 pups. Quantification of the intensity of DRP1 normalized to loading control SDHA is shown on the right. n = 3 per genotype for all experiments.

4.1.3 Lack of *Afg3l2* triggers tauopathy

Ultrastructural analysis of mitochondrial morphology in the brain of L2 KO mice unexpectedly showed that microtubules were disorganized and fragmented in neurons (Figure 4.3 A) (Kondadi et al., 2014). Tau is a well-known microtubule associated protein, and tau hyperphosphorylation has been implicated in Alzheimer's diseases (AD) (Alonso et al., 1996; Butner and Kirschner, 1991; Cleveland et al., 1977; Drubin et al., 1986; Mandelkow and Mandelkow, 1998; Stoothoff and Johnson, 2005). Hyperphosphorylated tau detaches from microtubules, forms neurofibrillary tangles and results in microtubular disintegration and eventually neuronal death (Stoothoff and Johnson, 2005). To test if tauopathy is linked to *Afg3l2* deficiency, we analysed tau levels in the L2 KO mice at P12. Immunoblot showed a dramatic increase of phosphorylated tau at various sites including T181, S199, S202, T205, S396, hyperphosphorylation of which has been involved in the pathogenesis of Alzheimer's disease (Martin et al., 2013b), whereas total tau level was not changed in the brain of L2 KO mice (Figure 4.3 B) (Kondadi et al., 2014). Importantly, a significant increase of insoluble phosphorylated tau was present in the brain lysate pellets of L2 KO mice (Figure 4.3 C). These data indicate that *Afg3l2* deficiency triggers tau hyperphosphorylation and tau pathology.

4.1.4 Investigation of possible kinases involved in tau hyperphosphorylation

Protein kinases regulate tau phosphorylation, and abnormal kinase activation has been implicated in tau hyperphosphorylation observed in the brain of AD patients (Martin et al., 2013b). To investigate potential kinases leading to tau hyperphosphorylation in the brain of the L2 KO mice, I tested steady state levels of multiple tau kinases, such as PKA, CDK5, JNK, ERK1/2, which have been shown to cause tau hyperphosphorylation in AD (Martin et al., 2013b). However, none of the kinases examined was dysregulated either in the total brain lysates or mitochondrial lysates in the L2 KO mice (Figure 4.4 A, B).

Oxidative stress has been identified as one of the earliest events in the pathogenesis of AD (Lovell and Markesbery, 2007; Onyango and Khan, 2006; Zafrilla et al., 2006; Zhu et al., 2004). Moreover, haploinsufficiency of *Afg3l2* mouse model showed increased reactive oxygen species (ROS) production (Maltecca et al., 2009). We therefore explored possible oxidative damage in our L2 KO mice. Unexpectedly, oxidative stress

markers SOD2, and carbonyl groups in oxidative proteins were comparable to the control (Figure 4.4 B, C) (Kondadi et al., 2014).

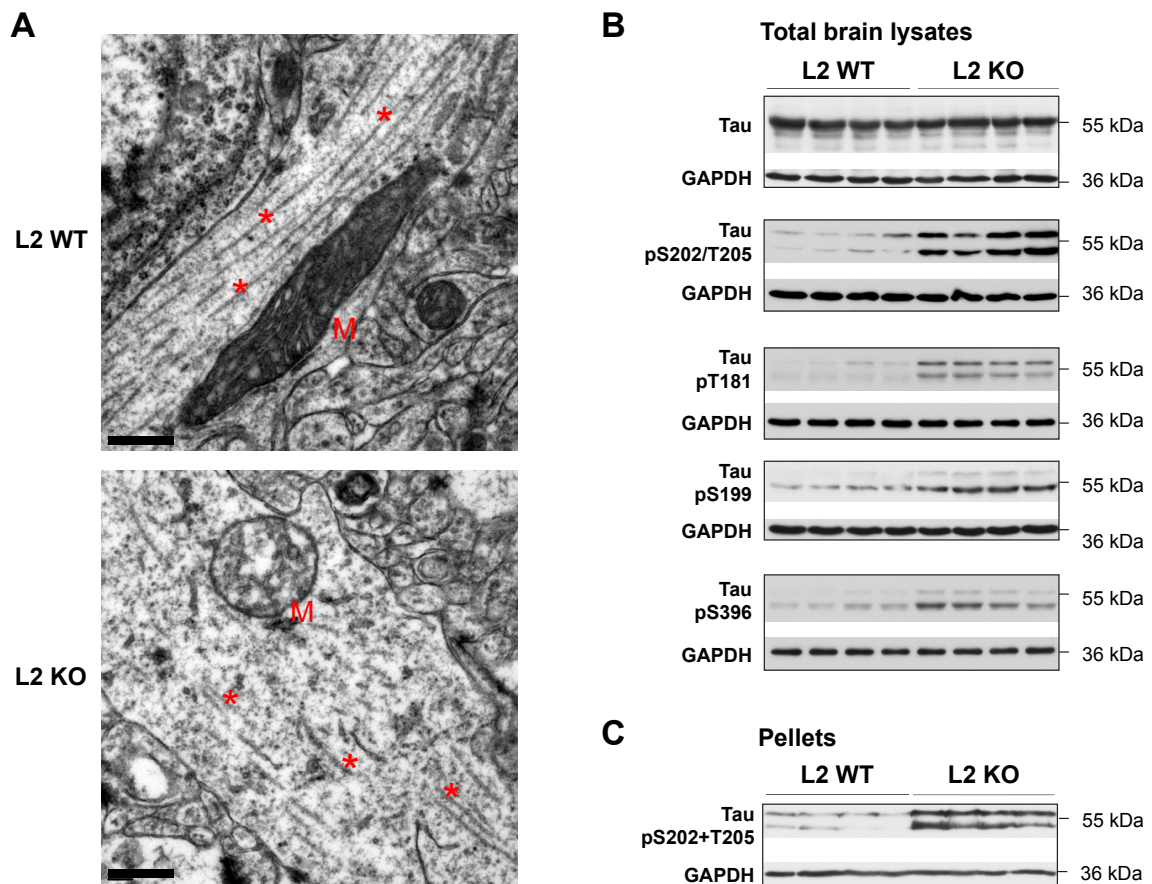


Figure 4.3 Microtubule fragmentation and tau hyperphosphorylation in the L2 KO mice.

(A) Electron micrographs of cortical neuronal processes show microtubule disruption in the L2 KO mice. M: mitochondrion; asterisks: microtubules. Scale bar, 0.5 μ m. n = 3 per genotype. (B) Immunoblot analysis of tau and phospho-tau levels in the total brain lysates. While total tau levels were not changed, the levels of phosphorylated tau at various sites were increased. (C) Immunoblot analysis of insoluble phospho-tau at sites S202 and T205 in the brain.

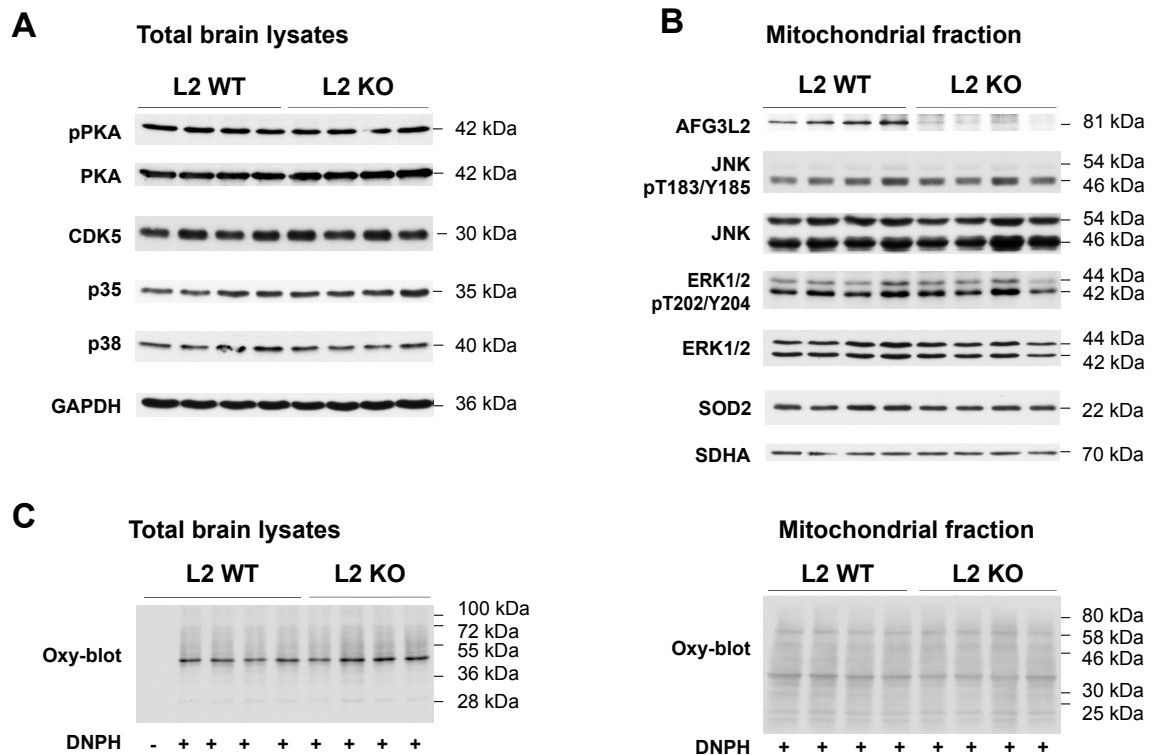


Figure 4.4 L2 KO mice show normal kinase activity and no overt signs of oxidative damage

(A, B) Total lysates (A) and mitochondrial fraction (B) from the brain of P12 pups were subjected to western blot and indicated antibodies were probed. No overt kinase upregulation was observed in this mouse model. (C) Oxy-blot showed similar levels of protein carbonyl groups in brain total lysates and mitochondrial fraction of pups at P12.

4.2 *Afg3l2* forebrain-neuron specific knockout mice show early-onset neurodegeneration

Since L2 KO mice show developmental phenotype and tau phosphorylation is increased during neonatal development, tau hyperphosphorylation observed in the L2 KO mice might be explained by general developmental dysregulation or a possible link between AFG3L2 and tau phosphorylation levels. To circumvent effects of *Afg3l2* deletion during embryogenesis and early development, we generated a forebrain-neuron specific conditional knockout (AFG3L2^{NKO}) mice by crossing *Afg3l2*^{fl^{ox}/fl^{ox}} mice to mice constitutively expressing the Cre recombinase postnatally under control of the *CaMKII α* promoter, which is active specifically in the forebrain starting at P20 (Minichiello et al., 1999).

4.2.1 Signs of neurodegeneration in AFG3L2^{NKO} mice

AFG3L2^{NKO} mice developed a severe progressive phenotype starting at 8 weeks, and generally died at 12 weeks of age (observations by Anne Korwitz). At 8 weeks of age and later on, AFG3L2^{NKO} mice showed lordokyphosis and abnormal behaviour, such as hind-limb clasping phenotype, and weight reduction (Figure 4.5 A, B). As expected, deletion of AFG3L2 was observed in the cortex and in the hippocampus, but not in the cerebellum (Figure 4.5 C) (Kondadi et al., 2014). We therefore analyzed AFG3L2^{NKO} mice and the littermates at 8-10 weeks of age and focused on the cortex and the hippocampus. As early as 8 weeks, Nissl staining revealed massive neuronal loss in both cortex and hippocampus in the AFG3L2^{NKO} mice (Figure 4.5 D) (Kondadi et al., 2014). Thus, loss of AFG3L2 postnatally in neurons causes early onset neurodegeneration and subsequent premature death.

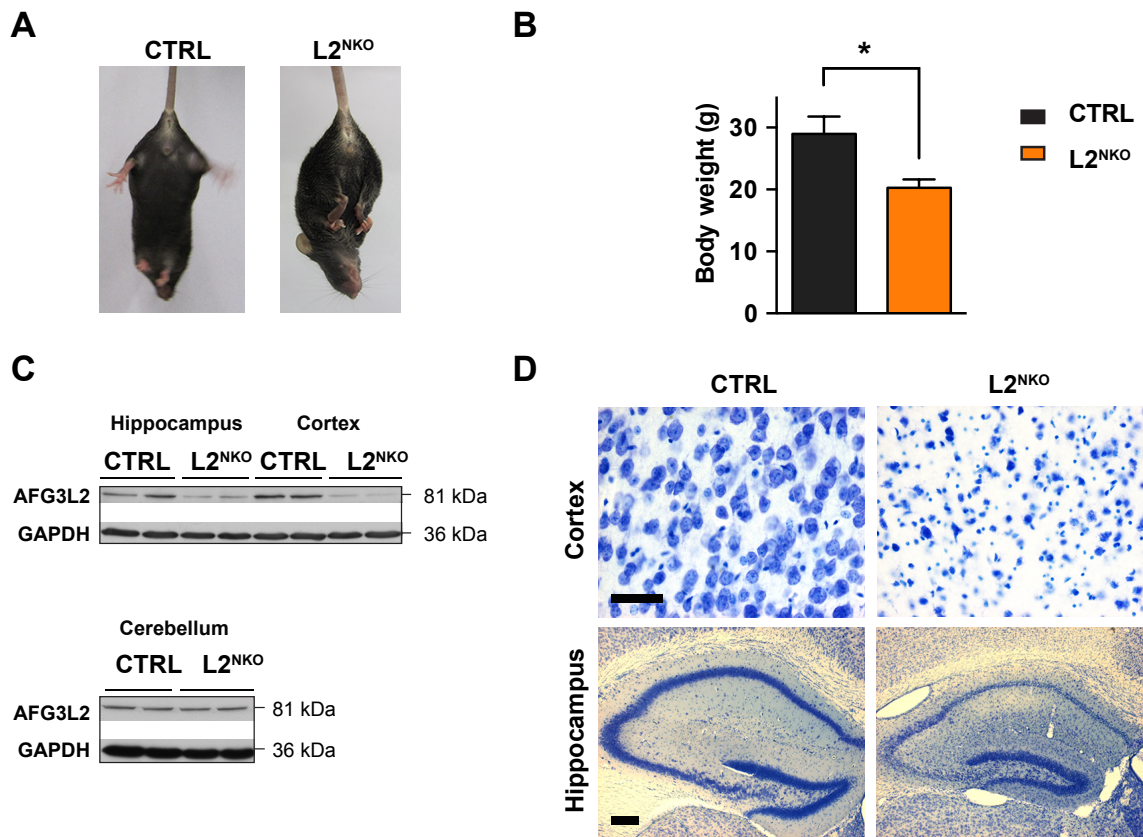


Figure 4.5 Deletion of *Afg3l2* in forebrain-neurons causes neurodegeneration.

(A) All $AFG3L2^{NKO}$ ($L2^{NKO}$) mice showed limb-clasping phenotype, which is a sign of neurodegeneration. (B) The body weight was reduced in 8-10 week-old $L2^{NKO}$ mice. Females and males were pooled. CTRL: n = 10; $L2^{NKO}$ n = 9. (C) Immunoblot showed efficient AFG3L2 depletion in the hippocampus and cerebral cortex, while its expression level in the cerebellum was normal. (D) Brain coronal sections from 8-week old mice were stained with Nissl solution. Pronounced neuronal degeneration was shown in the cerebral cortex and hippocampus. n = 3 mice per group. Scale bar, 50 μ m (cortex), 200 μ m (hippocampus).

4.2.2 Mitochondrial morphology aberration in AFG3L2^{NKO} mice

Ablation of the AFG3L2 in Purkinje cells in the cerebellum leads to mitochondrial fragmentation and altered distribution in the dendritic tree (Almajan et al., 2012), we therefore investigated the mitochondrial morphology upon postnatal deletion of the AFG3L2 in forebrain neurons. In line with the observations in *Afg3l2* conditional Purkinje cell-specific KO (Almajan et al., 2012) and constitutive full-body KO mice (Figure 4.2 A), immunostaining of COX1 showed that mitochondria were fragmented and swollen in cortical neurons of AFG3L2^{NKO} mice (Figure 4.6 A). Ultrastructural studies further revealed that these abnormal mitochondria were dramatically devoid of cristae (Figure 4.6 B). Hence, we conclude that postnatal deletion of *Afg3l2* is sufficient to cause mitochondrial morphological alternations in neurons.

4.2.3 Tau hyperphosphorylation in AFG3L2^{NKO} mice

To exclude that tau hyperphosphorylation in the L2 KO mice is because of developmental defects, we next examined tau levels in the adult AFG3L2^{NKO} mice. As expected, similar to what was observed in the L2 KO mice (Figure 4.3 B), western blot revealed more phosphorylation of tau in the cortex and in the hippocampus of AFG3L2^{NKO} mice (Figure 4.7 A) (Kondadi et al., 2014), indicating that a causal link between AFG3L2 deficiency and tauopathies.

In comparison to L2 KO mice that die before 3 weeks, AFG3L2^{NKO} is an adult mouse model, which is more representative of the progressive phenotype of the human diseases. We then set out to investigate whether kinases are activated in this model and could account for tau hyperphosphorylation. Remarkably, the activated form of kinase ERK1/2 and PKA at corresponding phosphorylation sites were enhanced in the AFG3L2^{NKO} mice (Figure 4.7 B) (Kondadi et al., 2014). In contrast, the activity of other kinases was unchanged, with the exception of increased levels of the inactivate form of GSK3 kinase phosphorylated at Ser9/21, indicating that GSK3 kinase was inhibited in our mouse model. To determine whether oxidative damage evoked the observed kinases activation, I checked the SOD2 levels and protein carbonyl groups. However, in comparison to the controls, AFG3L2^{NKO} showed identical levels of carbonylated proteins and SOD2 (Figure 4.7 C) (Kondadi et al., 2014).

To address whether mitochondrial dysfunction *per se* could cause tau hyperphosphorylation, I analysed brains from Surf1, Sco2 and NDUF54 mouse models with mitochondrial respiration defects. Surf1 locus protein 1 (Surf1) is a putative assembly factor of respiratory complex IV, which mutations have been found in a severe neurological disorder Leigh Syndrome characterized by bilaterally symmetrical necrotic lesions in the brain (Zhu et al., 1998). Surf1 mutation or deletion causes COX activity reduction (Viscomi et al., 2011; Zhu et al., 1998). Deficiency of COX assembly protein isoform 2 (Sco2), a copper chaperone of the COX subunit II (COX2), results in decreased COX activity and leads to fatal infantile cardioencephalomyopathy (Dickinson et al., 2000; Papadopoulou et al., 1999; Yang et al., 2010). Ndufs4 is a complex I subunit, which mutations also has been implicated in Leigh Syndrome (Benit et al., 2003). Ndufs4 deficiency impairs complex I assembly and decreases its activity (Ingraham et al., 2009; Papa, 2002). Interestingly, negligible phosphorylated tau levels were detected in these mutated mice compared to the controls (Figure 4.7 D). Hence, we conclude that tauopathy is specially associated to AFG3L2 deficiency, and is not a feature for all mitochondrial dysfunction.

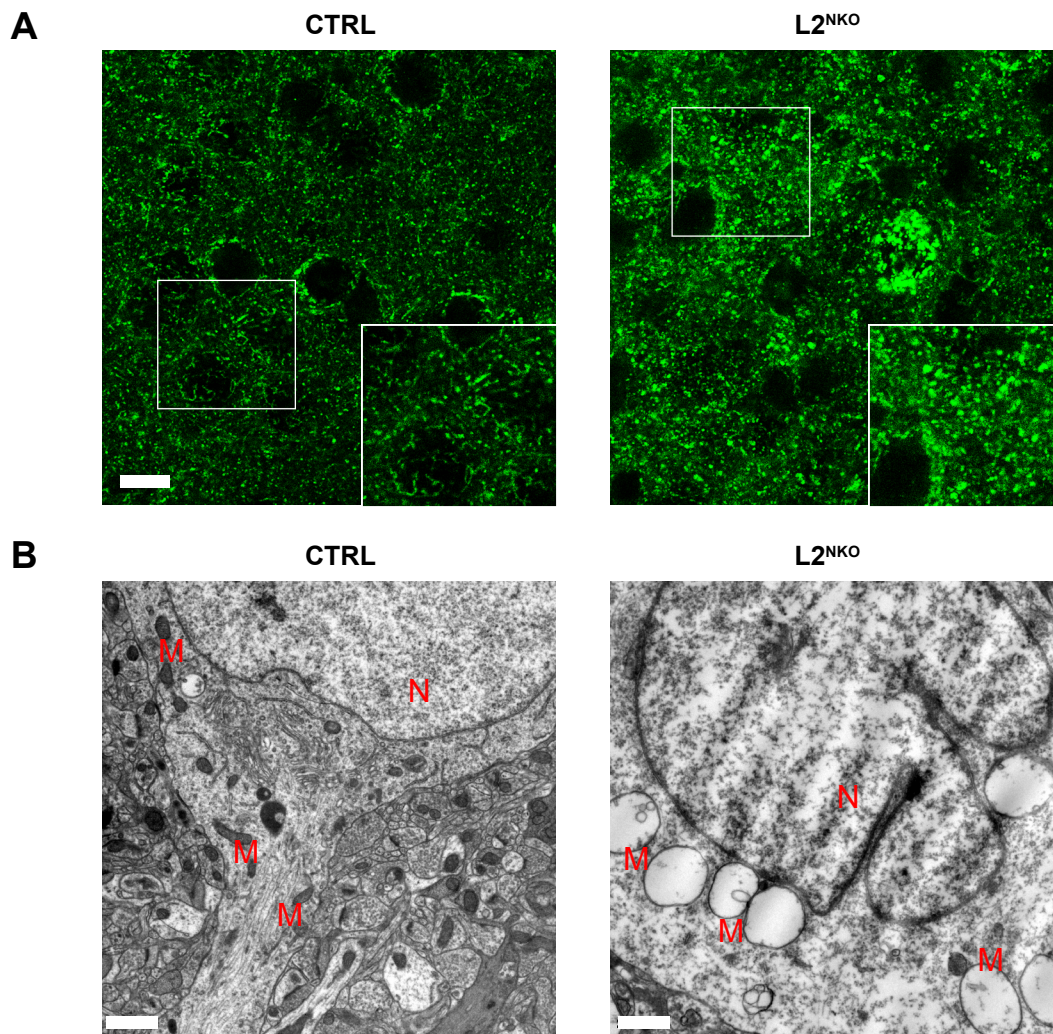


Figure 4.6 Loss of *Afg3l2* in forebrain neurons postnatally leads to mitochondrial disruption.

(A) Immunofluorescence staining of COX1 on brain coronal sections indicates mitochondrial morphological aberration in the cortical neurons of $L2^{NKO}$ mice at 8 weeks of age. $n = 2$ per group. Scale bar, $10 \mu\text{m}$. (B) Electron micrographs of cortical neurons show swollen mitochondria with few cristae in the brain of $L2^{NKO}$ mice at 8 weeks of age. M: mitochondria; N, nucleus. $n = 3$ per group. Scale bar, $1 \mu\text{m}$.

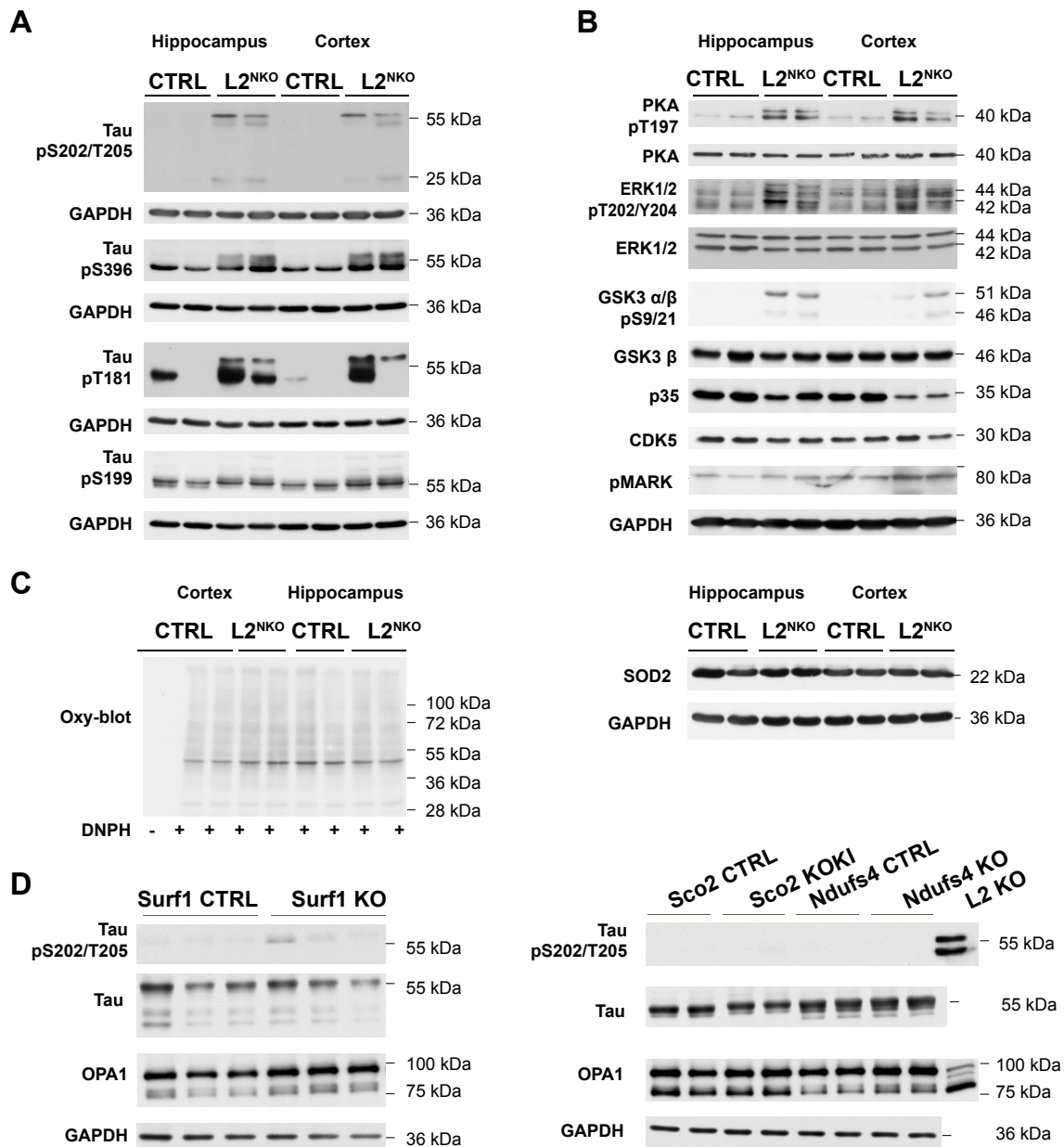


Figure 4.7 Tau hyperphosphorylation and kinases investigation in the adult AFG3L2^{NKO} mice

(A) Tau was hyperphosphorylated at various sites in the hippocampus and cerebral cortex of AFG3L2^{NKO} (L2^{NKO}) mice. (B) The ERK1/2 and PKA kinases were activated in the hippocampus and the cortex of AFG3L2^{NKO} mice. GSK3 kinase was inhibited at the phosphorylation sites S9/21, whereas other kinases appeared unchanged. (C) Oxy-blot and western blot analyses revealed neither any evident oxidative damage in the hippocampus and cerebral cortex, nor an overexpression of SOD2 was detected. (D) Mitochondrial respiration deficient mouse models showed negligible tau phosphorylation and comparable OPA1 isoforms in the brain. Brains of Surf1^{-/-} (Surf1 KO) mice, Sco2 knockout/knockin mice (Sco2 KOKI) harboring a Sco2 knockout allele and a Sco2 knockin allele expressing a mutation of E129K, and Ndufs4^{-/-} (Ndufs4 KO) and control mice were kindly provided by Massimo Zeviani.

4.3 *Afg3l2* oligodendrocytes-specific knockouts display late-onset myelin abnormalities

Previous results have clearly indicated that AFG3L2 is essential for the survival of neurons, yet its role in glial cells is unknown. Oligodendrocytes and Schwann cells are myelinating glial cells in the central nervous system (CNS) and peripheral nervous system (PNS), respectively. To investigate the role of AFG3L2 in myelinating cells, I investigated the expression levels of the *m*-AAA protease subunits in oligodendrocytes and explored the effects of deleting *Afg3l2* specifically in adult oligodendrocytes.

4.3.1 AFG3L2 is abundantly expressed in oligodendrocytes

AFG3L2 is highly expressed in the murine brain (Koppen et al., 2007), but its expression in myelin-forming cells remains undetermined. To address this question, I isolated immature oligodendrocytes from P5 pups using magnetic anti-O4 microbeads. Western blotting showed that the isolation was successful as indicated in the elution fraction, in which the oligodendrocytes marker MBP was highly enriched whereas the neuronal marker β -III tubulin was present in negligible amount (Figure 4.8). Notably, AFG3L2 was abundantly expressed in purified oligodendrocytes in comparison to other *m*-AAA protease subunits AFG3L1 and paraplegin (Figure 4.8).

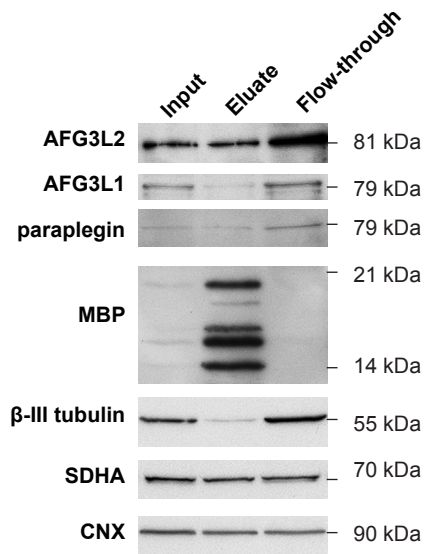


Figure 4.8 The expression levels of *m*-AAA protease subunits in oligodendrocytes.

O4⁺ immature oligodendrocytes were isolated from the brain of P5 pups by using anti-O4 magnetic beads. Immunoblot for the oligodendrocyte marker MBP and the neuronal marker β -III tubulin showed successful isolation in the eluate compared to the input and the flow-through. Succinate dehydrogenase A (SDHA) and calnexin (CNX) were used as loading controls. n = 2 experiments on pups at P5, and similar results were obtained from one experiment on pups at P4.

4.3.2 The *PLP1* promoter is efficiently and specifically expressed in oligodendrocytes in the adult mice

The *PLP1* promoter drives the expression of the major component of myelin in CNS- the proteolipid protein 1 (PLP1), and its splice variant DM-20, which is largely expressed during early development in both neuronal and oligodendrocyte precursors (Ikenaka et al., 1992; Timsit et al., 1995). The *PLP1* promoter is therefore expressed in multi-lineage cells during embryonic and early postnatal stages (Delaunay et al., 2008; Guo et al., 2009; Michalski et al., 2011). To further evaluate the temporal and spatial expression of Cre under the *PLP1* promoter, I crossed tamoxifen inducible PLP1-CreERT transgenic mice (Doerflinger et al., 2003) with mice expressing a mitochondrially targeted YFP (mt-YFP) activated upon Cre recombination (*ROSA26^{+SmY}*) (Sterky et al., 2011). Tamoxifen was administered either to a pregnant female mouse at embryonic day 15.5 (E15.5) for one day or to adult mice at 4 weeks of age for 5 consecutive days. Pups from the female mouse that received tamoxifen at E15.5 were analysed at P15. In the CNS, the mt-YFP signal was mainly localized in cells that were stained with the mature oligodendrocytes marker APC in the brain stem, and also partially in cells showing the morphology of immature oligodendrocytes in the ventral brain (Figure 4.9). Moreover, the mt-YFP was expressed in molecular layers of the cerebellum likely in Bergmann glial cells, but was not observed in the corpus callosum or in the cortex (Figure 4.9). In contrast, in mice that had received tamoxifen at 4 weeks and were analysed at 10 weeks of age (Figure 4.10 A), the mt-YFP⁺ signal was selectively present in mature oligodendrocytes, recognized by their expression of the marker APC⁺ throughout the CNS (Figure 4.10 B). Quantification of the colocalization of the mt-YFP⁺ and the APC⁺ cells showed that Cre excision occurred in approximately 50% of mature oligodendrocytes in different regions (Figure 4.10 C). In addition, the specificity of the *PLP1* promoter was approximately 97% in the CNS, which was obtained by calculating the number of mt-YFP⁺ that also APC⁺ cells dividing the total number of mt-YFP⁺ cells. In the PNS, dispersed mito-YFP signal was present in Schwann cells (Figure 4.10 D). Thus, despite that the Cre expression is not restricted to myelinating cells at the embryonic stage, *PLP1* promoter driven Cre expression is highly specific at a later postnatal stage. Based on this, all mice in the following experiments were injected with tamoxifen at 4 weeks of age for 5 consecutive days.

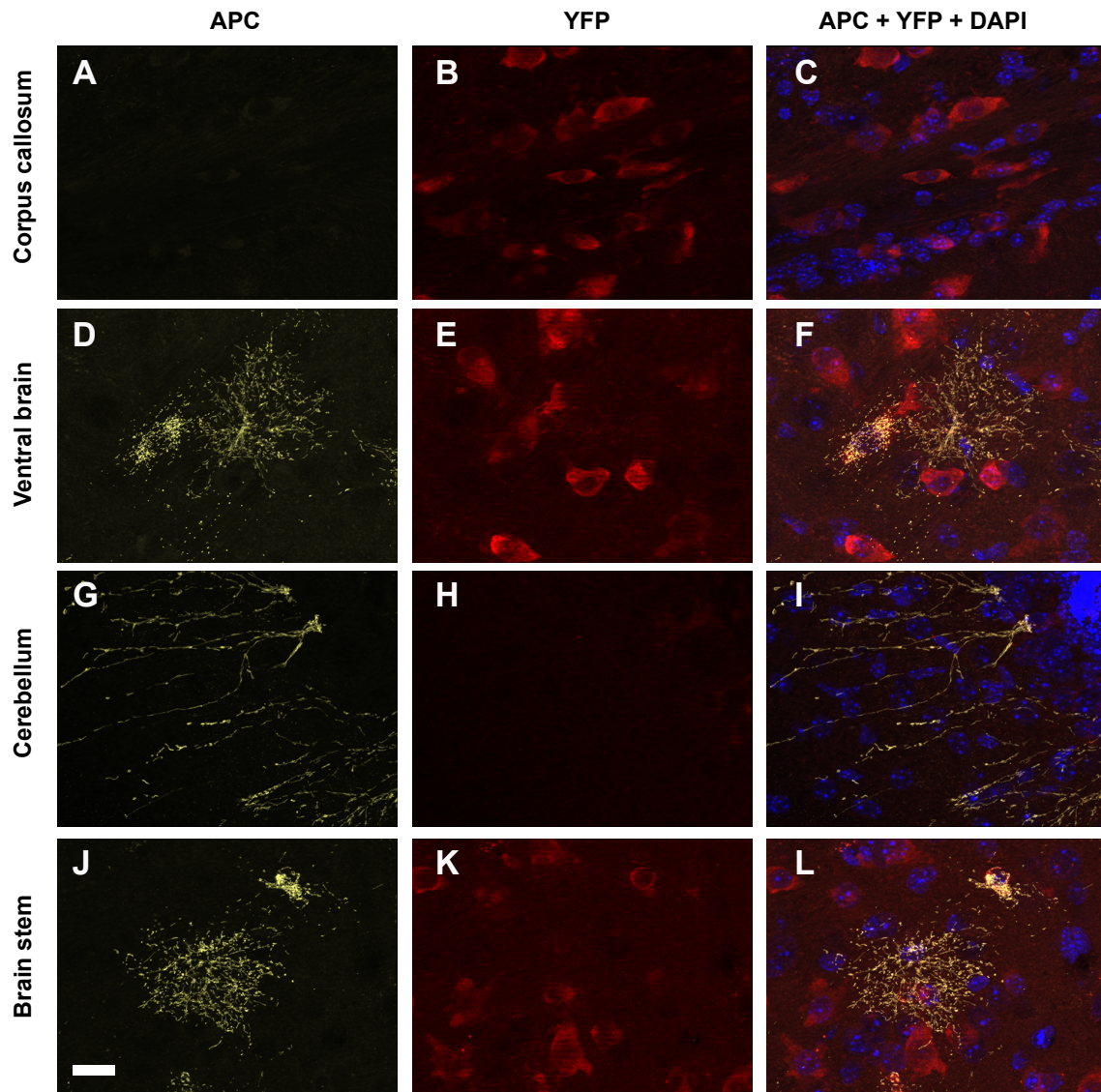


Figure 4.9 *PLP1* promoter-driven Cre recombination is not restricted to oligodendrocytes lineage at early developmental stage.

Tamoxifen was administered to a pregnant female mouse at ~E15.5 for one day, and the pups were analyzed at P15. Representative brain sections were stained with APC, a marker for mature oligodendrocytes (B, E, H, K) and mitochondria in recombined cells were visualized by endogenous YFP signal (A, D, G, J). Nuclei were counterstained with DAPI (C, F, I, L). Scale bar: 20 μ m. n = 3 pups from one litter were analyzed.

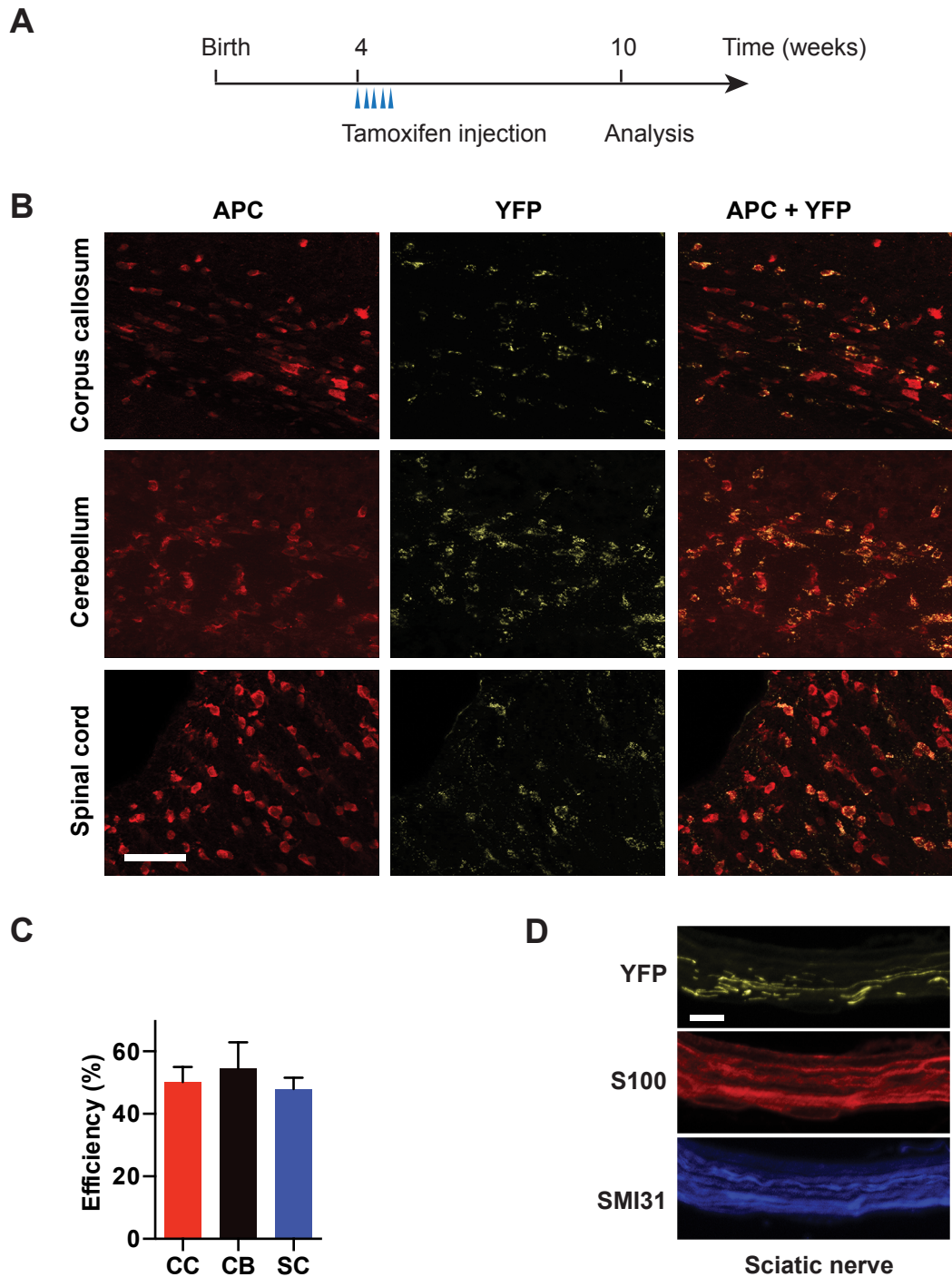


Figure 4.10 PLP1 expression is restricted to myelinating cells in the adult.

(A) Schematic representation of the timeline of tamoxifen injection and analysis. (B) Brain and spinal cord sections from *PLP1-CreERT^{+/tg} ROSA26^{+/SmY}* mice treated as described in (A) were stained with the mature oligodendrocyte marker APC. Mitochondria in targeted cells were visualized by endogenous YFP signal. Scale bar, 50 μ m. (C) Quantitative analysis of recombination efficiency. n = 3 mice. CC: corpus callosum; CB: cerebellum; SC: spinal cord. (D). Dispersed YFP-labeled mitochondrial signal was observed in the sciatic nerve. S100, Schwann cell marker; SMI31, neurofilaments marker. n = 3 mice. Scale bar, 10 μ m.

4.3.3 Deletion of *Afg3l2* induces mitochondrial abnormalities in oligodendrocytes

Since loss of AFG3L2 in adult forebrain neurons (Figure 4.6) and cerebellar Purkinje cells leads to fragmented and swollen mitochondria (Almajan et al., 2012), we investigated the mitochondrial morphology in AFG3L2-deficient oligodendrocytes. To this end, we generated *Afg3l2* myelinating cells-specific knockout mice ($L2^{MC-KO}$) by crossing conditional *Afg3l2* floxed mice (Almajan et al., 2012) to PLP1-CreERT mice (Doerflinger et al., 2003). To visualize the mitochondrial morphology when *Afg3l2* is deleted, mice from this double line were mated with ROSA26^{+/SmY} mice (Sterky et al., 2011). Remarkably, mitochondria in the $L2^{MC-KO}$ mice were fragmented and swollen as early as at 8 weeks, and this alteration persisted at 56 weeks of age (Figure 4.11 A). Indeed, ultrastructural analysis of 56-week-old $L2^{MC-KO}$ mice further confirmed the presence of enlarged mitochondria with reduced cristae (Figure 4.11 B). To examine the functionality of these mitochondria, I performed immunostaining of COX1 that is a mitochondrially encoded subunit of the respiratory chain complex IV. Confocal microscopy validated that these mitochondria appeared fragmented and swollen in the $L2^{MC-KO}$ mice, but COX1 staining was retained in these abnormal mitochondria (Figure 4.11 C). Notably, since the targeting presequence of YFP is from a mitochondrial matrix protein in ROSA26^{+/SmY} (Sterky et al., 2011), the YFP should be homogenous expressed in the mitochondrial matrix under normal conditions. However, in the brain of $L2^{MC-KO}$ mice at the age of 56 weeks, the YFP signal was heterogeneous with clumps in the periphery and little intensity in the centre of mitochondria. Co-staining with COX1, which is supposed to localize to the mitochondrial inner membrane, was also clumped but more towards the centre of the mitochondria (Figure 4.11 C), indicating that mitochondrial cristae was remodelled in oligodendrocytes lacking of AFG3L2. The intensity of COX1 did not reduce, indicating that the mitochondrial translation was not impaired in oligodendrocytes. Together, these data indicate that in the absence of AFG3L2, mitochondrial morphological alteration is an early event and mitochondrial translation might not be affected in oligodendrocytes.

4.3.4 Lack of AFG3L2 does not affect the survival of oligodendrocytes

AFG3L2 deficiency in neurons leads to early neuronal death (Almajan et al., 2012; Kondadi et al., 2014), thus the next question was to address whether the survival of oligodendrocytes is affected upon loss of AFG3L2. Notably, the number of targeted

oligodendrocytes labeled with mt-YFP⁺ in the L2^{MC-KO} mice was comparable to control mice at 56 weeks of age (Figure 4.12 A, B), indicating normal viability of oligodendrocytes lacking AFG3L2. Therefore, it was not surprising that the total number of APC⁺ mature oligodendrocytes was not statistically different (Figure 4.12 A, C). However, quantitative analysis showed that the number of mt-YFP⁺ cells that were not stained by the mature oligodendrocyte marker APC antibody was significantly increased (Figure 4.12 A, D), suggesting that these mt-YFP⁺ cells were not mature oligodendrocytes. Thereby, we conclude that deletion of AFG3L2 in adult oligodendrocytes does not cause oligodendrocyte death but possibly affects their maturation.

4.3.5 Late-onset motor impairment and axonal dysmyelination in the L2^{MC-KO} mice

To explore whether axonal myelination and integrity are affected in the spinal cord of L2^{MC-KO} mice at 56 weeks of age, I analysed the semithin sections of the spinal cord, and did not observe evident axonal demyelination or degeneration (Figure 4.13 A). However, electron microscopy study revealed some pathological axons with adaxonal myelin detachment and vacuolization (Figure 4.13 B). I then analysed the aged 90-week-old L2^{MC-KO} mice. Despite that L2^{MC-KO} mice displayed identical body weight compared to the control littermates (Figure 4.13 C) and no obvious phenotype in the cage for all the time of analyses, these mice showed significant reduction of latency time to fall in the rotarod test, suggesting motor impairment at 90 weeks of age (Figure 4.13 D). I further analysed the semithin sections of the spinal cord in these mice, and found evident axonal dysmyelination and degeneration in the corticospinal tracts (Figure 4.13 E, F). Thus, loss of AFG3L2 in oligodendrocytes in adult mouse causes age-dependent axonopathy in the spinal cord.

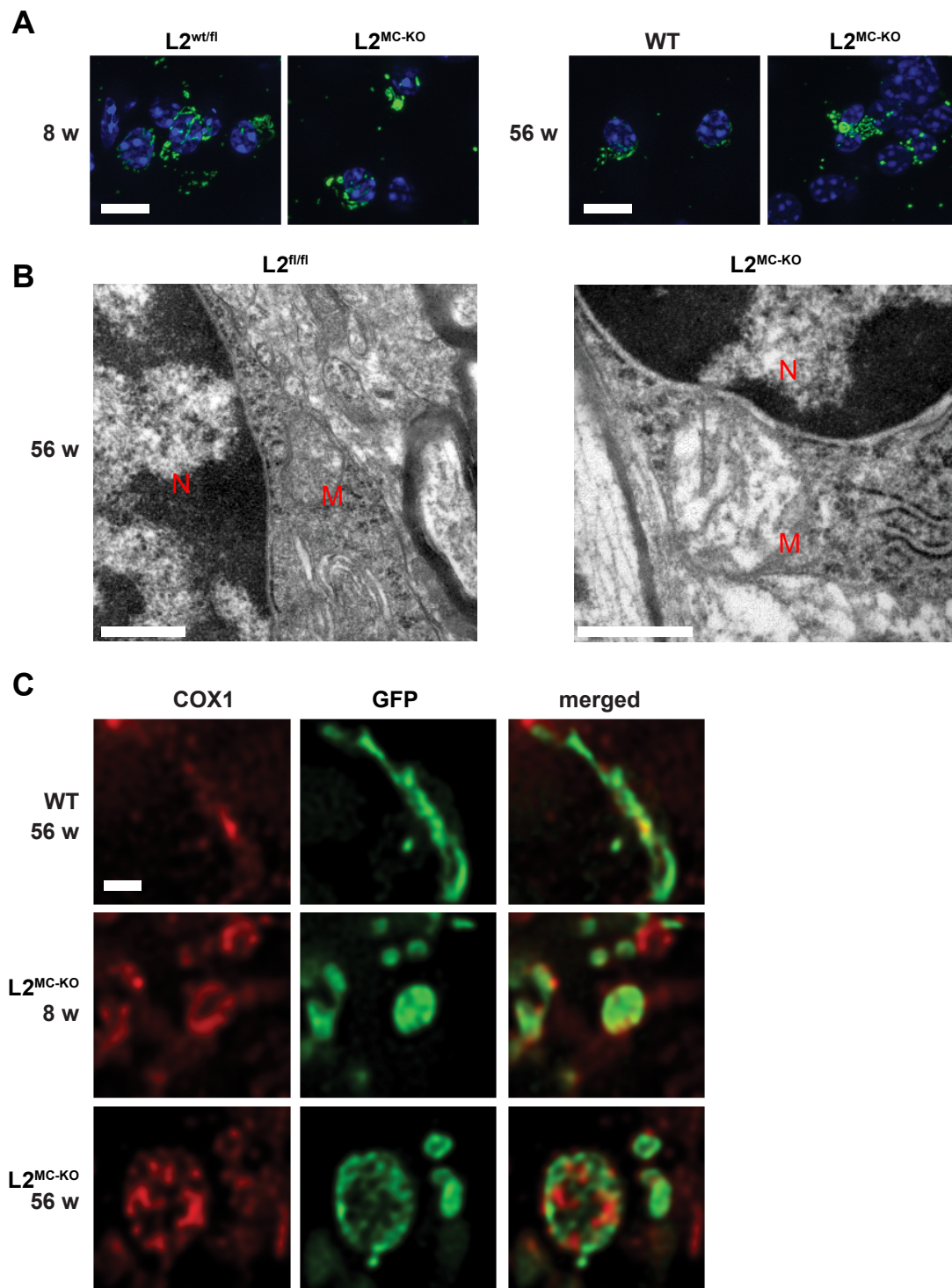


Figure 4.11 Disturbed mitochondrial dynamics in oligodendrocytes of $L2^{MC-KO}$ mice.

(A) YFP^+ mitochondria in targeted oligodendrocytes were visualized by anti-GFP immunostaining. Nuclei were counterstained with DAPI. At 8 weeks of age, $L2^{wt/fl}$ ($PLP1-CreERT^{+/tg}/Afg3l2^{wt/fl}/ROSA26^{+/SmY}$) littermates were compared to $L2^{MC-KO}$ ($PLP1-CreERT^{+/tg}/Afg3l2^{fl/fl}/ROSA26^{+/SmY}$). At 56 weeks of age, wild type mice ($PLP1-CreERT^{+/tg}/Afg3l2^{wt/wt}/ROSA26^{+/SmY}$) were compared to $L2^{MC-KO}$ ($PLP1-CreERT^{+/tg}/Afg3l2^{fl/fl}/ROSA26^{+/SmY}$) mice. Scale bar, 10 μm . (B) Electron micrographs of cortical oligodendrocytes show a swollen mitochondrion lack of cristae in the $L2^{MC-KO}$ mice. N, nucleaus; M, mitochondrion. Scale bar, 0.5 μm . (C) Deconvoluted single-plane confocal images showing that COX1 staining was retained in swollen mt- YFP^+ mitochondria in $L2^{MC-KO}$ mice. Scale bar, 1 μm . $n = 3$ or 4 mice per group for all experiments.

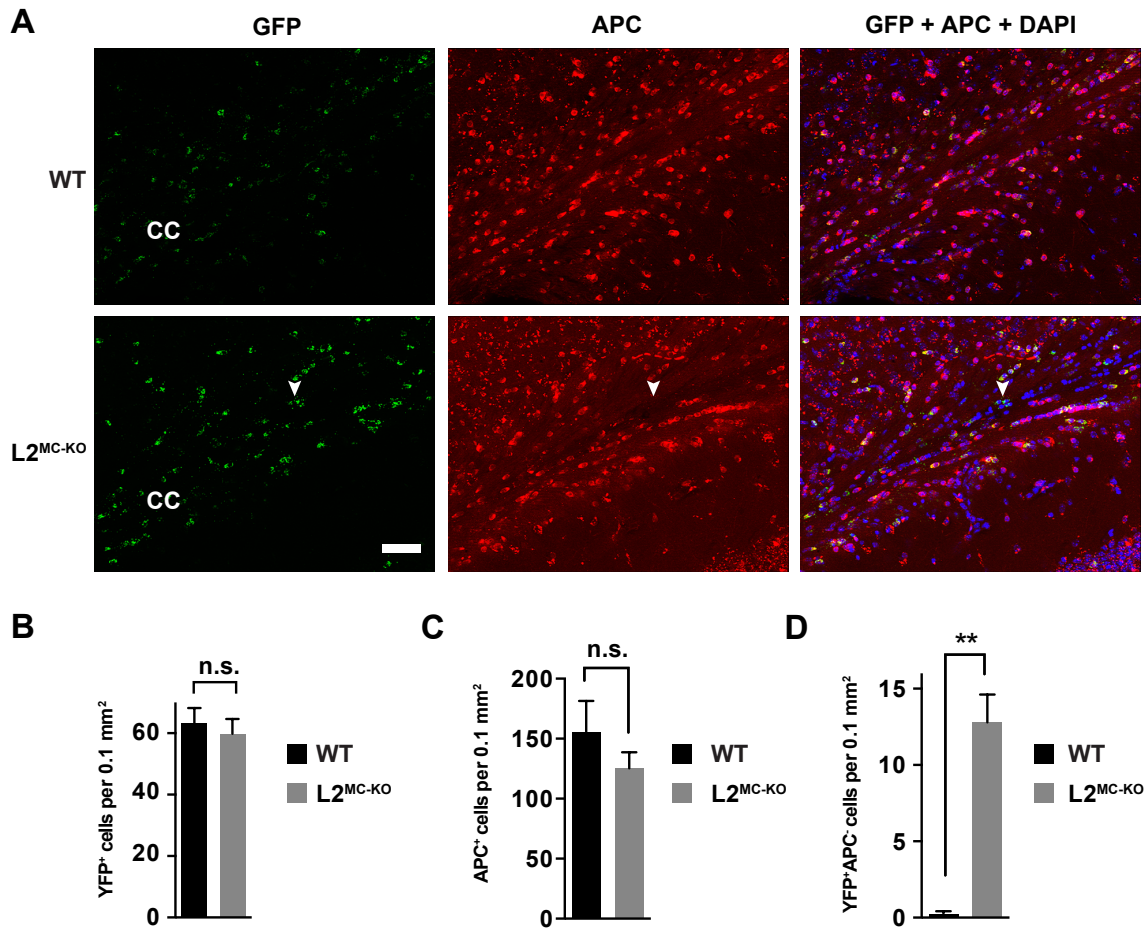


Figure 4.12 AFG3L2 is essential for oligodendrocyte maturation not for their survival.

(A) Immunofluorescence double staining of GFP and APC in coronal brain sections from 56-week-old mice. $n = 3$ or 4 animals per group. GFP staining visualizes targeted mt-YFP⁺ cells, and mature oligodendrocytes were labeled by APC in the corpus callosum. Nuclei were counterstained with DAPI. CC: corpus callosum. Arrowhead indicates mt-YFP⁺ cells that are APC⁻, indicating that these cells are not mature oligodendrocytes. Scale bar, $50 \mu\text{m}$. (B-D) Quantification of mt-YFP⁺ cells (B), APC⁺ cells (C), and mt-YFP⁺ cells that were not stained by APC (D) in the panel A.

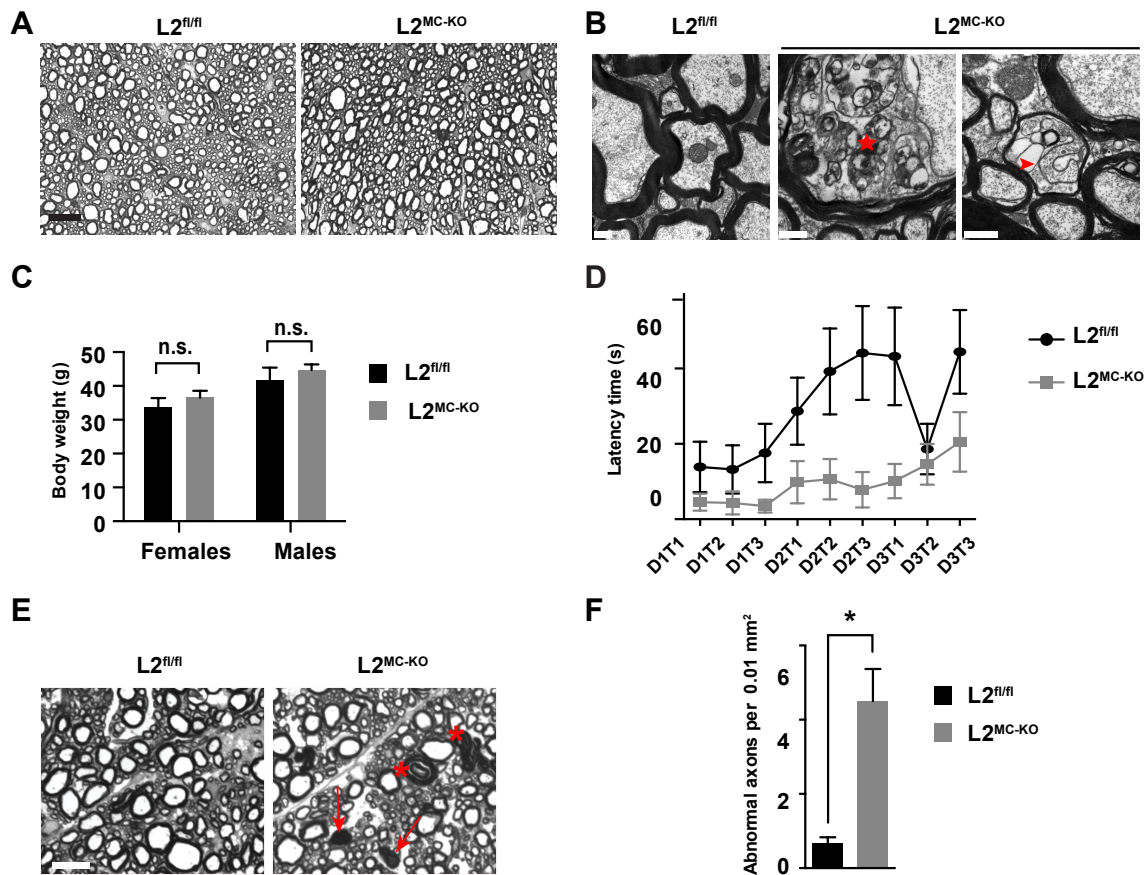


Figure 4.13 Deletion of *Afg3l2* in oligodendrocytes causes late-onset motor impairment and dysmyelination.

(A) Representative semithin micrographs of the white matter in the lumbar spinal cord showed comparable myelination and axonal integrity in 56-week-old $L2^{fl/fl}$ and $L2^{MC-KO}$ mice ($n = 3$ per genotype). Scale bar, 20 μm . (B) Ultrastructural analysis of the lumbar spinal cord white matter in 56-week-old mice showing adaxonal vacuolization (star) and myelin detachment (arrowhead) in $L2^{MC-KO}$ mice. Scale bar, 0.5 μm . (C) Body weight of 90-week-old $L2^{fl/fl}$ and $L2^{MC-KO}$ mice. (Females: $L2^{fl/fl}$ $n = 6$, $L2^{MC-KO}$ $n = 3$; males: $L2^{fl/fl}$ $n = 3$, $L2^{MC-KO}$ $n = 4$). (D) Latency time to fall from a rotarod apparatus of 90-week-old mice ($n = 10$ mice per genotype). 3 trials (T) per 3 consecutive days (D) were performed. Two-way ANOVA test, $p < 0.0001$. (E) Representative semithin micrographs of the spinal cord white matter in 90-week-old mice. Arrows indicate dark degenerating axons and asterisks show thickened myelin. Scale bar, 10 μm . (F) Quantification of abnormal axons (dark degeneration or dysmyelination) in ventral corticospinal tracts of the spinal cord. $n = 3$ per group.

4.4 *Afg3l1* full-body knockout mice show no evident sign of neurodegeneration

The murine genome has a third *m*-AAA protease subunit, AFG3L1, which is similar to AFG3L2, and is capable of forming both homo- and hetero-oligomeric complexes (Koppen et al., 2007). In the mouse, AFG3L1 is expressed at high level in the liver but at low level in the brain (Koppen et al., 2007; Sacco et al., 2010). The function of AFG3L1 in the mouse is not well known, but it has been proposed to play compensatory role when AFG3L2 is absent (Ehse et al., 2009; Maltecca et al., 2008). To test whether AFG3L1 compensates for the loss of AFG3L2 in myelinating cells, I analysed the *Afg3l1* full-body knockout mice, which was generated by our group but has not been published.

4.4.1 Normal growth curve of *Afg3l1* KO mice

Afg3l1 constitutive KO mice were produced by deletion of exons 2 and 3 (Figure 4.14 A), and were born at expected Mendelian ratio (Figure 4.14 B). These mice were fertile, and did not show any overt behavioral abnormalities. Moreover, the body weight of *Afg3l1* KO mice (referred to as L1^{-/-}) was comparable to the wild type (referred to as L1^{+/+}) littermates till 1 year of age (Figure 4.14 C). Thus, we concluded that *Afg3l1* KO mice grow normally compared to the wild type mice.

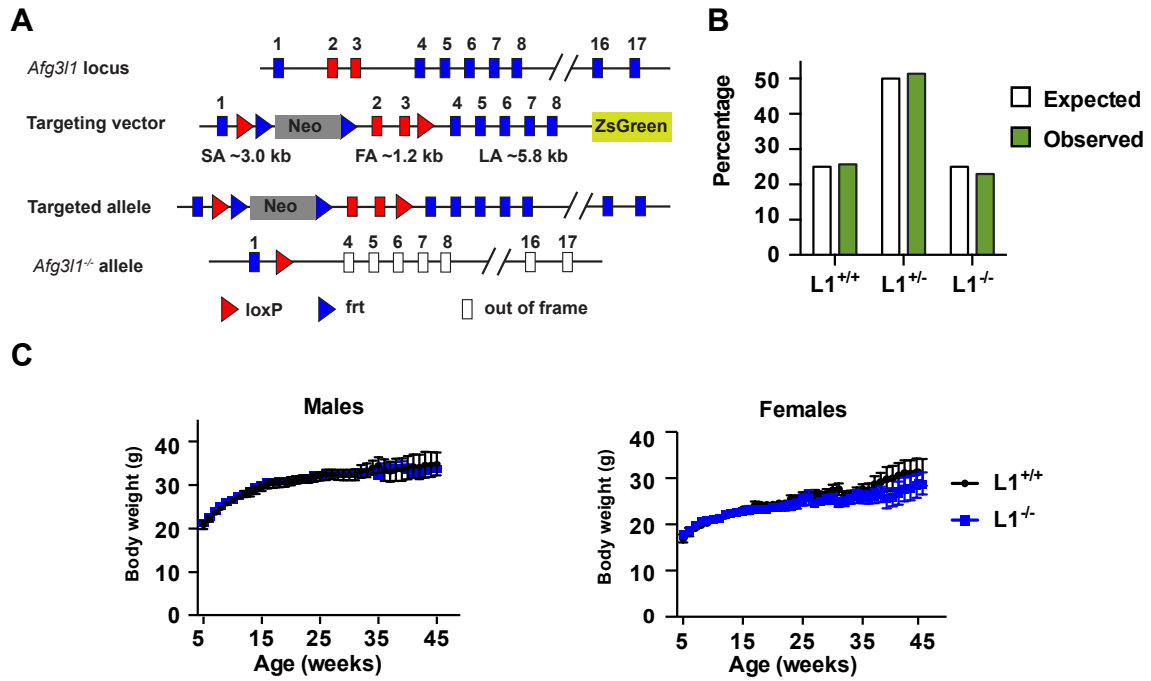


Figure 4.14 Generation of *Afg3l1* full-body knockout (L1^{-/-}) mice.

(A) Schematic illustration of the gene targeting strategy. (B) Observed versus expected genotype distribution of *Afg3l1* animal at ~ 4 weeks of age. *Chi-square* test, $\chi^2 = 0.13$, probability 0.94. Wild type (L1^{+/+}) mice n = 19, *Afg3l1*^{+/-} (L1^{+/-}) mice n = 38, and L1^{-/-} mice n = 17. (C) Growth curves of L1^{+/+} and L1^{-/-} mice. n \geq 4 L1^{+/+} females and males, n \geq 3 L1^{-/-} females and males at each age group.

4.4.2 Preserved axonal myelination and integrity in *Afg3l1* KO mice

I have shown that lack of AFG3L2 is sufficient to induce stress-activated OPA1 processing in the brain (Figure 4.2). This finding prompted us to examine the OPA1 levels in the brain of *Afg3l1* KO mice. Since AFG3L1 is highly expressed in murine liver (Koppen et al., 2007), I also investigated OPA1 cleavage in the liver. Immunoblots showed no evident accumulation of OPA1 short isoforms in tissues of 50-week-old $L1^{KO}$ mice (Figure 4.15 A), indicating that the absence of AFG3L1 is not sufficient to trigger extensive OPA1 processing *in vivo*. Gallyas myelin staining of the brain sections showed similar myelin patterns between *Afg3l1*^{+/-} (referred to as $L1^{+/-}$) and *Afg3l1*^{-/-} (referred to as $L1^{-/-}$) mice at 50 weeks of age (Figure 4.15 B). At the same age, axonal myelination and integrity in the $L1^{-/-}$ mice were comparable to the control $L1^{+/-}$ mice (Figure 4.15 C). In summary, *Afg3l1* KO mice do not show any behavioural or obvious pathological abnormality in the CNS at least until 1 year of age.

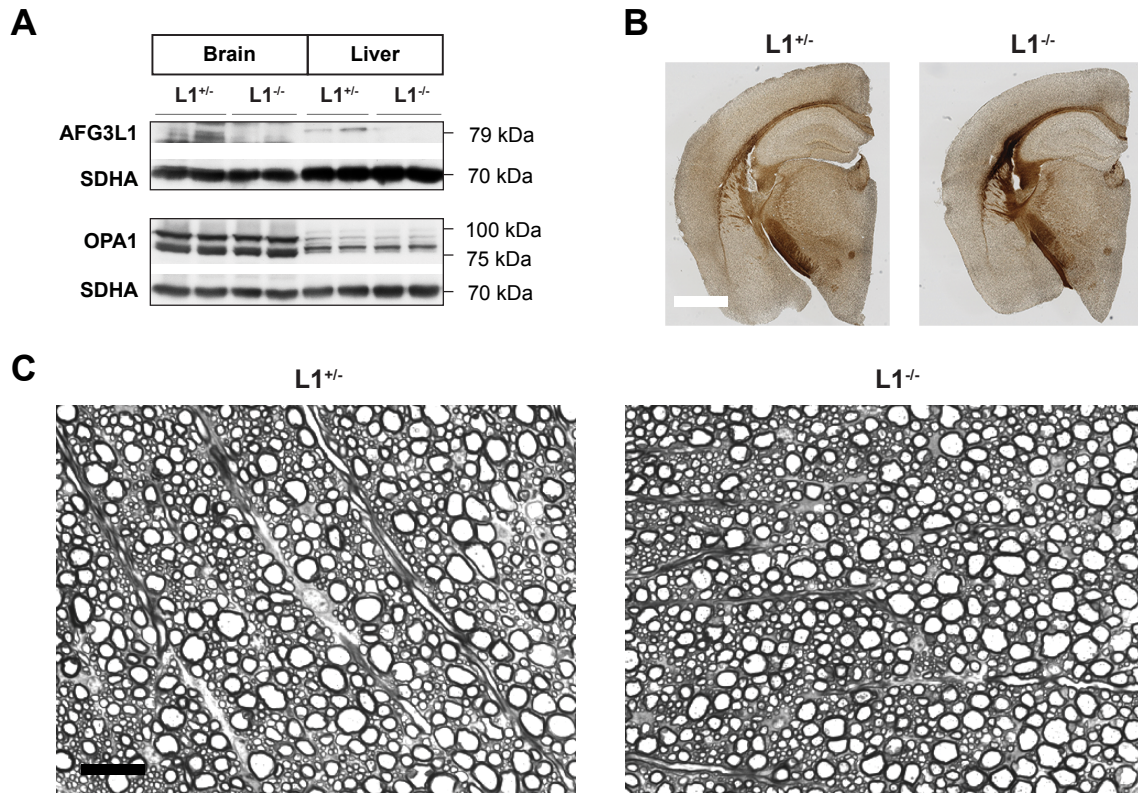


Figure 4.15 Characterization of L1^{-/-} mice.

(A) Crude mitochondria were isolated from brains and livers of 50-week-old L1^{+/-} and L1^{-/-} mice, and immunoblots showed no overt OPA1 cleavage in both tissues of L1^{-/-} mice. (B) Representative images of Gallyas myelin staining of the brain showing comparable myelin pattern between 50-week-old L1^{+/-} and L1^{-/-} mice. Scale bar, 1 mm. (C) Semithin micrographs of the white matter of the lumbar spinal cord revealing similar axonal integrity and myelination in 50-week-old L1^{+/-} and L1^{-/-} mice. n = 3 mice per genotype. Scale bar, 20 μ m.

4.5 Ablation of the *m*-AAA protease in myelinating cells causes axonal demyelination and hair greying

To achieve complete deletion of the *m*-AAA protease in myelinating cells, *PLP1-CreERT^{wt/tg}* mice (Doerflinger et al., 2003) were crossed with *Afg3l2^{lox/lox}* mice (Almajan et al., 2012) in an *Afg3l1* null background. Mice with the genotype *PLP1-CreERT^{wt/tg}/Afg3l2^{lox/lox}/Afg3l1^{-/-}* were referred to as DKO, and the control littermates with the genotype *PLP1-CreERT^{wt/wt}/Afg3l2^{lox/lox}/Afg3l1^{-/-}* were referred to as CTRL. All CTRL and DKO mice were injected with tamoxifen at 4 weeks of age as previously described.

4.5.1 DKO mice showed progressive motor impairment and hair greying

DKO mice gained less weight compared to CTRL mice starting at 8 weeks of age (Figure 4.16 A). Interestingly, the fat content was also significantly lowered in the DKO mice (Figure 4.16 B). To test the motor balance and coordination, we performed rotarod and beam-walking tests. At about 13 weeks of age, DKO mice showed significant motor deficits in both tests, and progressive motor impairment was observed in the beam-walking test (Figure 4.16 C, D). These mice were bred in cages wherein they were required to balance themselves to grasp the grid to access their food. Therefore, since the DKO mice display motor deficits, it is conceivable that they potentially had difficulties to reach the food and hence showed body weight reduction. To exclude this possibility, we decided to put food pellets directly in the cage instead of on the grid after weaning. Remarkably, the body weight reduction of DKO mice persisted (Figure 4.16 E). Furthermore, DKO mice displayed a specific and progressive hair-greying pattern. Hair greying started at ventral forelimbs, later at ventral hindlimbs, then proceeded to dorsal and head (Figure 4.16 F). Thus, loss of the *m*-AAA protease in *PLP* expression cells causes progressive neurological phenotype and hair greying.

4.5.2 Genetic tracing of targeted cells in the skin

The premature hair greying phenotype prompted us to study melanocytes, melanin-producing cells localized in the skin. Previous studies have shown that the *PLP1* is expressed in melanocytes or Schwann cells precursors (SCP) that also give rise to melanocytes, when the Cre is activated during embryonic development (Adameyko et al., 2009; Leone et al., 2003). However, the expression pattern of the *PLP* in adult mice

is unknown. To address this question, we first performed fate-mapping experiments with the PLP1-CreERT/ROSA26^{+SmY} line. Mice with the genotype *PLP1-Cre^{wt/tg}/ROSA26^{+tg}* were injected with tamoxifen for 5 consecutive days starting from P29 and were sacrificed at P36. The ventral skin close to the forelimbs and the dorsal skin close to the thorax were examined. We detected mt-YFP⁺ signal mostly in Schwann cells in the subcutaneous plexus and to a less extent in the deep cutaneous plexus. We also identified moderate mt-YFP⁺ signal in melanocyte stem cells in the bulge, in melanoblasts in the outer root sheath, and in pigmented bulbar melanocytes in the hair follicle (Figure 4.17 A, B). Notably, we observed more mt-YFP⁺ signal in the ventral forelimb skin than in the dorsal part (Figure 4.17 A, B), indicating that the targeting efficiency is higher in the ventral skin, which is reflected in ventral to dorsal hair-greying progression in the DKO mice.

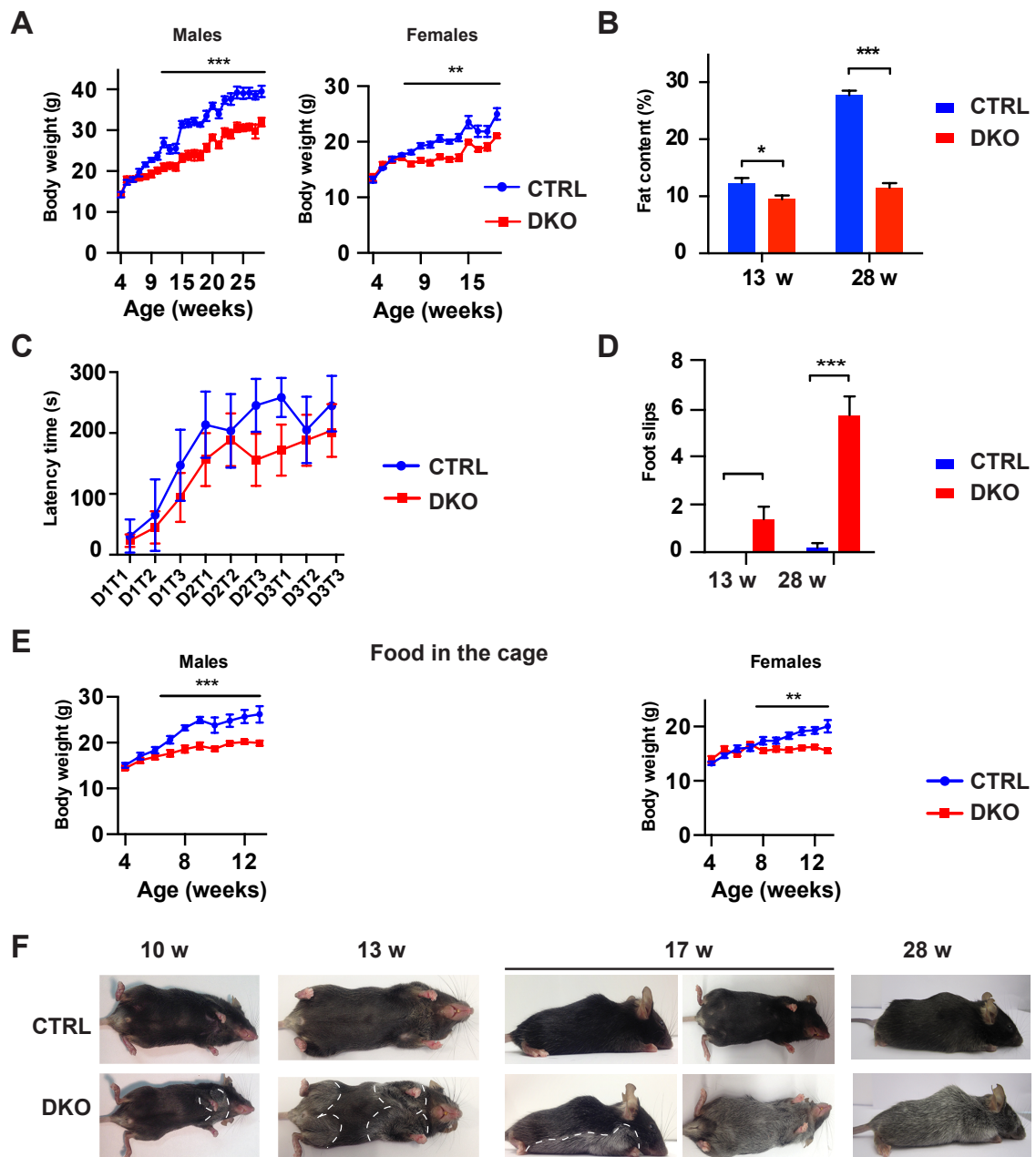


Figure 4.16 DKO mice show a progressive neurological phenotype and hair greying

(A) Weight curves of CTRL and DKO mice (males: $n \geq 5$ per genotype; females: $n \geq 6$ per genotype). (B) The fat content of mice determined by the quantitative magnetic resonance analyser (represent percentage of fat mass to body weight) at 13 weeks ($n = 5$ per genotype) and at 28 weeks of age ($n = 4$ CTRL and 5 DKO). (C) Latency time to fall from a rotarod apparatus of mice at 11-13 weeks old. 5 CTRL and 10 DKO mice were tested for 3 trials (T) in 3 consecutive days (D). Two-way ANOVA test, $p < 0.05$. (D) Quantification of foot slips during the beam walking test of mice at 13 weeks ($n = 5$ per genotype) and at 28 weeks of age ($n = 5$ CTRL and 7 DKO). (E) Weight curves of DKO mice and CTRL mice when food was directly added in the cage (males: $n \geq 6$ per genotype; females: $n \geq 8$ per genotype). (F) All DKO mice ($n > 15$) displayed progressive ventral limbs to dorsal hair greying.

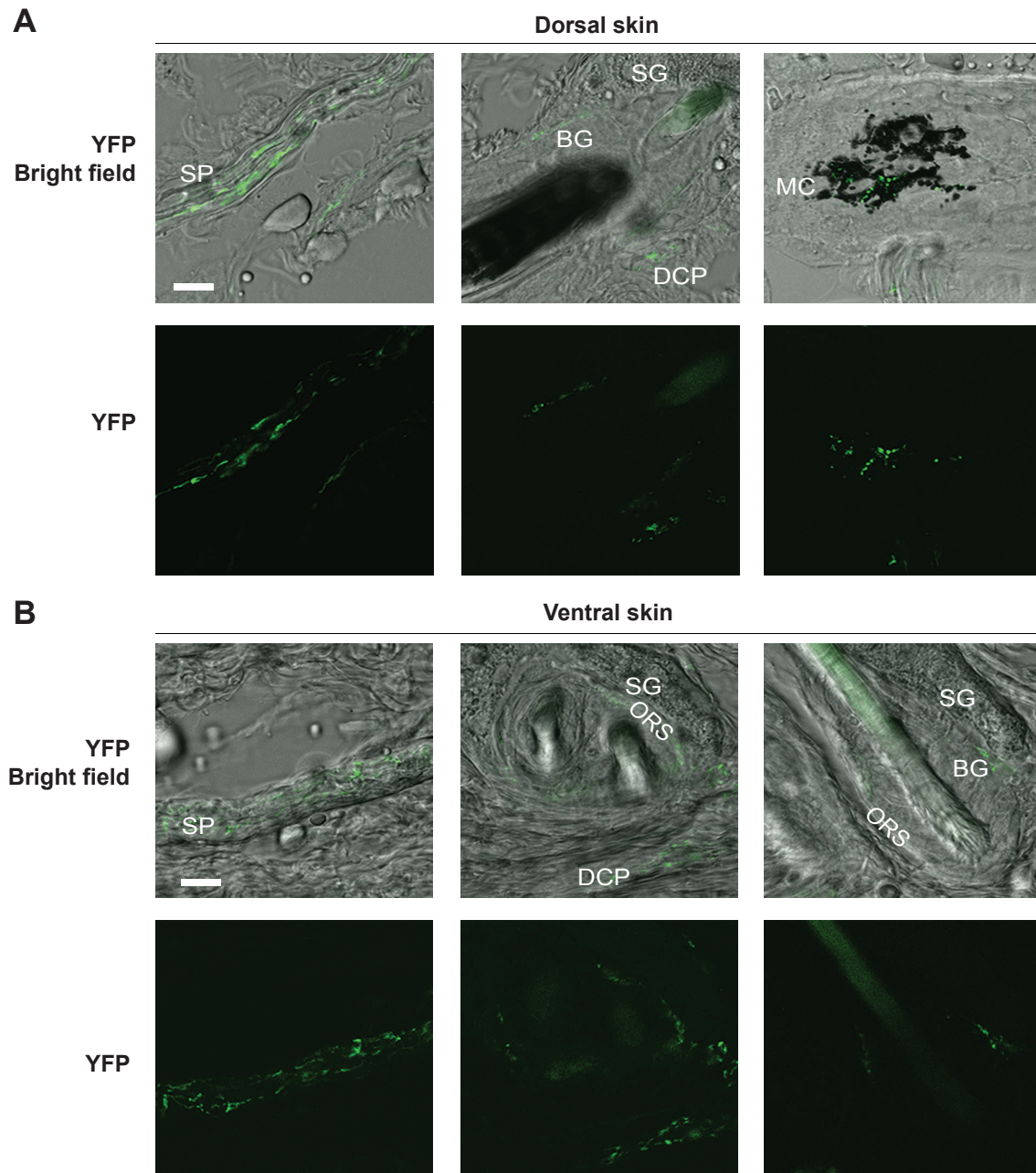


Figure 4.17 Fate mapping in the skin using *PLP1-CreERT^{+/tg} ROSA26^{+SmY}* mice

(A, B) Single-plane confocal images of dorsal (A) and ventral (close to forelimbs) (B) skin sections from *PLP1-CreERT^{+/tg} ROSA26^{+SmY}* mice. Mice were injected with tamoxifen at P29 for five consecutive days and the skin was collected at P36. Endogenous mt-YFP⁺ signal in the cryosections is shown in green. SP: subcutaneous plexus; SG: sebaceous glands; BG: bulge area; DCP: deep cutaneous plexus; MC: melanocytes; ORS: outer root sheath. Scale bar, 10 μ m. n = 3 mice.

Note: Julie Jacquemyn contributed to Figure 4.17 A and B.

4.5.3 Loss of melanocytes and melanoblasts in the skin of DKO mice

To monitor the fate of targeted cells in the DKO mice by using the mt-YFP reporter line, a quadruple line $PLP1-CreERT/Afg3l2^{lox/lox}/Afg3l1^{-}/ROSA26$ was generated. Given the extreme low chance to get the ideal genotype of control and DKO mice from the same litter, DKO mt-YFP^{Tg} mice ($PLP1-CreERT^{wt/tg}/Afg3l2^{lox/lox}/Afg3l1^{-}/ROSA26^{+/SmY}$) were compared to the WT mt-YFP^{Tg} mice ($PLP1-CreERT^{wt/tg}/ROSA26^{+/SmY}$) from the $PLP1-CreERT/ROSA26$ line. In 10-week-old DKO mt-YFP^{Tg} mice, we observed an evident decrease of mt-YFP signal in melanoblasts in the outer root sheath of hair follicle, and in the non-myelinating Schwann cells in the subcutaneous nerve plexus (Figure 4.18 A). At 28 weeks of age, despite a reduction of deposited fat in the dermis, the skin structure and hair cycle were preserved in DKO mice (Figure 4.18 B). Therefore, we surmised that the hair greying in the DKO mice is not caused by hair cycle disturbance, but is possibly due to melanocytes maintenance failure. As expected, in the anagen phase in the dorsal skin, melanocytes and melanoblasts identified by the marker c-KIT were dramatically reduced in 28-week-old DKO mice (Figure 4.18 C), and consistently, the number of pigmented hair follicles was also significantly diminished ($79.7 \pm 2.9\%$ in the CTRL versus $28 \pm 12.3\%$ in the DKO mice, $n = 3$, $p < 0.05$, Julie Jacquemyn performed the quantification). Thus, our data suggest that the phenotype of hair greying in the DKO mice is caused by loss of melanocytes and melanoblasts.

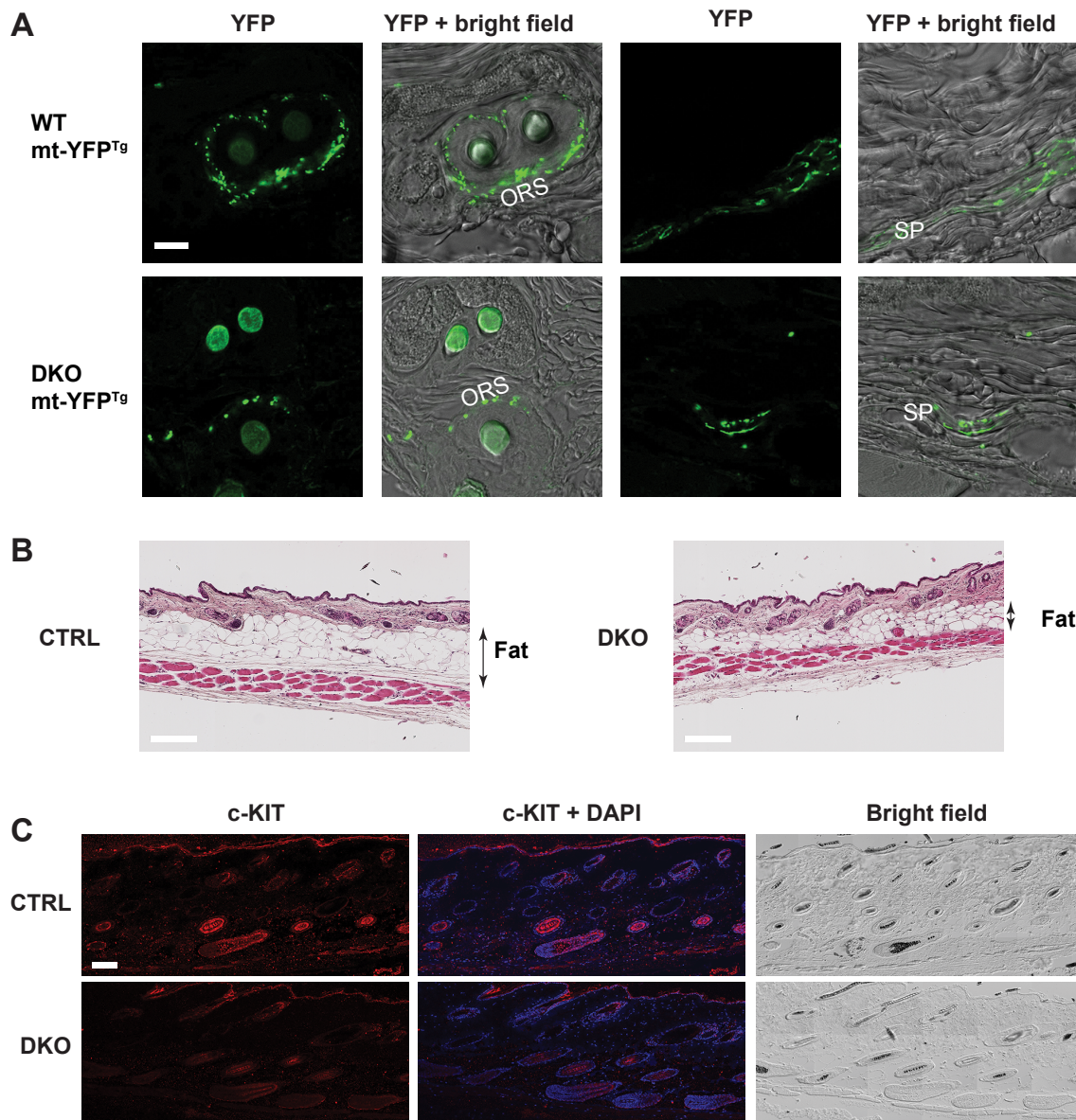


Figure 4.18 Melanoblasts and melanocytes reduction in DKO mice

(A) Confocal micrographs of the dorsal skin of 10-week-old CTRL and DKO mice carrying the mt-YFP transgene show loss of mt-YFP signal in the subcutaneous plexus (SP) and the outer root sheath (ORS). Scale bar, 10 μm . (B) Hematoxylin and eosin staining of dorsal skin of CTRL and DKO mice at 28 weeks. Double-head arrows indicate the fat layer. Scale bar, 200 μm . (C) Confocal fluorescent and bright field images of the dorsal skin of 28-week-old CTRL and DKO mice. Several images were stitched using the tile scan function and show a total area of 0,74 mm^2 . c-KIT positive cells and pigmented HF were largely decreased in DKO mice. Nuclei were counterstained with DAPI. Scale bar, 100 μm . At least 3 mice per group were used for all experiments.

Note: Julie Jacquemyn contributed to Figure 4.18 A and C.

4.5.4 Peripheral neuropathy in the DKO mice

Non-myelinating Schwann cell reduction in the nerve plexus in the skin of DKO mice prompted us to examine whether Schwann cells in the sciatic nerve were also affected. Consistent with the loss of mt-YFP⁺ Schwann cells in the subcutaneous nerve plexus (Figure 4.18 A), mt-YFP⁺ Schwann cells in the sciatic nerve were also prominently reduced in the 10-week-old DKO mice (Figure 4.19 A). In spite of this, from the semithin sections of sciatic nerves, we could not see obvious differences between DKO and CTRL at both 10 weeks and 28 weeks of age (Figure 4.19 B). Given the fact that PLP1 is not highly expressed in Schwann cells in the adult (Doerflinger et al., 2003), presumably we need a more refined technique to assess these limited amount of targeted Schwann cells, To this end, we conducted electron microscopy studies. Ultrastructural analysis showed pathological signs of unmyelinated C fibers (also known as Remark bundles) in the DKO mice (Figure 4.19 C). At 10 weeks of age, while non-myelinated axons were separated by the cytoplasm of Schwann cells in the CTRL, individual axons were intimately touching each other in the DKO mice (Figure 4.19 C). We also observed adaxonal myelin detachment in a few big calibre axons in the DKO mice (Figure 4.19 C). These signs of axonal degeneration were more pronounced at 28 weeks of age, where a few non-myelinated large-calibre axons were found (Figure 4.19 C). Taken together, we conclude that deletion of *m*-AAA protease in adult mice leads to Schwann cell loss and preferentially affects C fibers at early stage.

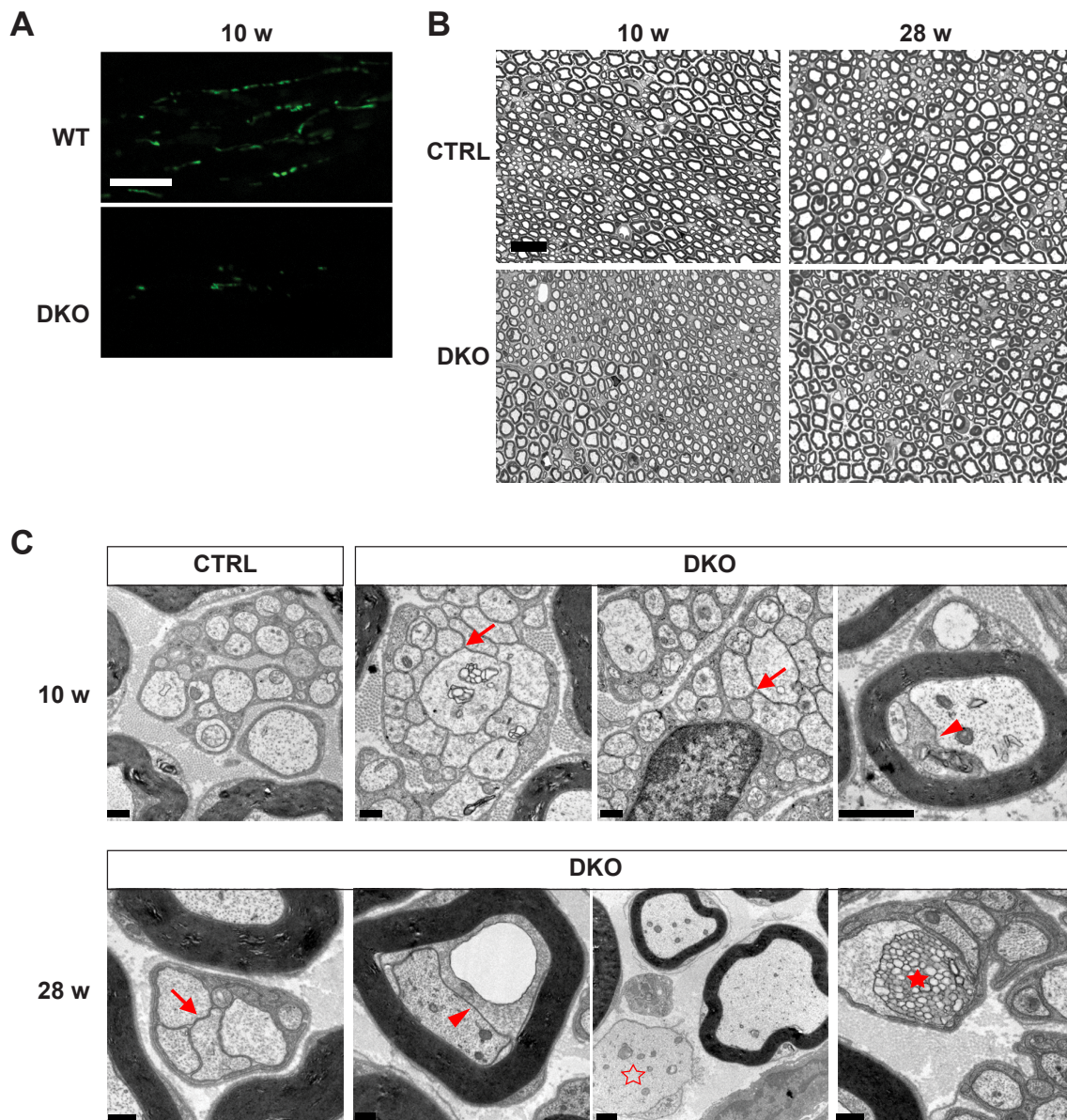


Figure 4.19 Neuropathy in the sciatic nerve of the DKO mice

(A) Representative single-plane confocal images showing endogenous mt-YFP signal in the sciatic nerve of mice at 10 weeks of age (10 w). Reduction of the signal was prominent in DKO mice. Scale bar, 10 μ m (B) Representative semithin micrographs of the sciatic nerves. No overt demyelination was observed in DKO mice. Scale bar, 20 μ m. (C) Electron micrographs of the sciatic nerve at 10 weeks and at 28 weeks (28 w). While in CTRL mice normal Remak bundles were found, in DKO mice some unmyelinated axons were touching each other (arrow), and showed pathological alteration of adaxonal vacuolization (arrowhead). 28-week-old DKO mice also showed non-myelinated large caliber axon (empty star) and multivesicular disintegration of adaxonal myelin lamellae (filled star). Scale bar 1 μ m. n=3 per genotype per age for all experiments.

Note: Julie Jacquemyn contributed Figure 4.19 A.

4.5.5 Axonal demyelination and neuroinflammation in the DKO mice

Despite the fact that large-caliber axons of motor neurons in the peripheral nerves were predominantly intact in the DKO mice, given the fact that the *PLP1* promoter is more efficient in the CNS, we therefore sought to investigate the axonal myelination and integrity in the CNS. Overt signs of axonal demyelination were observed in the white matter of the forebrain and the cerebellum in the 28-week DKO mice (Figure 4.20 A). Similarly, at this age, axonal demyelination was evident in the spinal cord of DKO mice characterized by a decrease of myelinated fibers and an increase of the g ratio (the ratio of the inner axon diameter to the fiber diameter) (Figure 4.20 B-E). Moreover, the number of abnormal dark cells was significantly enhanced in the DKO mice (Figure 4.20 B, C). Ultrastructural analysis further confirmed the progressive axonal demyelination and dysmyelination in the DKO mice, and secondary axonal degeneration was also observed (Figure 4.20 F). The dark cells were identified as oligodendrocytes because they clearly wrapped axons (Figure 4.20 F), and possibly were attempting to remyelinate. Interestingly, we found that the number of mitochondria within axons was increased in the spinal cord of 28-week-old DKO mice (Figure 4.20 G). Consistently, in the crude myelin fraction, the mitochondrial proteins were increased in the DKO mice (Figure 4.20 H). In line with previous studies that demyelinated axons increase mitochondrial content to fulfil their energy demand (Andrews et al., 2006; Mahad et al., 2009). AMP-activated protein kinase (AMPK) is a cellular energy sensor (Hardie et al., 2012). Remarkably, the activated form of AMPK phosphorylated at Thr 172 was upregulated in the spinal cord of 13-week-old DKO mice and in the brain of 28-week-old DKO, while the total AMPK level was not altered (Figure 4.20 I). Hence, our results indicate that the loss of the *m*-AAA protease in oligodendrocytes causes progressive demyelination and influences profoundly energy homeostasis.

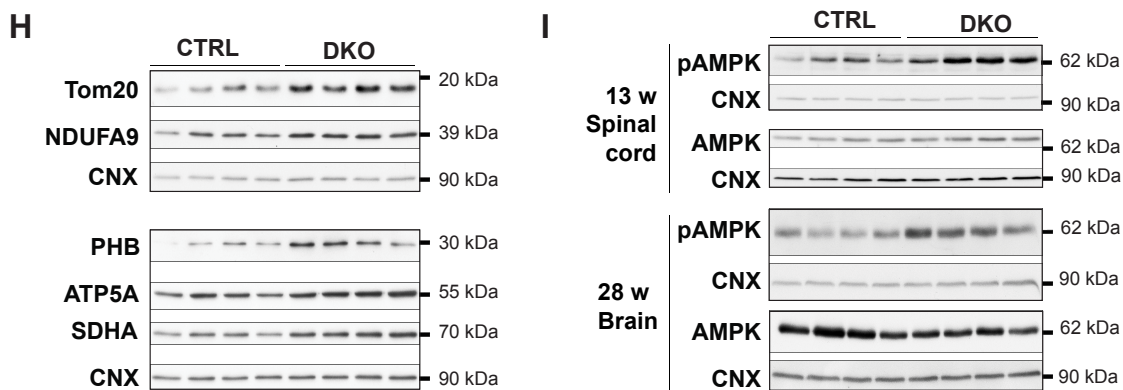
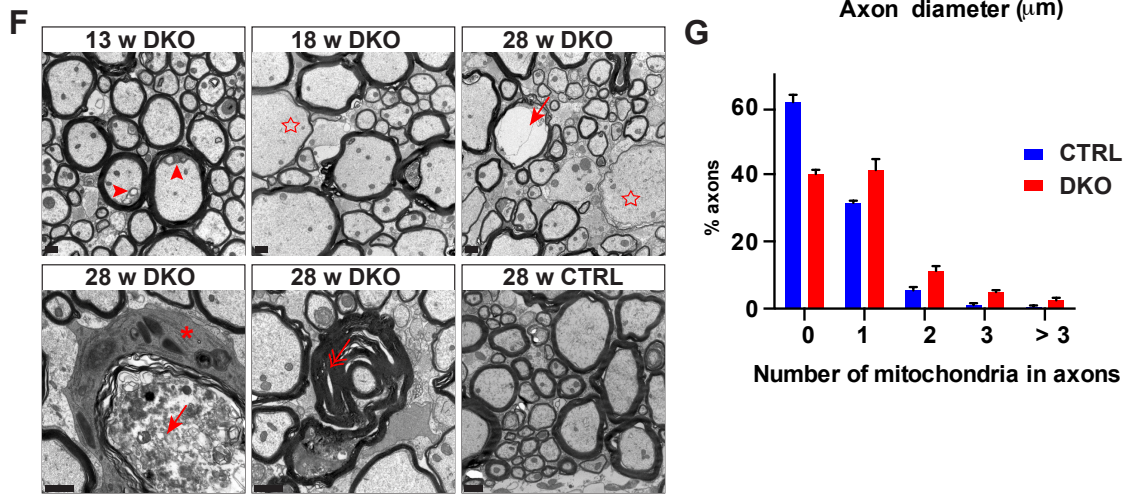
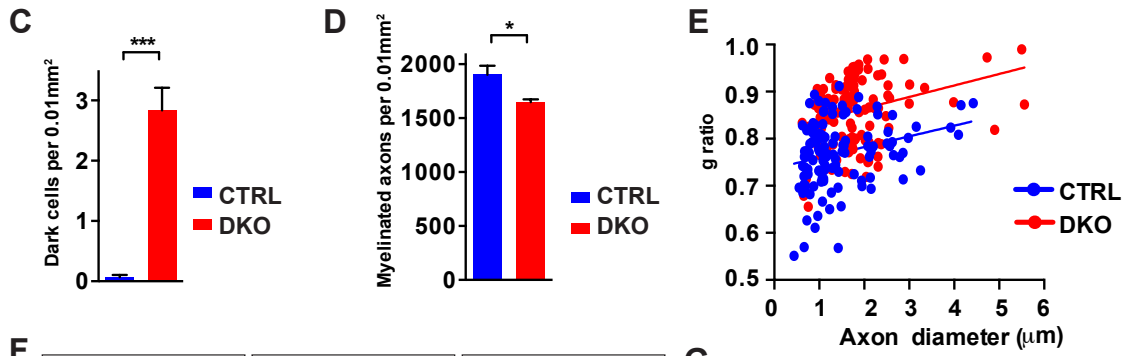
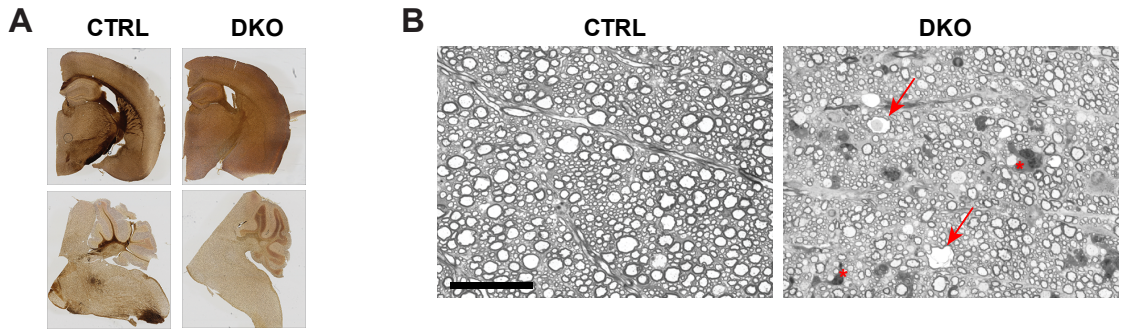


Figure 4.20 Progressive axonal demyelination and energy deficiency in DKO mice

(A) Gallyas myelin staining of the forebrain and cerebellum sections from 28-week-old mice. $n = 3$ mice per genotype. (B) Representative semithin sections of the white matter of the lumbar spinal cord of 28-week-old mice. Degenerating axons (arrow) and dark cells (asterisk) are prominent in DKO mice. Scale bar, $50 \mu\text{m}$. (C, D) Quantification of dark cells (C) and myelinated axons (D) in the white matter of the spinal cord of 28-week-old mice. (E) G ratio of axons in the white matter of the lumbar spinal cord of 28-week-old CTRL and DKO mice. $n = 3$ mice per group and in total 118 axons in the CTRL and 117 axons in the DKO were calculated. (F) Electron micrographs of the white matter of the lumbar spinal cord of CTRL and DKO at the indicated ages. Progressive myelin defects and secondary axonal degeneration (arrows) were evident in the spinal cord of DKO mice. Arrowheads indicate adaxonal detachment of myelin, while an arrow with two heads points to myelin folding. Several axons showed thin myelin layers, a feature of remyelination (empty stars). A dark remyelinating oligodendrocyte surrounding a swollen axon has membrane-like myelin debris is indicated with an asterisk. $n = 3$ mice per genotype were used in all experiments. Scale bar, $1 \mu\text{m}$. (G) Quantification of the number of axonal mitochondria in the spinal cord of CTRL and DKO mice at 28 weeks of age ($n = 3$ mice per group; in total 404 axons in CTRL and 479 axons in the DKO were assessed). (H) Mitochondrial proteins were increased in the crude myelin fractions isolated from the brain CTRL and in DKO at 28 weeks of age were. (I) Western blots revealed phospho-AMPK α (Thr172) upregulation in the spinal cord and in the brain of DKO mice at 13 weeks and 28 weeks of age, respectively.

We further addressed whether axonal demyelination is associated with neuroinflammation. In the DKO mice at 28 weeks of age, western blot analysis confirmed myelin protein MBP and CNP reduction, and astrocytes marker GFAP upregulation (Figure 4.21 A). At 10 weeks of age, DKO mice showed only mild demyelination in the spinal cord; however, the GFAP levels were increased in the brain and in the spinal cord (Figure 4.21 B). These results were further confirmed by immunostaining of MBP and GFAP antibodies in the brain. Astrocytes were amplified in number and were intensively stained by the GFAP antibody in the corpus callosum of DKO mice at both 10 weeks and 28 weeks of age, whereas the staining of MBP was comparable at 10 weeks and reduced at 28 weeks of age (Figure 4.21 C). Notably, immunostaining with microglia marker IBA1 also revealed obvious microglial activation represented by morphological enlargement and quantitative increase in the DKO mice at 28 weeks of age (Figure 4.21 C). Taken together, these data suggest that inflammation is evoked in the DKO mice, and astrogliosis is an early event that precedes microgliosis and myelination defect.

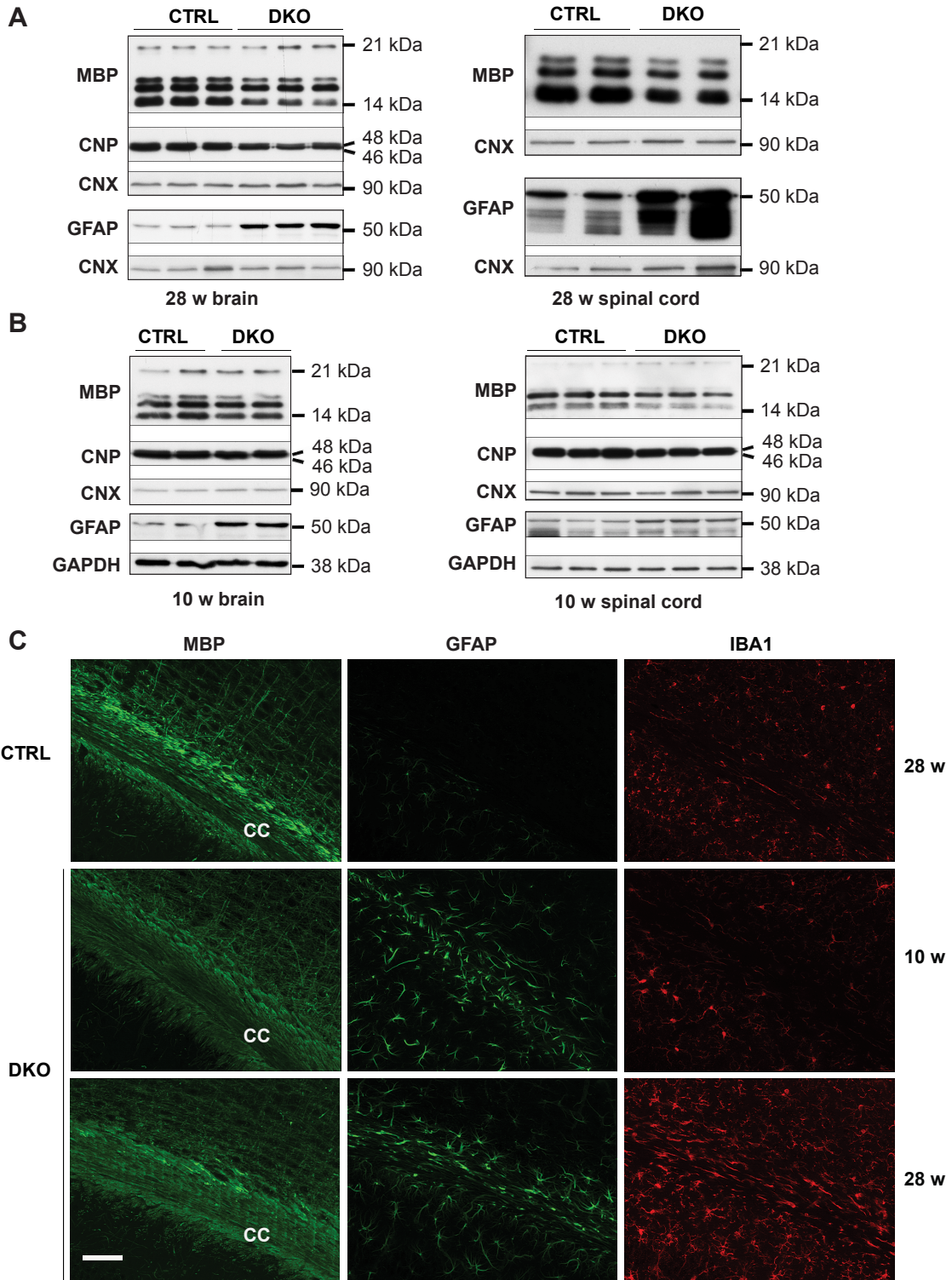


Figure 4.21 Early neuroinflammation followed by axonal demyelination in the DKO mice.

(A) Western blots showed a reduction of myelin proteins MBP and CNP in both brain and spinal cord of 28-week DKO mice. The number of astrocytes stained by GFAP antibody was obviously increased in both tissues at this age. (B) At 10 weeks of age, while myelin proteins in the brain of DKO mice were not evidently reduced, the levels of GFAP already were upregulated suggesting that astrogliosis was an early event prior to overt demyelination. In the spinal cord, the myelin proteins MBP and CNP were slightly decreased at 10 weeks of age. (C) Immunostaining of MBP, GFAP, and IBA1 in the corpus callosum (CC) of coronal brain sections of CTRL and DKO mice at the indicated ages. Demyelination in the DKO mice was associated with astrogliosis and microglial activation. n = 3 mice per group at each time point. Scale bar, 100 μ m.

4.5.6 Rapid loss of targeted cells in the DKO mice

The early-onset astrocytes activation followed by demyelination prompted us to investigate the fate of oligodendrocytes temporally in the central nervous system. Using the quadruple PLP1-CreERT/*Afg3l2*^{fllox/fllox}/*Afg3l1*^{-/-}/ROSA26^{+SmY} line, we observed rapid and progressive mt-YFP⁺ oligodendrocytes loss in the corpus callosum of DKO mice older than 6 weeks of age. Only a few mt-YFP⁺ oligodendrocytes existed at 28 weeks of age (Figure 4.22 A-B). Cell loss was in line with what was previously observed in the skin and in the peripheral nerves. Moreover, the number of mature oligodendrocytes stained by APC was significantly declined in the brain and in the spinal cord of DKO mice at 10 weeks of age (Figure 4.22 C-E). Interestingly, APC⁺ oligodendrocytes were replenished at 28 weeks of age (Figure 4.22 A, C), indicating compensatory proliferation and differentiation of untargeted oligodendrocyte precursors. Indeed, APC⁺ cells appeared enlarged (Figure 4.23 A-B) and more intensively stained by Olig2 (Figure 4.23 A), a key transcription factor necessary for oligodendrocyte development and expressed at high levels in oligodendrocyte precursors and at low levels in mature oligodendrocytes (Kuhlmann et al., 2008; Mei et al., 2013). Despite this, when I quantified Olig2⁺ cells in the corpus callosum, I did not observe statistical difference between CTRL and DKO mice at 6 weeks, 10 weeks and 28 weeks of age (Figure 4.23 C-D). Together, these results illustrate that ablation of the *m*-AAA protease in oligodendrocytes in adult mice causes cell death within a few weeks followed by compensatory oligodendrocyte precursor replenishment.

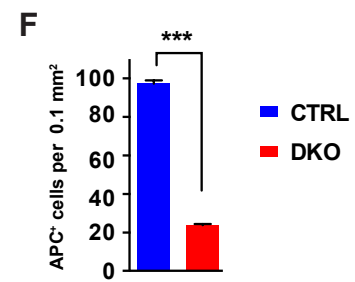
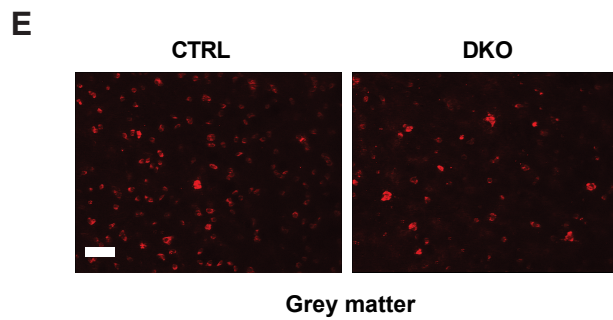
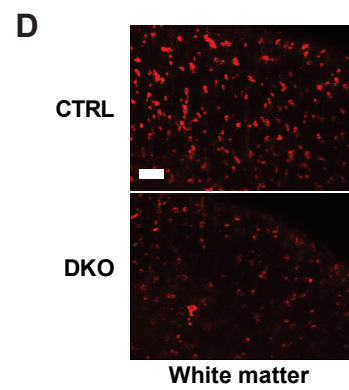
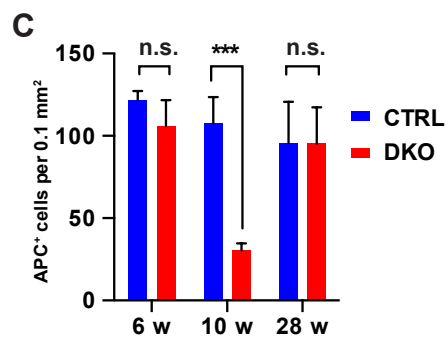
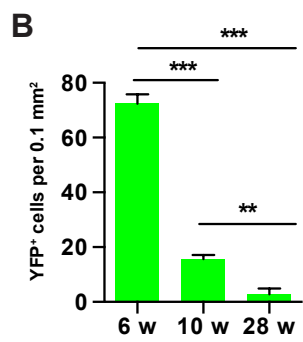
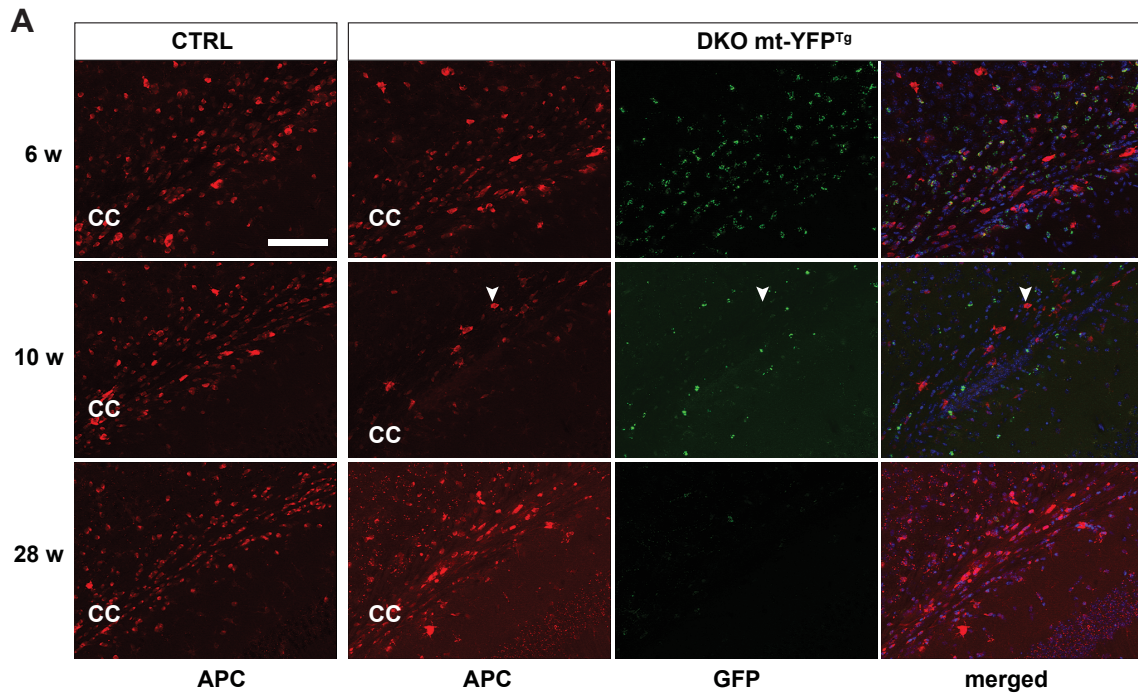


Figure 4.22 Death of targeted oligodendrocytes and compensatory proliferation of untargeted oligodendrocytes in DKO mice

(A) Immunofluorescence double staining of GFP and APC in coronal brain sections from mice at indicated ages. GFP staining allowed us to visualize targeted mt-YFP⁺ cells, and mature oligodendrocytes were labeled by APC in the corpus callosum. Nuclei were counterstained with DAPI. CC: corpus callosum. Arrowhead shows an enlarged APC⁺ mature oligodendrocyte without the mt-YFP signal. (B) Quantification of mt-YFP⁺ cells in the corpus callosum revealed rapid progressive loss of targeted oligodendrocytes in the DKO. (C) Quantification of APC⁺ cells in the corpus callosum. (D-E) Immunofluorescence staining of APC⁺ cells in the white matter (D) and in the grey matter (E) of the spinal cord of 10-week-old CTRL and DKO mice. (F) Quantification of APC⁺ cells in the grey matter of the spinal cord. For all experiments, n = 3 or 4 mice per group at each time point.

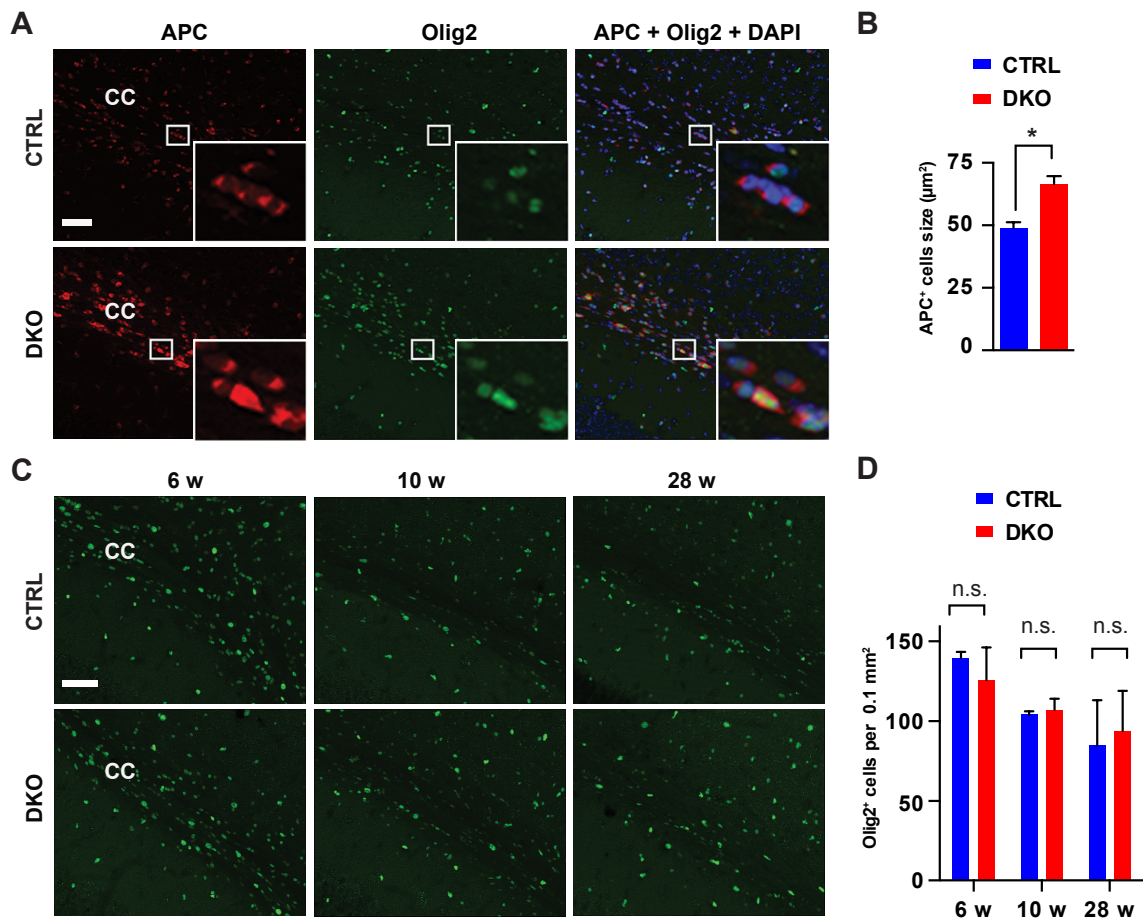


Figure 4.23 Oligodendrocyte regeneration in the brain of DKO mice.

(A) Double immunofluorescence staining of APC and Olig2 in the corpus callosum of CTRL and DKO mice at 28 weeks of age. Enlarged APC⁺ oligodendrocytes were more intensively stained by Olig2 in the DKO mice, suggesting these oligodendrocytes were developing. Scale bar, 50 µm. (B) Quantification of the size of APC⁺ oligodendrocytes in the corpus callosum of CTRL and DKO mice at 28 weeks of age. n = 3 mice per group, and in total 244 oligodendrocytes in the CTRL and 205 oligodendrocytes in the DKO were measured. (C, D) Immunofluorescence staining and quantification of Olig2⁺ cells in the corpus callosum (CC) of CTRL and DKO mice at the indicated ages. n = 3 mice per genotype per age.

To explore the mechanism of oligodendrocytes death caused by the loss of the *m*-AAA protease, we firstly examined the morphology and functionality of the mitochondria. Interestingly, mitochondria appeared fragmented and swollen in DKO mice at 6 weeks of age, only 2 weeks after tamoxifen injection. At this age, mitochondria in targeted cells tended to be less intensively stained for COX1 in the DKO mice. Strikingly, at 8 weeks of age, COX1 staining disappeared (Figure 4.24 A), revealing that deletion of *m*-AAA protease causes loss of the COX1 subunit of the respiratory chain complex IV and a potential impairment of mitochondrial respiration. Furthermore, *in situ* TUNEL assay detected significantly more apoptotic cells in the corpus callosum of 7-week-old DKO mice (Figure 4.24 B, C). Consistently, ultrastructural study showed mitochondrial abnormalities, and apoptotic features, such as intact cell membrane and condensed nucleus, in the oligodendrocytes of DKO mice (Figure 4.24 D). It has been shown that cytochrome c release from the mitochondria may lead to apoptosis (Cai et al., 1998), hence, we performed cytochrome c immunostaining in the brain sections from 8-week-old mice. Cytochrome c was localized into mitochondria in the WT mice; however, it was released from the swollen mitochondria in the DKO mice (Figure 4.24 E). In summary, deletion of the *m*-AAA protease in oligodendrocytes impairs mitochondrial respiration, induces cytochrome c release and eventually causes apoptosis.

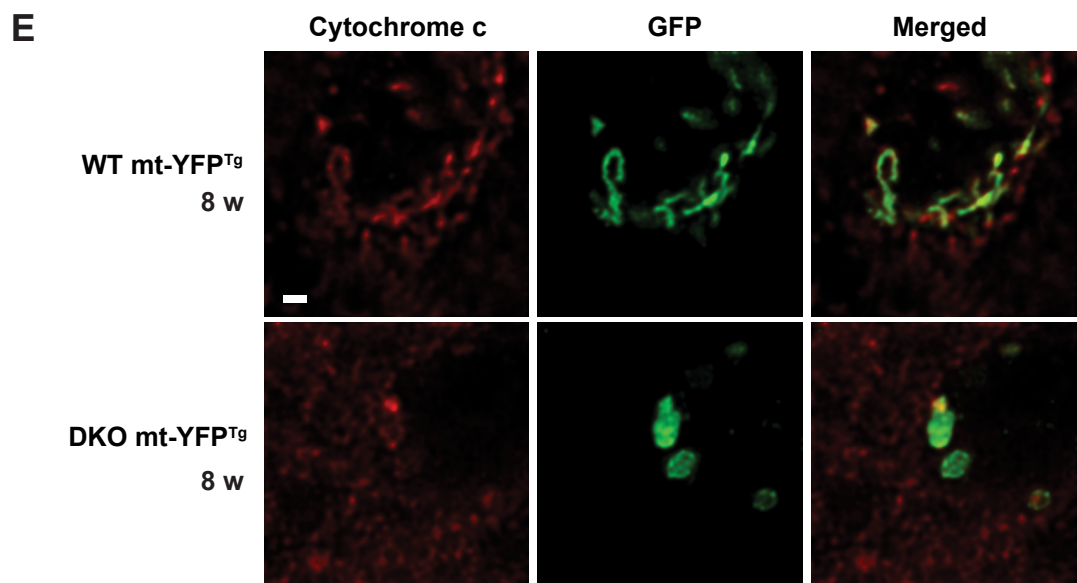
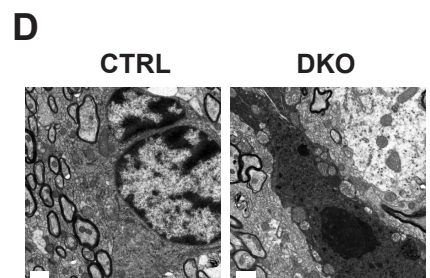
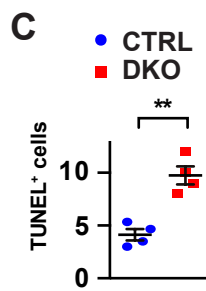
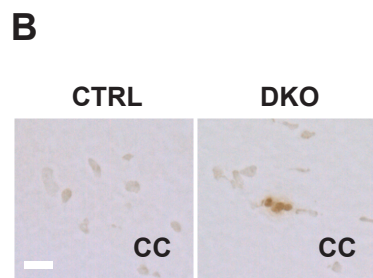
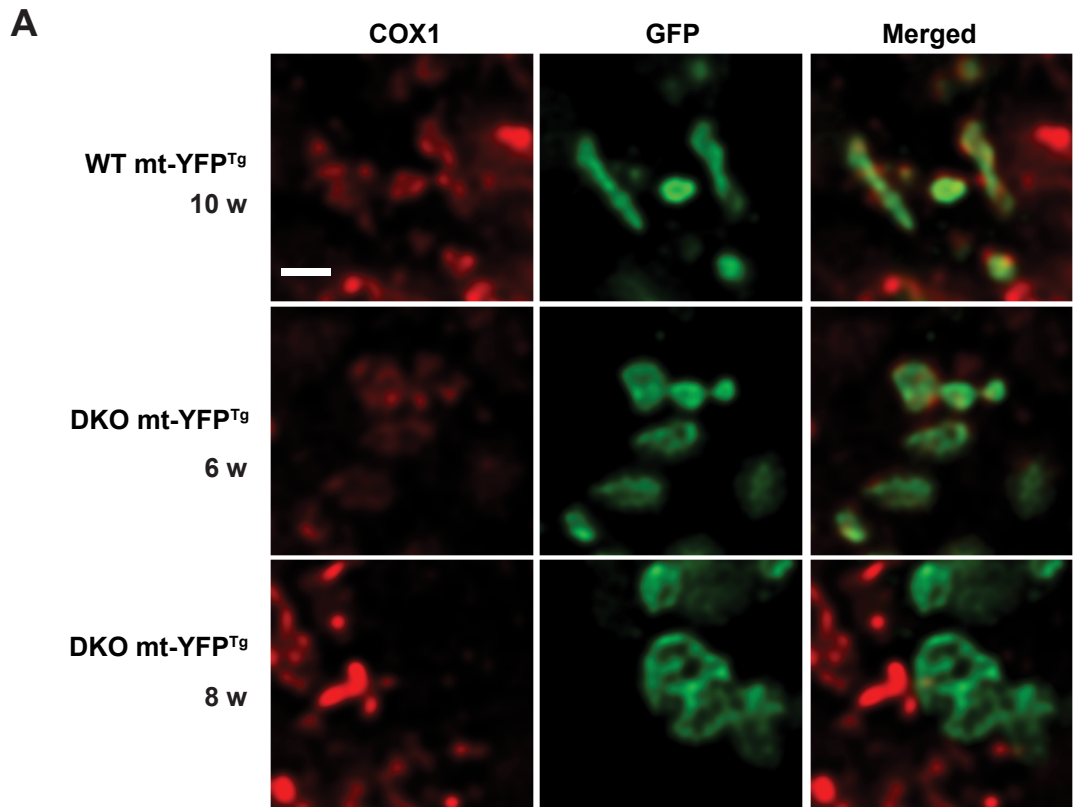


Figure 4.24 Loss of the *m*-AAA protease in oligodendrocytes causes mitochondrial dysfunction and triggers apoptotic death

(A) Deconvoluted single-plane confocal images of double immunofluorescence staining of mt-YFP and COX1 in WT and DKO mice at the indicated age. mt-YFP⁺ mitochondria in DKO lost COX1 staining. n = 3 mice per group per time point. Scale bar, 1 μ m. (B) Representative images of TUNEL assay in the corpus callosum of mice at 7 weeks of age. n = 4 mice per group. Scale bar, 10 μ m. (C) Quantification of TUNEL⁺ cells in the corpus callosum. Data are plotted as individual values from each mouse with mean \pm S.E.M. (D) Ultrastructural analysis showed apoptotic oligodendrocytes in the corpus callosum of DKO mice at 8 weeks of age. n = 3 mice per group. Scale bar, 1 μ m. (E) Deconvoluted single-plane confocal images of double immunofluorescence staining of GFP and cytochrome c in WT and DKO mice at 8 weeks of age. n = 3 mice per group. Scale bar, 1 μ m.

5 Discussion

5.1 Mitochondrial morphology alteration upon loss of the *m*-AAA protease

Aberrant mitochondrial dynamics has been implicated in the pathogenesis of neurodegenerative diseases (Cho et al., 2010; Knott et al., 2008; Lu, 2009), such as Charcot-Marie-Tooth disease type 2A (Kijima et al., 2005; Zuchner et al., 2004) and autosomal dominant optic atrophy (Alexander et al., 2000), caused by mutations of mitochondrial fusion gene *Mfn2* and *Opa1* respectively. Little is known about the cell-autonomous role of mitochondrial dynamics in neurodegeneration. In this study, I have shown that deletion of mitochondrial protease AFG3L2 in both forebrain neurons and myelinating glial cells cause similar mitochondrial fragmentation and enlargement; however, the fate of these cells is distinct. Early neuronal death and normal oligodendrocyte survival highlight that neurons are preferentially susceptible to mitochondrial fission/fusion imbalance. This is reasonable as neurons are highly polarized cells with the axonal extension up to one meter in humans (Williamson et al., 1996), they are particularly vulnerable to mitochondrial morphological disturbance, which influences the activity of respiratory complexes, Ca²⁺ buffering and quality control maintenance (Burte et al., 2015; Chan, 2006; Chen and Chan, 2009; Cho et al., 2010; Itoh et al., 2013).

On the other hand, the significance of mitochondrial dynamics in glial cells has not been extensively investigated yet. Depletion of *COX10* or *Tfam* in Schwann cells causes mitochondrial enlargement (Funfschilling et al., 2012; Viader et al., 2011); however, mitochondrial fusion and fission in these mouse models have been not explored in detail, presumably due to lack of any dramatic difference. In comparison with neurons, a specific feature of glial cells is the capability of glycolysis (Kasischke et al., 2004; Pellerin and Magistretti, 1994; Vega et al., 2003). Whether the effects of mitochondrial dynamics abnormalities in glycolytic cells are attenuated remains presently not well understood. In this study, disturbed mitochondrial morphology in *Afg3l2*-deficient myelinating cells and long-term survival of these cells, support the idea that glial cells could be more tolerant to mitochondrial dynamics abnormalities. Moreover, mitochondrial fragmentation *per se* may serve as a cellular stress response and facilitate cellular adaption dependent on the metabolic profile of the cell. Consistently, mitochondrial fission is utilized by brown adipocytes to increase energy expenditure by shifting nutrient oxidation towards thermogenesis (Wikstrom et al., 2014).

We have found that mitochondrial fusion protein OPA1 is cleaved and fission protein DRP1 and active form of DRP1 at phosphorylation site Ser616 are decreased in the brain of *Afg3l2* full-body knockout mice. AFG3L2 deficiency triggers stress-induced OMA1 peptidase activation (Ehse et al., 2009), and OMA1 mediates the degradation of OPA1 long isoforms into short isoforms (Baker et al., 2014; Ehse et al., 2009). Furthermore, short isoforms of OPA1 promote mitochondrial fission and inhibit fusion, resulting in mitochondrial fragmentation (Anand et al., 2014). Normally, enhanced mitochondria fission should recruit more active DRP1 to mitochondria (Ingeman et al., 2005; Legesse-Miller et al., 2003); however, we unexpectedly observed reduced levels of total DRP1, active phospho-DRP1 S616 and DRP1 in mitochondrial fraction. Interestingly, DRP1 is the only fusion/fission protein that shows an alteration or a reduction in SCA28 patient lymphoblasts (Mancini et al., 2013). Thus, we open the question whether decreased recruitment of DRP1 to mitochondria might be a compensatory mechanism to balance excessive fission.

Postnatal deletion of *Afg3l2* in forebrain-neurons and myelinating cells circumvents the potential impacts on embryonic development; nevertheless, similar mitochondrial morphological alteration still occurs, which highlights the essential role of AFG3L2 to maintain proper mitochondrial morphology and function in neuronal tissues. AFG3L2 plays pleiotropic roles in mitochondria, including processing of respiratory chain subunits and mitochondrial ribosomal protein MRPL32 in mitochondria (Bonn et al., 2011; Hornig-Do et al., 2012; Leonhard et al., 1996; Nolden et al., 2005) and mitochondrial Ca^{2+} buffering (Maltecca et al., 2015; Maltecca et al., 2012). Is there a primary cause to induce mitochondrial fragmentation and enlargement in the absence of AFG3L2 protease? Based on the published studies, this question might be difficult to address currently, however, some hints can be obtained. Considering lack of significant OPA1 processing in the brain of *Surf1* KO, *Sco2* KO/KI and *Nduf4* KO mice (this study), which clearly show respiratory complex deficiency (Ingraham et al., 2009; Viscomi et al., 2011; Yang et al., 2010), it is unlikely that purely affecting mitochondrial respiration to a certain extent triggers extensive mitochondrial fusion and fission disturbance *in vivo*. Since mitochondrial fission is also regulated by mitochondrial membrane potential, ROS levels and calcium homeostasis (Baker et al., 2014; Jeyaraju et al., 2009), these aspects should be taken into account for the mitochondrial fragmentation resulting from AFG3L2 loss. Further studies to uncouple

the role of AFG3L2 are required to understand the primary cause of mitochondrial fragmentation in cells lacking AFG3L2.

Additionally, mitochondrial fragmentation is regarded as a prerequisite for autophagy or mitophagy to eliminate damaged mitochondria or mitochondrial proteins (Narendra et al., 2008; Twig et al., 2008; Youle and van der Bliek, 2012). Whether autophagy or mitophagy is enhanced in the *Afg3l2*-deficient cells remains not well known. Remarkably, deficiency of AFG3L2 not only causes mitochondrial fragmentation, but also mitochondrial enlargement. Speculatively, these gigantic mitochondria would be difficult to be removed by autophagy. Regarding the phenotype of mitochondrial enlargement, it is noteworthy to mention that the non-specific mitochondrial permeability transition pore (MPTP) opening enables free passage of molecules up to about 1.5 kDa into the mitochondria leading to matrix swelling, under pathological condition of mitochondrial calcium overload (Bernardi, 2013; Halestrap, 2009). Investigating calcium influx and determining which component of the MPTP is affected will allow us to know the mechanism of mitochondrial enlargement alteration upon loss of AFG3L2.

5.2 Tau hyperphosphorylation evoked by AFG3L2 deficiency in neurons

Tau is a microtubule-associated phosphoprotein abundantly expressed in neurons, which stabilizes axonal microtubules (Breuzard et al., 2013; Butner and Kirschner, 1991; Cleveland et al., 1977; Drubin et al., 1986; Shin et al., 1991; Stoothoff and Johnson, 2005). In AD, many kinases have been shown to increase their activity and trigger tau hyperphosphorylation (Martin et al., 2013b). Hyperphosphorylated tau detaches from microtubules, aggregates into paired helical filaments and results in microtubule breakdown, intracellular transport defect and ‘dying-back’ of axons (Mandelkow and Mandelkow, 1998). Remarkably, in our two *Afg3l2* mouse models, constitutive full-body knockout and conditional forebrain neuron-specific knockout, tau is hyperphosphorylated in the brain of both models.

During development, tau is phosphorylated to match the period of active neurite outgrowth (Yu et al., 2009). Since *Afg3l2* full-body knockout mice generally die before at P16 (Maltecca et al., 2008) when the kinases are still active (Yu et al., 2009), it could be difficult to detect the kinases up-regulation at this stage. Not surprisingly, none of the kinases we assessed was hyperactivated neither in the total brain lysates nor mitochondrial fraction. In the absence of AFG3L2, mitochondrial respiration is defective (Almajan et al., 2012; Maltecca et al., 2008) because of mitochondrial protein synthesis impairment (Almajan et al., 2012). Inefficient mitochondrial respiration further leads to decreased ATP synthesis rate (Maltecca et al., 2008) and ultimately cAMP elevation; besides, it may also result in raised ROS production. For instance, *Afg3l2* haploinsufficiency mouse model shows increased ROS level at one year old (Maltecca et al., 2009). Consequence of the secondary effects of cAMP and ROS enhancement in the *Afg3l2* full-body knockout mice might be difficult to detect because of the early death. In contrast, in the adult model, *Afg3l2* is deleted postnatally, giving us relatively sufficient time for the analysis. Consequently, we found cAMP-dependent PKA and oxidative stress-induced ERK1/2 kinases activation in AFG3L2^{NKO} mice (Kondadi et al., 2014). Notably, tau hyperphosphorylated sites including T181, S199, S202, T205 and S396 in AFG3L2-deficient mouse models have been found in Alzheimer's disease patients shown to be phosphorylated by PKA and ERK1/2 (Martin et al., 2013b). On the other hand, tau phosphorylation is also regulated by phosphatase activity (Braithwaite et al., 2012; Martin et al., 2013a). Downregulation of phosphatases,

such as protein phosphatase 2A, has been implicated in the pathogenesis of AD. Therefore, the phosphatases activity could be a direction to understand tau pathogenesis of neurodegenerative diseases associated with AFG3L2 deficiency.

No evident hyperphosphorylated tau levels in the brain of mitochondrial respiratory chain complex-deficient *Surf1* KO, *Sco2* KO/KI and *Ndufs4* KO mice, reveals a particular link of the *m*-AAA protease and tau phosphorylation. Interestingly, PHB1/2, form ring-shaped scaffolds in the inner mitochondrial membrane that regulate the turnover of membrane proteins by the *m*-AAA protease (Merkwirth and Langer, 2009; Steglich et al., 1999), ablation of which in forebrain neurons with the same *CaMKII α* -Cre line also leads to tau hyperphosphorylation (Merkwirth et al., 2012). Thus, our data provide genetic evidence for a casual relationship of the *m*-AAA protease and tauopathy. Interestingly, tau reduction produces beneficial effects on mitochondrial transport in a mouse model of Alzheimer's disease (Vossel et al., 2010). Likewise, downregulation of tau partially rescued mitochondrial anterograde transport defect in *Afg3l2* knockdown primary neurons (Kondadi et al., 2014). Additionally, in these neurons, antioxidants, such as N-acetyl-cysteine and vitamin E, restored the mitochondrial transport impairment, further implying the role of ROS in the causative signaling pathway (Kondadi et al., 2014).

5.3 Physiological role of AFG3L1 in the mouse

In humans, *AFG3L1* is pseudogene, and is transcribed into four mRNA isoforms that are not translated (Kremmidiotis et al., 2001). AFG3L1, which shares highly sequence identity (68.5%) with its homolog AFG3L2, is expressed in mouse in tissue-specific manner (Koppen et al., 2007; Sacco et al., 2010). However, no mouse model of *Afg3l1* has been published yet. Here we generated a full-body knockout mouse model of *Afg3l1* and have shown that loss of *Afg3l1* can be tolerated in mouse. In contrast to severe developmental defects of *Afg3l2* null mice, *Afg3l1* full-body knockout mice have normal growth curve and display no obvious sign of neurodegeneration at least till one year of age. Our study and others have shown that AFG3L1 is not highly expressed in the brain (Koppen et al., 2007; Sacco et al., 2010), suggesting that the complexes of mitochondrial *m*-AAA protease, formed by AFG3L2 and paraplegin, are sufficient for mitochondrial dynamics and cell survival.

Surprisingly, despite high expression levels of AFG3L1 and AFG3L2, in the liver of *Afg3l1* full-body knockout (this study) or *Afg3l2* null mice (Ehse et al., 2009), no abnormal OPA1 cleavage was observed, indirectly suggesting normal mitochondrial dynamics. Consistently, the morphology of mitochondria in the liver in *Afg3l2* null mice was comparable to the wildtype mice (Maltecca et al., 2008). How liver mitochondria cope with the loss of the *m*-AAA protease is a very interesting question, which has to be addressed. Further investigations are required to understand whether the function of the *m*-AAA protease correlates with the features of mitochondria among different tissues.

Despite the fact that AFG3L1 may compensate the loss of AFG3L2 or paraplegin, most published *m*-AAA protease mouse studies till now have neglected the existence of AFG3L1 in the mouse models (Almajan et al., 2012; Ferreira et al., 2004; Kondadi et al., 2014; Maltecca et al., 2008; Maltecca et al., 2015; Maltecca et al., 2009). Therefore, the availability of *Afg3l1* full-body knockout mouse model will allow future studies to better model the human diseases associated with the *m*-AAA protease mutations.

5.4 AFG3L2 is required for oligodendrocyte maturation but is dispensable for the survival of adult oligodendrocytes

Previous *in vitro* studies have shown that mitochondria are required for oligodendrocyte differentiation and myelin production, and whether mitochondrial dysfunction causes glial cell demise is not clear (Schoenfeld et al., 2010; Ziabreva et al., 2010). In the absence of AFG3L2, the viability of oligodendrocytes is not affected; instead, their maturation is impaired as shown by the significant reduction of mt-YFP⁺ cells not localized with mature oligodendrocytes marked by APC antibody. This would make a significant consequence if *Afg3l2* were depleted during early postnatal or developmental stage when mature oligodendrocytes are required during the peak of myelin formation. Given the fact that PLP1-CreERT transgenic line targets not only myelinating cells but also astrocytes and neurons during development (Guo et al., 2009; Michalski et al., 2011), it is difficult to explore the role of AFG3L2 or *m*-AAA protease in the process of myelin formation using this promoter. Although AFG3L1 and paraplegin are expressed at low levels in oligodendrocytes, presumably the amount of *m*-AAA protease composed of AFG3L1 and paraplegin in these cells is sufficient for mitochondrial quality control maintenance and cell survival for relatively long time. However, ultimately myelinating cells lacking AFG3L2 become sick and cannot support long-term axonal integrity and proper myelin maintenance. Probably this is one explanation for axonal degeneration and dysmyelination in the 90-week-old mice.

How to explain the long-term survival of myelinating cells in the absence of AFG3L2? *In vivo* studies conducted by other groups have proposed that oligodendrocytes and Schwann cells utilize glycolysis to survive when mitochondrial respiration is impaired (Funfschilling et al., 2012; Viader et al., 2011). This hypothesis might be applied to our mouse model, in which low amount of the *m*-AAA protease composed by AFG3L1 and paraplegin maintains mitochondrial quality control, and adapted metabolism supports cell survival and axonal integrity.

5.5 Lack of the *m*-AAA protease causes death of myelinating cells

In this study, we generated and characterized a mouse model that lacks the whole *m*-AAA protease complexes for the first time. Interestingly, despite that the loss of AFG3L2 does not affect the viability of oligodendrocytes, deletion of entire *m*-AAA protease causes rapid cell death and results in progressive motor deficit and hair greying of the mutant mice.

5.5.1 Oligodendrocyte death and axonal demyelination in the central nervous system

In the literature, common approaches to ablate oligodendrocytes in the mouse used either diphtheria toxin (DTX)-diphtheria toxin receptor (DTR) system or genetically activation of diphtheria toxin fragment A (DTA) expression in oligodendrocytes (Ghosh et al., 2011; Gritsch et al., 2014; Locatelli et al., 2012; Oluich et al., 2012; Traka et al., 2010; Traka et al., 2016). Here, we induced oligodendrocytes death by mitochondrial *m*-AAA protease deletion. To my knowledge, only two mouse studies carrying deletion of mitochondrial genes in myelinating cells have been reported so far (Funfschilling et al., 2012; Viader et al., 2011). Coincidentally, in both studies, Schwann cells or oligodendrocytes survive well in the absence of mitochondrial transcriptional factor *Tfam* or respiratory complex IV assembly factor *Cox10*, as these cells have the capability of glycolysis (Funfschilling et al., 2012; Viader et al., 2011). Thus, independent from oxidative capacity, an anti-cell death function of the *m*-AAA protease is highlighted. Another evidence to support the idea that the functions of *m*-AAA protease are beyond just having an impact on mitochondrial respiration is that deleting postnatally *Afg3l2* in forebrain neurons using *CaMKII α* -Cre line causes massive neuronal loss at 2 months of age (Kondadi et al., 2014), which is much earlier than at 4 to 5 months of deleting OXPHOS genes *Tfam* or *Cox10* using the same *CaMKII α* promoter and Cre recombinase strategy (Diaz et al., 2012; Fukui et al., 2007; Sorensen et al., 2001).

Our work demonstrates that deletion of whole *m*-AAA protease in oligodendrocytes leads to apoptosis. Consistently, apoptotic pathway activation is revealed in the SCA28 patients by genome-wide expression profiling (Mancini et al., 2013). Moreover, the mitochondrial *i*-AAA protease YME1L deficiency in human embryonic kidney 293 cells or in *Drosophila* leads to impaired apoptotic resistance (Qi et al., 2016; Stiburek et

al., 2012). However, increase necrotic cell death is revealed in the YME1L knockout cardiomyocytes (Wai et al., 2015). Notably, our data demonstrate that the death of myelinating cells is independent of mitochondrial dynamics, and presumably also is not caused by respiration deficiency. However, based on our experiments, we cannot exclude that there are other concomitant cell death pathways upon loss of *m*-AAA protease. Further studies are required to explore unknown substrates or interactors of *m*-AAA protease, which might directly or indirectly play a role in apoptosis or other cell death pathways.

Since one of the significant functions of oligodendrocytes is to produce myelin (Bradl and Lassmann, 2010), ablation of oligodendrocytes in adult circumvents gene deletion during the period of myelin formation and more possible affects myelin maintenance. Indeed, oligodendrocytes death is followed by progressive axonal demyelination and degeneration. In line with our observation, demyelination occurs as early as several weeks after oligodendrocyte ablation (Locatelli et al., 2012; Pohl et al., 2011; Traka et al., 2016). Interestingly, prior to the overt demyelination, I have shown that astrogliosis is an early event accompanied by oligodendrocytes demise, and is followed by microglial activation. The roles of astrogliosis and microgliosis in demyelinating diseases are controversial, both protective and destructive effects are being discussed (Aguzzi et al., 2013; Williams et al., 2007). However, in recent studies, astrocytes and microglia are suggested to exert beneficial roles (Kocur et al., 2015; Lampron et al., 2015; Masuch et al., 2015; Nikolakopoulou et al., 2013; Skripuletz et al., 2013). For instance, astrocytes secrete chemokine to recruit microglia to remove myelin debris, which facilitates oligodendrocytes regeneration during remyelination (Skripuletz et al., 2013). Although the consequence of astrocyte and microglia activation in our double mutants needs deep investigation, complete replenishment of oligodendrocytes in these mice indicates that oligodendrocyte regeneration is not impaired. Thus, beneficial effects of astrogliosis and microgliosis in this context are favored.

Oligodendrocyte regeneration, in other words, oligodendrocyte precursor cells (OPC) proliferation, is considered as a prerequisite for myelin repair in demyelinating disorders, such as multiple sclerosis (MS) (Franklin and Ffrench-Constant, 2008). As expected, oligodendrocyte regeneration results in remyelination to a certain extent, but our mice still show axonal demyelination and degeneration. One explanation is that regenerated oligodendrocytes have inadequate myelination capability. Secondly, axonal

damage or loss may occur during the gap of oligodendrocyte death and regeneration. Due to lack of more time-course analyses, I could not catch the time point when the OPC generation takes place. Additionally, it has been shown that genetic oligodendrocyte ablation triggers sufficiently adaptive autoimmune response against myelin (Traka et al., 2016). Whether oligodendrocyte death in our double mutant mice is associated with T- and B-cell infiltration in the CNS is still an open question.

Mitochondrial accumulation in the axons of DKO mice is of particular interest because increased mitochondrial content has been implicated within demyelinated axons in chronic myelin-deficient Shiverer mouse or in MS patients (Andrews et al., 2006; Mahad et al., 2009; Zamboni et al., 2011). Syntrophin (SNPH), which controls axonal mitochondria docking through the interaction with microtubules (Kang et al., 2008), is upregulated in Shiverer mouse or in MS patients (Joshi et al., 2015; Mahad et al., 2009). Further studies demonstrate that mitochondrial mobilization by deletion of *SNPH*, deteriorates the survival of demyelinated axons in acute demyelination (Ohno et al., 2014), but produces benefits in the chronic demyelinating Shiverer mouse (Joshi et al., 2015). Thus, a biphasic model is proposed for the role of SNPH during MS: mitochondrial anchoring by SNPH is adaptive in the early phase and maladaptive in the late phase (Joshi et al., 2015). The expression level of SNPH in the absence of *m-AAA* protease remains undetermined. Considering the progressive process of demyelination and AMPK activation in our DKO mice, it is conceivable that stationary mitochondrial congestion is compensatory to fit the energy-demand in the demyelinated axons; however, exhausted mitochondria might get stuck in the axons and ultimately generate substantial molecules such as ROS to fuel a vicious cycle (Joshi et al., 2015).

5.5.2 Peripheral neuropathy

In contrast to extensive axonal demyelination in the CNS of the DKO mice, moderate phenotype was observed in the PNS. This is possibly because the efficiency of Cre-mediated recombination under *PLP1* promoter in the PNS is much less than in the CNS (Doerflinger et al., 2003). Although PLP1 only constitutes 0.15% of total myelin proteins in the murine sciatic nerve (Patzig et al., 2011), it is expressed in both myelinating and nonmyelinating Schwann cells in adult mouse (Jiang et al., 2000). Here we induced the Cre recombinase activation using PLP1-CreERT line at 4 weeks, a time point when it is still enigmatic which cell populations in the PNS expressed PLP1.

Targeted Schwann cells are significantly diminished in the DKO mice, and our results highlight that the loss of *m*-AAA protease preferentially affects nonmyelinating Schwann cells and small C-fibers. This is in line with previous findings that these cells are more susceptible to mitochondrial dysfunction in a mouse model of *Tfam* deletion in Schwann cells (Viader et al., 2011). The susceptibility of unmyelinating small-caliber axons is also shown in the diabetic peripheral neuropathies (Kennedy et al., 1996; Polydefkis et al., 2004) and small-fiber sensory neuropathies (Lacomis, 2002; Sommer and Lauria, 2007). However, since small fibers are sensory nerves, their sensory phenotype of our DKO needs to be further explored. Mild demyelination and adaxonal myelin detachment of large-caliber axons in the 28-week DKO mice indicate that motor nerve fibers are eventually damaged, which may contribute to the motor deficit in the beam-walking test of these mice.

After nerve injury, Schwann cells digest myelin by selective autophagy-myelinophagy for regeneration (Gomez-Sanchez et al., 2015). This is a particular feature of Schwann cells in comparison with oligodendrocytes (Brosius Lutz and Barres, 2014), therefore, it is not surprising that we could observe few myelin debris in the PNS but numerous myelin debris accumulation in the CNS of the DKO mice. Failure to detect myelinophagy in the Schwann cells lacking the *m*-AAA protease is probably owing to very low targeting efficiency in the PNS therefore limited number of autophagosomes.

5.5.3 Melanocytes reduction and hair greying in the skin

A remarkable phenotype of our DKO mice is age-related premature hair greying. We have shown that loss of melanocytes is the cause of hair greying. Skin melanocytes originate from two sources: one is directly from neural crest cells with dorsal migration (Rawles, 1947), the other is indirectly from neural crest-derived Schwann cell precursors with ventral migration (Adameyko et al., 2009; Nitzan et al., 2013). Transcription factor FoxD3 regulates the balance between these two populations of melanocytes (Nitzan et al., 2013). Additionally, transcriptomic analysis of embryo skin reveals that *PLP1* gene is expressed in melanoblasts (Colombo et al., 2012). Moreover, it has been shown that melanocytes are targeted by *PLP1*-promoter driven Cre expression during embryogenesis (Leone et al., 2003). *PLP1*-Cre is active in Schwann cell precursors-bipotential progenitors of Schwann cells and melanocytes, rather than in melanocytes (Adameyko et al., 2009). However, all these studies are conducted during

embryonic development. Is PLP1 expressed in melanoblasts/melanocytes in adult? What are the cellular sources for melanoblasts/melanocyte stem cells in adult? Are Schwann cells /Schwann cell precursors contributing to them in adult? All these questions are not clear.

Our preliminary data unveil that the reporter mitochondrial YFP signal was localized to mature melanocytes and melanoblasts after activating Cre recombinase, and c-KIT⁺ melanocytes were diminished in the skin of the DKO mice. To my knowledge, these are the first findings suggesting that melanocytes/melanoblasts could be eventually targeted by inducible PLP1-CreERT line in adult mouse, and the mitochondrial *m*-AAA protease is essential for Schwann cell/melanocyte lineage survival. Based on our preliminary results, there are three hypotheses to explain the hair greying phenotype. First of all, at 4 weeks of age, *PLP1* promoter is expressed not only in myelinating cell lineage but also in melanocyte lineage; in other words, melanocytes are directly targeted by *PLP1*-promoter driven Cre recombinase in adult. Although this is not in agreement with the observation that PLP1-Cre is not active in melanocytes at embryonic stages (Adameyko et al., 2009), our ‘direct’ evidence to support this hypothesis is that minor mitochondrial YFP signal was found in hair follicles in the skin as early as one day after tamoxifen induction (Julie Jacquemyn’s data not shown). However, if this were true for the DKO mice, I would expect to see an early dorsal hair greying phenotype since neural crest cells-derived melanocytes migrate dorsally. Instead, we saw a progressive forelimbs-hindlimbs-ventral to lateral body wall-dorsal-head hair greying pattern. This is reminiscent of a previous study demonstrating that Schwann cell precursors give rise to a large number of melanocytes in the limbs, lateral and dorsal skin during the embryonic development (Adameyko et al., 2009). Furthermore, deletion of the *m*-AAA protease leads to dramatic Schwann cell death in the peripheral nerves and preferentially has early effects on nonmyelinating Schwann cells. Whether Schwann cell precursors exist in adulthood is still an open question. Interestingly, in bone marrow, adult nonmyelinating Schwann cells contact with hematopoietic stem cells (HSC) and express HSC factor TGF- β to regulate HSC hibernation (Yamazaki et al., 2011). Thus, nonmyelinating Schwann cells in the adult may express factors for melanocyte stem cells maintenance, or act as precursors instead of embryonic Schwann cell precursors. This brings me to the second hypothesis: the absence of the *m*-AAA protease causes nonmyelinating Schwann cells death, thereby leading to lack of Schwann cell-derived

melanocytes replenishment and ultimately resulting in hair greying. The third is accepting the former two hypotheses: the hair greying is caused partially by direct targeting melanocyte death and largely by loss of Schwann cell-originated melanocytes. This hypothesis is more preferable in the scenario of hair greying pattern, but does not exclude the possibility of directly targeting a small population of melanocytes.

Skin biopsy has been widely used to investigate peripheral neuropathies (Sommer and Lauria, 2007), and skin denervation is one of the initial signs of pathology and correlates with disease progression (Ebenezer et al., 2007). Considering the phenotypes of peripheral neuropathies in the DKO mice, I would expect to see denervation in the skin of the aged mice, and this could potentially account for the hair greying because the source of melanocytes from Schwann cells-associated peripheral nerve is cut out. However, because of incompatibility of antibody applications or lack of optimization, I could not address this point yet.

5.6 Conclusions

In summary, using various genetic mouse models, we have shown:

1. Postnatal Lack of AFG3L2 in neurons triggers tau hyperphosphorylation, which provides new insights to the pathogenesis of neurodegenerative diseases associated with AFG3L2 mutations.
2. AFG3L2 is highly expressed in oligodendrocytes, and AFG3L2 deficiency is sufficient to cause mitochondrial fragmentation in myelinating glial cells.
3. Loss of AFG3L2 in neurons and myelinating glial cells shows similar mitochondrial morphological alterations, but the outcomes are distinct. Whereas neurons die rapidly, the survival of oligodendrocytes is not affected but their maturation is delayed.
4. *Afg3l1* full-body knockout mice display no neurological phenotype till one year old of age. AFG3L1 is dispensable for mitochondrial quality control when AFG3L2 is present.
5. Despite the capacity of glycolysis in myelinating glial cells, these cells die in the absence of the *m*-AAA protease, indicating a novel role of the *m*-AAA protease to prevent cell death.
6. Oligodendrocyte death caused by the *m*-AAA protease ablation results in progressive axonal demyelination and profound energy deficiency.
7. In adulthood, deletion of the *m*-AAA protease using the PLP1-CreERT line leads to premature hair greying.

Therefore, we have expanded the basic understanding of the *m*-AAA protease functions in neurons and myelinating cells. We also provide a valuable mitochondria-based animal model to study chronic demyelinating diseases. Further investigation to unravel cell death mechanism in the absence of *m*-AAA protease may suggest novel therapeutic target for human neurodegenerative diseases such as SCA28 and hair greying.

Zusammenfassung

Die *m*-AAA Protease ist ein hexamerischer Proteinkomplex, welcher sich in der inneren Membran des Mitochondriums befindet. Zum einen spielt die *m*-AAA Protease eine Rolle in der Weiterverarbeitung von speziellen Substraten, zum anderen ist sie wichtig für den Abbau fehlgefalteter Polypeptide. Im Menschen besteht die *m*-AAA Protease aus AFG3L2 und paraplegin. Mutationen in dem *AFG3L2* Gen sind verbunden mit den Krankheiten dominante Spinozerebelläre Ataxia 28 und dem rezessiven spastic ataxia-neuropathy syndrome 5 (SPAX5). Weiterhin wurde gezeigt, dass Mutationen in dem *SPG7* Gen, welches für paraplegin codiert, zur Hereditären Spastischen Paraplegie führen kann. In der Maus gibt es neben AFG3L2 und paraplegin eine dritte *m*-AAA Untereinheit, genannt AFG3L1. Obwohl verschiedene Maus Krankheitsmodelle den neurodegenerativen Phentypen der oben genannten Krankheiten rekapitulieren konnten, ist der molekulare Mechanismus der dem zu Grunde liegt noch nicht verstanden.

In dieser Arbeit wurde mit Hilfe verschiedener Mausmodelle die zellautonome Funktion der *m*-AAA Protease in Neuronen und in Myelin produzierenden Zellen erforscht. Wir konnten zeigen, dass in Knock-Out-Mäusen, in denen AFG3L2 entweder im ganzen Körper oder spezifisch im Vorderhirn fehlt, Mitochondrien fragmentieren und anschwellen und dass das Protein tau hyperphosphoryliert wird. Weiterhin führt das Fehlen von AFG3L2 in ausgewachsenen Myelin produzierenden Zellen zu früh auftretenden mitochondrialen Abnormalitäten wie auch vorher in Neuronen beobachtet werden konnte. Im Gegensatz zu der Beobachtung in Neuronen, konnten wir keine reduzierte Lebensdauer der Myelin produzierenden Zellen feststellen. Desweiteren ist bekannt, dass Myelin produzierende Zellen Probleme in der Atmungskette durch Glykolyse kompensieren können. Interessanterweise konnten wir jedoch zeigen, dass der komplette Verlust der *m*-AAA Protease durch den Knock-out (KO) von *Afg3l2* in einem *Afg3l1* KO Hintergrund (Doppelter Knock-out (DKO)), zum absterben von Myelin produzierenden Zellen führt, was letztendlich zum fortschreitenden Verlust des Myelins um das neuronale Axons führt. Ausserdem haben wir ein frühzeitiges Ergrauen der Haare in DKO Mäusen festgestellt, was auf den Verlust von Melanozyten zurückzuführen ist.

Zusammenfassend konnten wir zeigen, dass es einen zellautonomen Grenzwert für die *m*-AAA Protease gibt, welcher nicht unterschritten werden darf, da sonst das Überleben der Zelle in Gefahr ist. Die essentielle Rolle von AFG3L2 in der Vorbeugung gegen den Zelltod ist unabhängig von der Teilung und Fusionierung von Mitochondrien und der Fähigkeit der Zelle Oxidative Phosphorylierung zu betreiben. Unsere Ergebnisse bringen neue Erkenntnisse über Krankheiten die mit dem Verlust der *m*-AAA Protease verbunden sind. Weiterhin können die von uns etablierten Mausmodelle wertvolle Werkzeuge in der Forschung über andere Krankheiten sein, die der Mitochondrialen Dysfunktion zu Grunde liegen. Dies könnte helfen andere neurodegenerative Krankheiten, wie Tauopathien und Krankheiten, in denen ein Myelin Defizit vorliegt, besser zu erforschen.

References

- Adameyko, I., Lallemand, F., Aquino, J.B., Pereira, J.A., Topilko, P., Muller, T., Fritz, N., Beljajeva, A., Mochii, M., Liste, I., *et al.* (2009). Schwann cell precursors from nerve innervation are a cellular origin of melanocytes in skin. *Cell* *139*, 366-379.
- Aggarwal, S., Yurlova, L., and Simons, M. (2011). Central nervous system myelin: structure, synthesis and assembly. *Trends Cell Biol* *21*, 585-593.
- Aguzzi, A., Barres, B.A., and Bennett, M.L. (2013). Microglia: scapegoat, saboteur, or something else? *Science* *339*, 156-161.
- Alexander, C., Votruba, M., Pesch, U.E., Thiselton, D.L., Mayer, S., Moore, A., Rodriguez, M., Kellner, U., Leo-Kottler, B., Auburger, G., *et al.* (2000). OPA1, encoding a dynamin-related GTPase, is mutated in autosomal dominant optic atrophy linked to chromosome 3q28. *Nat Genet* *26*, 211-215.
- Almajan, E.R., Richter, R., Paeger, L., Martinelli, P., Barth, E., Decker, T., Larsson, N.G., Kloppenburg, P., Langer, T., and Rugarli, E.I. (2012). AFG3L2 supports mitochondrial protein synthesis and Purkinje cell survival. *J Clin Invest* *122*, 4048-4058.
- Alonso, A.C., Grundke-Iqbal, I., and Iqbal, K. (1996). Alzheimer's disease hyperphosphorylated tau sequesters normal tau into tangles of filaments and disassembles microtubules. *Nat Med* *2*, 783-787.
- Anand, R., Langer, T., and Baker, M.J. (2013). Proteolytic control of mitochondrial function and morphogenesis. *Biochimica et Biophysica Acta (BBA) - Molecular Cell Research* *1833*, 195-204.
- Anand, R., Wai, T., Baker, M.J., Kladt, N., Schauss, A.C., Rugarli, E., and Langer, T. (2014). The i-AAA protease YME1L and OMA1 cleave OPA1 to balance mitochondrial fusion and fission. *J Cell Biol* *204*, 919-929.
- Andrews, H., White, K., Thomson, C., Edgar, J., Bates, D., Griffiths, I., Turnbull, D., and Nichols, P. (2006). Increased axonal mitochondrial activity as an adaptation to myelin deficiency in the Shiverer mouse. *J Neurosci Res* *83*, 1533-1539.
- Antonicka, H., Leary, S.C., Guercin, G.H., Agar, J.N., Horvath, R., Kennaway, N.G., Harding, C.O., Jaksch, M., and Shoubridge, E.A. (2003). Mutations in COX10 result in a defect in mitochondrial heme A biosynthesis and account for multiple, early-onset clinical phenotypes associated with isolated COX deficiency. *Hum Mol Genet* *12*, 2693-2702.
- Arnoldi, A., Tonelli, A., Crippa, F., Villani, G., Pacelli, C., Sironi, M., Pozzoli, U., D'Angelo, M.G., Meola, G., Martinuzzi, A., *et al.* (2008). A clinical, genetic, and biochemical characterization of SPG7 mutations in a large cohort of patients with hereditary spastic paraplegia. *Hum Mutat* *29*, 522-531.
- Atorino, L., Silvestri, L., Koppen, M., Cassina, L., Ballabio, A., Marconi, R., Langer, T., and Casari, G. (2003). Loss of m-AAA protease in mitochondria causes complex I deficiency and increased sensitivity to oxidative stress in hereditary spastic paraplegia. *J Cell Biol* *163*, 777-787.
- Baker, M.J., Lampe, P.A., Stojanovski, D., Korwitz, A., Anand, R., Tatsuta, T., and Langer, T. (2014). Stress-induced OMA1 activation and autocatalytic turnover regulate OPA1-dependent mitochondrial dynamics. *Embo J* *33*, 578-593.
- Banfi, S., Bassi, M.T., Andolfi, G., Marchitello, A., Zanotta, S., Ballabio, A., Casari, G., and Franco, B. (1999). Identification and characterization of AFG3L2, a novel paraplegin-related gene. *Genomics* *59*, 51-58.

- Baumann, N., and Pham-Dinh, D. (2001). Biology of oligodendrocyte and myelin in the mammalian central nervous system. *Physiol Rev* *81*, 871-927.
- Benit, P., Steffann, J., Lebon, S., Chretien, D., Kadhom, N., de Lonlay, P., Goldenberg, A., Dumez, Y., Dommergues, M., Rustin, P., *et al.* (2003). Genotyping microsatellite DNA markers at putative disease loci in inbred/multiplex families with respiratory chain complex I deficiency allows rapid identification of a novel nonsense mutation (IVS1nt-1) in the NDUFS4 gene in Leigh syndrome. *Human Genetics* *112*, 563-566.
- Bernardi, P. (2013). The mitochondrial permeability transition pore: a mystery solved? *Front Physiol* *4*, 95.
- Bonn, F., Tatsuta, T., Petrungraro, C., Riemer, J., and Langer, T. (2011). Presequence-dependent folding ensures MrpL32 processing by the m-AAA protease in mitochondria. *Embo J* *30*, 2545-2556.
- Bradl, M., and Lassmann, H. (2010). Oligodendrocytes: biology and pathology. *Acta Neuropathol* *119*, 37-53.
- Braithwaite, S.P., Stock, J.B., Lombroso, P.J., and Nairn, A.C. (2012). Protein phosphatases and Alzheimer's disease. *Prog Mol Biol Transl Sci* *106*, 343-379.
- Braugher, J.M., Duncan, L.A., and Chase, R.L. (1986). The involvement of iron in lipid peroxidation. Importance of ferric to ferrous ratios in initiation. *J Biol Chem* *261*, 10282-10289.
- Breuzard, G., Hubert, P., Nouar, R., De Bessa, T., Devred, F., Barbier, P., Sturgis, J.N., and Peyrot, V. (2013). Molecular mechanisms of Tau binding to microtubules and its role in microtubule dynamics in live cells. *J Cell Sci* *126*, 2810-2819.
- Brinkmann, B.G., Agarwal, A., Sereda, M.W., Garratt, A.N., Muller, T., Wende, H., Stassart, R.M., Nawaz, S., Humml, C., Velanac, V., *et al.* (2008). Neuregulin-1/ErbB signaling serves distinct functions in myelination of the peripheral and central nervous system. *Neuron* *59*, 581-595.
- Brosius Lutz, A., and Barres, B.A. (2014). Contrasting the glial response to axon injury in the central and peripheral nervous systems. *Dev Cell* *28*, 7-17.
- Brugman, F., Scheffer, H., Wokke, J.H., Nillesen, W.M., de Visser, M., Aronica, E., Veldink, J.H., and van den Berg, L.H. (2008). Paraplegin mutations in sporadic adult-onset upper motor neuron syndromes. *Neurology* *71*, 1500-1505.
- Brussino, A., Brusco, A., and Durr, A. (2011, updated 2013). Spinocerebellar Ataxia Type 28. In *GeneReviews(R)*, R.A. Pagon, M.P. Adam, H.H. Ardinger, S.E. Wallace, A. Amemiya, L.J.H. Bean, T.D. Bird, C.T. Fong, H.C. Mefford, R.J.H. Smith, *et al.*, eds. (Seattle (WA)).
- Burte, F., Carelli, V., Chinnery, P.F., and Yu-Wai-Man, P. (2015). Disturbed mitochondrial dynamics and neurodegenerative disorders. *Nat Rev Neurol* *11*, 11-24.
- Butner, K.A., and Kirschner, M.W. (1991). Tau protein binds to microtubules through a flexible array of distributed weak sites. *J Cell Biol* *115*, 717-730.
- Cagnoli, C., Mariotti, C., Taroni, F., Seri, M., Brussino, A., Michielotto, C., Grisoli, M., Di Bella, D., Migone, N., Gellera, C., *et al.* (2006). SCA28, a novel form of autosomal dominant cerebellar ataxia on chromosome 18p11.22-q11.2. *Brain : a journal of neurology* *129*, 235-242.
- Cagnoli, C., Stevanin, G., Brussino, A., Barberis, M., Mancini, C., Margolis, R.L., Holmes, S.E., Nobili, M., Forlani, S., Padovan, S., *et al.* (2010). Missense mutations in the AFG3L2 proteolytic domain account for approximately 1.5% of European autosomal dominant cerebellar ataxias. *Hum Mutat* *31*, 1117-1124.

- Cai, J., Yang, J., and Jones, D.P. (1998). Mitochondrial control of apoptosis: the role of cytochrome c. *Biochim Biophys Acta* 1366, 139-149.
- Casari, G., De Fusco, M., Ciarmatori, S., Zeviani, M., Mora, M., Fernandez, P., De Michele, G., Filla, A., Coccozza, S., Marconi, R., *et al.* (1998). Spastic paraplegia and OXPHOS impairment caused by mutations in paraplegin, a nuclear-encoded mitochondrial metalloprotease. *Cell* 93, 973-983.
- Casari, G., and Marconi, R. (2006, updated 2010). Spastic Paraplegia 7. In GeneReviews(R), R.A. Pagon, M.P. Adam, H.H. Ardinger, S.E. Wallace, A. Amemiya, L.J.H. Bean, T.D. Bird, C.T. Fong, H.C. Mefford, R.J.H. Smith, *et al.*, eds. (Seattle (WA)).
- Chan, D.C. (2006). Mitochondria: dynamic organelles in disease, aging, and development. *Cell* 125, 1241-1252.
- Chen, H., and Chan, D.C. (2009). Mitochondrial dynamics--fusion, fission, movement, and mitophagy--in neurodegenerative diseases. *Hum Mol Genet* 18, R169-176.
- Cho, D.H., Nakamura, T., and Lipton, S.A. (2010). Mitochondrial dynamics in cell death and neurodegeneration. *Cell Mol Life Sci* 67, 3435-3447.
- Cleveland, D.W., Hwo, S.Y., and Kirschner, M.W. (1977). Purification of tau, a microtubule-associated protein that induces assembly of microtubules from purified tubulin. *J Mol Biol* 116, 207-225.
- Colombo, S., Champeval, D., Rambow, F., and Larue, L. (2012). Transcriptomic analysis of mouse embryonic skin cells reveals previously unreported genes expressed in melanoblasts. *J Invest Dermatol* 132, 170-178.
- De Michele, G., De Fusco, M., Cavalcanti, F., Filla, A., Marconi, R., Volpe, G., Monticelli, A., Ballabio, A., Casari, G., and Coccozza, S. (1998). A new locus for autosomal recessive hereditary spastic paraplegia maps to chromosome 16q24.3. *Am J Hum Genet* 63, 135-139.
- De Vos, K.J., Allan, V.J., Grierson, A.J., and Sheetz, M.P. (2005). Mitochondrial function and actin regulate dynamin-related protein 1-dependent mitochondrial fission. *Curr Biol* 15, 678-683.
- Delaunay, D., Heydon, K., Cumano, A., Schwab, M.H., Thomas, J.L., Suter, U., Nave, K.A., Zalc, B., and Spassky, N. (2008). Early neuronal and glial fate restriction of embryonic neural stem cells. *J Neurosci* 28, 2551-2562.
- Dewar, D., Underhill, S.M., and Goldberg, M.P. (2003). Oligodendrocytes and ischemic brain injury. *J Cereb Blood Flow Metab* 23, 263-274.
- Di Bella, D., Lazzaro, F., Brusco, A., Plumari, M., Battaglia, G., Pastore, A., Finardi, A., Cagnoli, C., Tempia, F., Frontali, M., *et al.* (2010). Mutations in the mitochondrial protease gene AFG3L2 cause dominant hereditary ataxia SCA28. *Nat Genet* 42, 313-321.
- Diaz, F., Garcia, S., Padgett, K.R., and Moraes, C.T. (2012). A defect in the mitochondrial complex III, but not complex IV, triggers early ROS-dependent damage in defined brain regions. *Hum Mol Genet* 21, 5066-5077.
- Dickinson, E.K., Adams, D.L., Schon, E.A., and Glerum, D.M. (2000). A human SCO2 mutation helps define the role of Sco1p in the cytochrome oxidase assembly pathway. *J Biol Chem* 275, 26780-26785.
- Doerflinger, N.H., Macklin, W.B., and Popko, B. (2003). Inducible site-specific recombination in myelinating cells. *Genesis* 35, 63-72.

- Dogan, S.A., Pujol, C., Maiti, P., Kukat, A., Wang, S., Hermans, S., Senft, K., Wibom, R., Rugarli, E.I., and Trifunovic, A. (2014). Tissue-specific loss of DARS2 activates stress responses independently of respiratory chain deficiency in the heart. *Cell metabolism* *19*, 458-469.
- Drubin, D., Kobayashi, S., and Kirschner, M. (1986). Association of tau protein with microtubules in living cells. *Ann N Y Acad Sci* *466*, 257-268.
- Ebenezer, G.J., Hauer, P., Gibbons, C., McArthur, J.C., and Polydefkis, M. (2007). Assessment of epidermal nerve fibers: a new diagnostic and predictive tool for peripheral neuropathies. *J Neuropathol Exp Neurol* *66*, 1059-1073.
- Edener, U., Wollner, J., Hehr, U., Kohl, Z., Schilling, S., Kreuz, F., Bauer, P., Bernard, V., Gillissen-Kaesbach, G., and Zuhlke, C. (2010). Early onset and slow progression of SCA28, a rare dominant ataxia in a large four-generation family with a novel AFG3L2 mutation. *Eur J Hum Genet* *18*, 965-968.
- Ehse, S., Raschke, I., Mancuso, G., Bernacchia, A., Geimer, S., Tondera, D., Martinou, J.C., Westermann, B., Rugarli, E.I., and Langer, T. (2009). Regulation of OPA1 processing and mitochondrial fusion by m-AAA protease isoenzymes and OMA1. *J Cell Biol* *187*, 1023-1036.
- El Waly, B., Macchi, M., Cayre, M., and Durbec, P. (2014). Oligodendrogenesis in the normal and pathological central nervous system. *Front Neurosci* *8*, 145.
- Elleuch, N., Depienne, C., Benomar, A., Hernandez, A.M., Ferrer, X., Fontaine, B., Grid, D., Tallaksen, C.M., Zemmouri, R., Stevanin, G., *et al.* (2006). Mutation analysis of the paraplegin gene (SPG7) in patients with hereditary spastic paraplegia. *Neurology* *66*, 654-659.
- Erickson, C.A. (1993). From the crest to the periphery: control of pigment cell migration and lineage segregation. *Pigment Cell Res* *6*, 336-347.
- Fancy, S.P., Chan, J.R., Baranzini, S.E., Franklin, R.J., and Rowitch, D.H. (2011). Myelin regeneration: a recapitulation of development? *Annual review of neuroscience* *34*, 21-43.
- Ferreirinha, F., Quattrini, A., Pirozzi, M., Valsecchi, V., Dina, G., Broccoli, V., Auricchio, A., Piemonte, F., Tozzi, G., Gaeta, L., *et al.* (2004). Axonal degeneration in paraplegin-deficient mice is associated with abnormal mitochondria and impairment of axonal transport. *J Clin Invest* *113*, 231-242.
- Franklin, R.J., and Ffrench-Constant, C. (2008). Remyelination in the CNS: from biology to therapy. *Nature reviews* *9*, 839-855.
- Friedman, J.R., and Nunnari, J. (2014). Mitochondrial form and function. *Nature* *505*, 335-343.
- Fukui, H., Diaz, F., Garcia, S., and Moraes, C.T. (2007). Cytochrome c oxidase deficiency in neurons decreases both oxidative stress and amyloid formation in a mouse model of Alzheimer's disease. *Proc Natl Acad Sci U S A* *104*, 14163-14168.
- Funfschilling, U., Supplie, L.M., Mahad, D., Boretius, S., Saab, A.S., Edgar, J., Brinkmann, B.G., Kassmann, C.M., Tzvetanova, I.D., Mobius, W., *et al.* (2012). Glycolytic oligodendrocytes maintain myelin and long-term axonal integrity. *Nature* *485*, 517-521.
- Garratt, A.N., Britsch, S., and Birchmeier, C. (2000). Neuregulin, a factor with many functions in the life of a schwann cell. *Bioessays* *22*, 987-996.
- Gerdes, F., Tatsuta, T., and Langer, T. (2012). Mitochondrial AAA proteases — Towards a molecular understanding of membrane-bound proteolytic machines. *Biochimica et Biophysica Acta (BBA) - Molecular Cell Research* *1823*, 49-55.

- Ghosh, A., Manrique-Hoyos, N., Voigt, A., Schulz, J.B., Kreutzfeldt, M., Merkler, D., and Simons, M. (2011). Targeted ablation of oligodendrocytes triggers axonal damage. *PLoS One* 6, e22735.
- Gomez-Sanchez, J.A., Carty, L., Iruarrizaga-Lejarreta, M., Palomo-Irigoyen, M., Varela-Rey, M., Griffith, M., Hantke, J., Macias-Camara, N., Azkargorta, M., Aurrekoetxea, I., *et al.* (2015). Schwann cell autophagy, myelinophagy, initiates myelin clearance from injured nerves. *J Cell Biol* 210, 153-168.
- Grinspan, J.B., Marchionni, M.A., Reeves, M., Coulaloglou, M., and Scherer, S.S. (1996). Axonal interactions regulate Schwann cell apoptosis in developing peripheral nerve: neuregulin receptors and the role of neuregulins. *J Neurosci* 16, 6107-6118.
- Gritsch, S., Lu, J., Thilemann, S., Wortge, S., Mobius, W., Bruttger, J., Karram, K., Ruhwedel, T., Blanfeld, M., Vardeh, D., *et al.* (2014). Oligodendrocyte ablation triggers central pain independently of innate or adaptive immune responses in mice. *Nat Commun* 5, 5472.
- Guo, F., Ma, J., McCauley, E., Bannerman, P., and Pleasure, D. (2009). Early postnatal proteolipid promoter-expressing progenitors produce multilineage cells in vivo. *J Neurosci* 29, 7256-7270.
- Halestrap, A.P. (2009). What is the mitochondrial permeability transition pore? *J Mol Cell Cardiol* 46, 821-831.
- Hardie, D.G., Ross, F.A., and Hawley, S.A. (2012). AMPK: a nutrient and energy sensor that maintains energy homeostasis. *Nat Rev Mol Cell Biol* 13, 251-262.
- Harding, A.E. (1983). Classification of the hereditary ataxias and paraplegias. *The Lancet* 321, 1151-1155.
- Harris, J.J., and Attwell, D. (2012). The energetics of CNS white matter. *J Neurosci* 32, 356-371.
- Hornig-Do, H.T., Tatsuta, T., Buckermann, A., Bust, M., Kollberg, G., Rotig, A., Hellmich, M., Nijtmans, L., and Wiesner, R.J. (2012). Nonsense mutations in the COX1 subunit impair the stability of respiratory chain complexes rather than their assembly. *Embo J* 31, 1293-1307.
- Hughes, E.G., Kang, S.H., Fukaya, M., and Bergles, D.E. (2013). Oligodendrocyte progenitors balance growth with self-repulsion to achieve homeostasis in the adult brain. *Nature neuroscience* 16, 668-676.
- Ikenaka, K., Kagawa, T., and Mikoshiba, K. (1992). Selective Expression of Dm-20, an Alternatively Spliced Myelin Proteolipid Protein Gene-Product, in Developing Nervous-System and in Nonglial Cells. *J Neurochem* 58, 2248-2253.
- Ingerman, E., Perkins, E.M., Marino, M., Mears, J.A., McCaffery, J.M., Hinshaw, J.E., and Nunnari, J. (2005). Dnm1 forms spirals that are structurally tailored to fit mitochondria. *J Cell Biol* 170, 1021-1027.
- Ingraham, C.A., Burwell, L.S., Skalska, J., Brookes, P.S., Howell, R.L., Sheu, S.S., and Pinkert, C.A. (2009). NDUFS4: creation of a mouse model mimicking a Complex I disorder. *Mitochondrion* 9, 204-210.
- Itoh, K., Nakamura, K., Iijima, M., and Sesaki, H. (2013). Mitochondrial dynamics in neurodegeneration. *Trends Cell Biol* 23, 64-71.
- Jessen, K.R., and Mirsky, R. (2005). The origin and development of glial cells in peripheral nerves. *Nature reviews neuroscience* 6, 671-682.
- Jeyaraju, D.V., Cisbani, G., and Pellegrini, L. (2009). Calcium regulation of mitochondria motility and morphology. *Biochimica et Biophysica Acta (BBA) - Bioenergetics* 1787, 1363-1373.

- Jiang, H., Duchala, C.S., Awatramani, R., Shumas, S., Carlock, L., Kamholz, J., Garbern, J., Scherer, S.S., Shy, M.E., and Macklin, W.B. (2000). Proteolipid protein mRNA stability is regulated by axonal contact in the rodent peripheral nervous system. *J Neurobiol* *44*, 7-19.
- Johnston, P.B., Gaster, R.N., Smith, V.C., and Tripathi, R.C. (1979). A clinicopathologic study of autosomal dominant optic atrophy. *Am J Ophthalmol* *88*, 868-875.
- Joshi, D.C., Zhang, C.L., Lin, T.M., Gusain, A., Harris, M.G., Tree, E., Yin, Y., Wu, C., Sheng, Z.H., Dempsey, R.J., *et al.* (2015). Deletion of mitochondrial anchoring protects dysmyelinating shiverer: implications for progressive MS. *J Neurosci* *35*, 5293-5306.
- Juurink, B.H. (1997). Response of glial cells to ischemia: roles of reactive oxygen species and glutathione. *Neurosci Biobehav Rev* *21*, 151-166.
- Kang, J.S., Tian, J.H., Pan, P.Y., Zald, P., Li, C., Deng, C., and Sheng, Z.H. (2008). Docking of axonal mitochondria by syntaphilin controls their mobility and affects short-term facilitation. *Cell* *132*, 137-148.
- Kasischke, K.A., Vishwasrao, H.D., Fisher, P.J., Zipfel, W.R., and Webb, W.W. (2004). Neural activity triggers neuronal oxidative metabolism followed by astrocytic glycolysis. *Science* *305*, 99-103.
- Kennedy, W.R., Wendelschafer-Crabb, G., and Johnson, T. (1996). Quantitation of epidermal nerves in diabetic neuropathy. *Neurology* *47*, 1042-1048.
- Kessarlis, N., Fogarty, M., Iannarelli, P., Grist, M., Wegner, M., and Richardson, W.D. (2006). Competing waves of oligodendrocytes in the forebrain and postnatal elimination of an embryonic lineage. *Nature neuroscience* *9*, 173-179.
- Kijima, K., Numakura, C., Izumino, H., Umetsu, K., Nezu, A., Shiiki, T., Ogawa, M., Ishizaki, Y., Kitamura, T., Shozawa, Y., *et al.* (2005). Mitochondrial GTPase mitofusin 2 mutation in Charcot-Marie-Tooth neuropathy type 2A. *Hum Genet* *116*, 23-27.
- Knott, A.B., Perkins, G., Schwarzenbacher, R., and Bossy-Wetzell, E. (2008). Mitochondrial fragmentation in neurodegeneration. *Nature reviews* *9*, 505-518.
- Kocur, M., Schneider, R., Pulm, A.K., Bauer, J., Kropp, S., Gliem, M., Ingwersen, J., Goebels, N., Alferink, J., Prozorovski, T., *et al.* (2015). IFN β secreted by microglia mediates clearance of myelin debris in CNS autoimmunity. *Acta Neuropathol Commun* *3*, 20.
- Kondadi, A.K., Wang, S., Montagner, S., Kladt, N., Korwitz, A., Martinelli, P., Herholz, D., Baker, M.J., Schauss, A.C., Langer, T., *et al.* (2014). Loss of the m-AAA protease subunit AFG(3)L(2) causes mitochondrial transport defects and tau hyperphosphorylation. *Embo J* *33*, 1011-1026.
- Koppen, M., and Langer, T. (2007). Protein degradation within mitochondria: versatile activities of AAA proteases and other peptidases. *Crit Rev Biochem Mol Biol* *42*, 221-242.
- Koppen, M., Metodiev, M.D., Casari, G., Rugarli, E.I., and Langer, T. (2007). Variable and tissue-specific subunit composition of mitochondrial m-AAA protease complexes linked to hereditary spastic paraplegia. *Mol Cell Biol* *27*, 758-767.
- Korobova, F., Ramabhadran, V., and Higgs, H.N. (2013). An actin-dependent step in mitochondrial fission mediated by the ER-associated formin INF2. *Science* *339*, 464-467.
- Kovacs, G.G., Hoffberger, R., Majtenyi, K., Horvath, R., Barsi, P., Komoly, S., Lassmann, H., Budka, H., and Jakab, G. (2005). Neuropathology of white matter disease in Leber's hereditary optic neuropathy. *Brain : a journal of neurology* *128*, 35-41.

- Kremmidiotis, G., Gardner, A.E., Settasatian, C., Savoia, A., Sutherland, G.R., and Callen, D.F. (2001). Molecular and functional analyses of the human and mouse genes encoding AFG3L1, a mitochondrial metalloprotease homologous to the human spastic paraplegia protein. *Genomics* 76, 58-65.
- Kuhlmann, T., Miron, V., Cui, Q., Wegner, C., Antel, J., and Bruck, W. (2008). Differentiation block of oligodendroglial progenitor cells as a cause for remyelination failure in chronic multiple sclerosis. *Brain : a journal of neurology* 131, 1749-1758.
- Lacomis, D. (2002). Small-fiber neuropathy. *Muscle Nerve* 26, 173-188.
- Lampron, A., Larochele, A., Laflamme, N., Prefontaine, P., Plante, M.M., Sanchez, M.G., Yong, V.W., Stys, P.K., Tremblay, M.E., and Rivest, S. (2015). Inefficient clearance of myelin debris by microglia impairs remyelinating processes. *J Exp Med* 212, 481-495.
- Larsson, N.G., Wang, J.M., Wilhelmsson, H., Oldfors, A., Rustin, P., Lewandoski, M., Barsh, G.S., and Clayton, D.A. (1998). Mitochondrial transcription factor A is necessary for mtDNA maintenance and embryogenesis in mice. *Nat Genet* 18, 231-236.
- Lee, Y., Morrison, B.M., Li, Y., Lengacher, S., Farah, M.H., Hoffman, P.N., Liu, Y., Tsingalia, A., Jin, L., Zhang, P.W., *et al.* (2012). Oligodendroglia metabolically support axons and contribute to neurodegeneration. *Nature* 487, 443-448.
- Legesse-Miller, A., Massol, R.H., and Kirchhausen, T. (2003). Constriction and Dnm1p recruitment are distinct processes in mitochondrial fission. *Mol Biol Cell* 14, 1953-1963.
- Leone, D.P., Genoud, S., Atanasoski, S., Grausenburger, R., Berger, P., Metzger, D., Macklin, W.B., Chambon, P., and Suter, U. (2003). Tamoxifen-inducible glia-specific Cre mice for somatic mutagenesis in oligodendrocytes and Schwann cells. *Mol Cell Neurosci* 22, 430-440.
- Leonhard, K., Herrmann, J.M., Stuart, R.A., Mannhaupt, G., Neupert, W., and Langer, T. (1996). AAA proteases with catalytic sites on opposite membrane surfaces comprise a proteolytic system for the ATP-dependent degradation of inner membrane proteins in mitochondria. *Embo J* 15, 4218-4229.
- Lobbe, A.M., Kang, J.S., Hilker, R., Hackstein, H., Muller, U., and Nolte, D. (2014). A novel missense mutation in AFG3L2 associated with late onset and slow progression of spinocerebellar ataxia type 28. *J Mol Neurosci* 52, 493-496.
- Locatelli, G., Wortge, S., Buch, T., Ingold, B., Frommer, F., Sobottka, B., Kruger, M., Karram, K., Buhlmann, C., Bechmann, I., *et al.* (2012). Primary oligodendrocyte death does not elicit anti-CNS immunity. *Nature neuroscience* 15, 543-550.
- Lovell, M.A., and Markesbery, W.R. (2007). Oxidative damage in mild cognitive impairment and early Alzheimer's disease. *J Neurosci Res* 85, 3036-3040.
- Lu, B. (2009). Mitochondrial dynamics and neurodegeneration. *Curr Neurol Neurosci Rep* 9, 212-219.
- Luong, T.N., Carlisle, H.J., Southwell, A., and Patterson, P.H. (2011). Assessment of Motor Balance and Coordination in Mice using the Balance Beam. *Jove-J Vis Exp*.
- Mahad, D., Ziabreva, I., Lassmann, H., and Turnbull, D. (2008). Mitochondrial defects in acute multiple sclerosis lesions. *Brain : a journal of neurology* 131, 1722-1735.
- Mahad, D.H., Trapp, B.D., and Lassmann, H. (2015). Pathological mechanisms in progressive multiple sclerosis. *Lancet Neurol* 14, 183-193.

- Mahad, D.J., Ziabreva, I., Campbell, G., Lax, N., White, K., Hanson, P.S., Lassmann, H., and Turnbull, D.M. (2009). Mitochondrial changes within axons in multiple sclerosis. *Brain : a journal of neurology* *132*, 1161-1174.
- Maltecca, F., Aghaie, A., Schroeder, D.G., Cassina, L., Taylor, B.A., Phillips, S.J., Malaguti, M., Previtali, S., Guenet, J.L., Quattrini, A., *et al.* (2008). The mitochondrial protease AFG3L2 is essential for axonal development. *J Neurosci* *28*, 2827-2836.
- Maltecca, F., Baseggio, E., Consolato, F., Mazza, D., Podini, P., Young, S.M., Jr., Drago, I., Bahr, B.A., Puliti, A., Codazzi, F., *et al.* (2015). Purkinje neuron Ca²⁺ influx reduction rescues ataxia in SCA28 model. *J Clin Invest* *125*, 263-274.
- Maltecca, F., De Stefani, D., Cassina, L., Consolato, F., Wasilewski, M., Scorrano, L., Rizzuto, R., and Casari, G. (2012). Respiratory dysfunction by AFG3L2 deficiency causes decreased mitochondrial calcium uptake via organellar network fragmentation. *Hum Mol Genet* *21*, 3858-3870.
- Maltecca, F., Magnoni, R., Cerri, F., Cox, G.A., Quattrini, A., and Casari, G. (2009). Haploinsufficiency of AFG3L2, the gene responsible for spinocerebellar ataxia type 28, causes mitochondria-mediated Purkinje cell dark degeneration. *J Neurosci* *29*, 9244-9254.
- Mancini, C., Roncaglia, P., Brussino, A., Stevanin, G., Lo Buono, N., Krmac, H., Maltecca, F., Gazzano, E., Bartoletti Stella, A., Calvaruso, M.A., *et al.* (2013). Genome-wide expression profiling and functional characterization of SCA28 lymphoblastoid cell lines reveal impairment in cell growth and activation of apoptotic pathways. *BMC medical genomics* *6*, 22.
- Mancuso, G., Barth, E., Crivello, P., and Rugarli, E.I. (2012). Alternative splicing of *Spg7*, a gene involved in hereditary spastic paraplegia, encodes a variant of paraplegin targeted to the endoplasmic reticulum. *PLoS One* *7*, e36337.
- Mandelkow, E.M., and Mandelkow, E. (1998). Tau in Alzheimer's disease. *Trends Cell Biol* *8*, 425-427.
- Mariotti, C., Bella, D.D., Di Donato, S., and Taroni, F. (2012). Spinocerebellar ataxia type 28. *Handb Clin Neurol* *103*, 575-579.
- Mariotti, C., Brusco, A., Di Bella, D., Cagnoli, C., Seri, M., Gellera, C., Di Donato, S., and Taroni, F. (2008). Spinocerebellar ataxia type 28: a novel autosomal dominant cerebellar ataxia characterized by slow progression and ophthalmoparesis. *Cerebellum* *7*, 184-188.
- Martin, L., Latypova, X., Wilson, C.M., Magnaudeix, A., Perrin, M.L., and Terro, F. (2013a). Tau protein phosphatases in Alzheimer's disease: the leading role of PP2A. *Ageing research reviews* *12*, 39-49.
- Martin, L., Latypova, X., Wilson, C.M., Magnaudeix, A., Perrin, M.L., Yardin, C., and Terro, F. (2013b). Tau protein kinases: involvement in Alzheimer's disease. *Ageing research reviews* *12*, 289-309.
- Martinelli, P., La Mattina, V., Bernacchia, A., Magnoni, R., Cerri, F., Cox, G., Quattrini, A., Casari, G., and Rugarli, E.I. (2009). Genetic interaction between the m-AAA protease isoenzymes reveals novel roles in cerebellar degeneration. *Hum Mol Genet* *18*, 2001-2013.
- Martinelli, P., and Rugarli, E.I. (2010). Emerging roles of mitochondrial proteases in neurodegeneration. *Biochim Biophys Acta* *1797*, 1-10.
- Masuch, A., Shieh, C.H., van Rooijen, N., van Calker, D., and Biber, K. (2015). Mechanism of microglia neuroprotection: Involvement of P2X7, TNFalpha, and valproic acid. *Glia*.

- McDermott, C.J., Dayaratne, R.K., Tomkins, J., Lusher, M.E., Lindsey, J.C., Johnson, M.A., Casari, G., Turnbull, D.M., Bushby, K., and Shaw, P.J. (2001). Paraplegin gene analysis in hereditary spastic paraparesis (HSP) pedigrees in northeast England. *Neurology* *56*, 467-471.
- Mei, F., Wang, H., Liu, S., Niu, J., Wang, L., He, Y., Etxeberria, A., Chan, J.R., and Xiao, L. (2013). Stage-specific deletion of Olig2 conveys opposing functions on differentiation and maturation of oligodendrocytes. *J Neurosci* *33*, 8454-8462.
- Merkwirth, C., and Langer, T. (2009). Prohibitin function within mitochondria: Essential roles for cell proliferation and cristae morphogenesis. *Biochimica et Biophysica Acta (BBA) - Molecular Cell Research* *1793*, 27-32.
- Merkwirth, C., Martinelli, P., Korwitz, A., Morbin, M., Bronneke, H.S., Jordan, S.D., Rugarli, E.I., and Langer, T. (2012). Loss of prohibitin membrane scaffolds impairs mitochondrial architecture and leads to tau hyperphosphorylation and neurodegeneration. *PLoS Genet* *8*, e1003021.
- Michailov, G.V., Sereda, M.W., Brinkmann, B.G., Fischer, T.M., Haug, B., Birchmeier, C., Role, L., Lai, C., Schwab, M.H., and Nave, K.A. (2004). Axonal neuregulin-1 regulates myelin sheath thickness. *Science* *304*, 700-703.
- Michalski, J.P., Anderson, C., Beauvais, A., De Repentigny, Y., and Kothary, R. (2011). The proteolipid protein promoter drives expression outside of the oligodendrocyte lineage during embryonic and early postnatal development. *PLoS One* *6*, e19772.
- Minichiello, L., Korte, M., Wolfer, D., Kuhn, R., Unsicker, K., Cestari, V., Rossi-Arnaud, C., Lipp, H.P., Bonhoeffer, T., and Klein, R. (1999). Essential role for TrkB receptors in hippocampus-mediated learning. *Neuron* *24*, 401-414.
- Muona, M., Berkovic, S.F., Dibbens, L.M., Oliver, K.L., Maljevic, S., Bayly, M.A., Joensuu, T., Canafoglia, L., Franceschetti, S., Michelucci, R., *et al.* (2015). A recurrent de novo mutation in KCNC1 causes progressive myoclonus epilepsy. *Nat Genet* *47*, 39-46.
- Musova, Z., Kaiserova, M., Kriegova, E., Fillerova, R., Vasovcak, P., Santava, A., Mensikova, K., Zumrova, A., Krepelova, A., Sedlacek, Z., *et al.* (2014). A novel frameshift mutation in the AFG3L2 gene in a patient with spinocerebellar ataxia. *Cerebellum* *13*, 331-337.
- Narendra, D., Tanaka, A., Suen, D.F., and Youle, R.J. (2008). Parkin is recruited selectively to impaired mitochondria and promotes their autophagy. *Journal of Cell Biology* *183*, 795-803.
- Nave, K.A. (2010). Myelination and the trophic support of long axons. *Nature reviews* *11*, 275-283.
- Nave, K.A., Sereda, M.W., and Ehrenreich, H. (2007). Mechanisms of disease: inherited demyelinating neuropathies--from basic to clinical research. *Nature clinical practice* *3*, 453-464.
- Nave, K.A., and Trapp, B.D. (2008). Axon-glia signaling and the glial support of axon function. *Annual review of neuroscience* *31*, 535-561.
- Niemann, A., Berger, P., and Suter, U. (2006). Pathomechanisms of mutant proteins in Charcot-Marie-Tooth disease. *Neuromolecular Med* *8*, 217-242.
- Nikolakopoulou, A.M., Dutta, R., Chen, Z., Miller, R.H., and Trapp, B.D. (2013). Activated microglia enhance neurogenesis via trypsinogen secretion. *Proc Natl Acad Sci U S A* *110*, 8714-8719.
- Nitzan, E., Pfaltzgraff, E.R., Labosky, P.A., and Kalcheim, C. (2013). Neural crest and Schwann cell progenitor-derived melanocytes are two spatially segregated populations similarly regulated by Foxd3. *Proc Natl Acad Sci U S A* *110*, 12709-12714.

- Nobrega, M.P., Nobrega, F.G., and Tzagoloff, A. (1990). COX10 codes for a protein homologous to the ORF1 product of *Paracoccus denitrificans* and is required for the synthesis of yeast cytochrome oxidase. *J Biol Chem* *265*, 14220-14226.
- Nolden, M., Ehses, S., Koppen, M., Bernacchia, A., Rugarli, E.I., and Langer, T. (2005). The m-AAA protease defective in hereditary spastic paraplegia controls ribosome assembly in mitochondria. *Cell* *123*, 277-289.
- Norton, W.T., and Poduslo, S.E. (1973). Myelination in rat brain: method of myelin isolation. *J Neurochem* *21*, 749-757.
- Ohno, N., Chiang, H., Mahad, D.J., Kidd, G.J., Liu, L., Ransohoff, R.M., Sheng, Z.H., Komuro, H., and Trapp, B.D. (2014). Mitochondrial immobilization mediated by syntaphilin facilitates survival of demyelinated axons. *Proc Natl Acad Sci U S A* *111*, 9953-9958.
- Olmos-Serrano, J.L., Kang, H.J., Tyler, W.A., Silbereis, J.C., Cheng, F., Zhu, Y., Pletikos, M., Jankovic-Rapan, L., Cramer, N.P., Galdzicki, Z., *et al.* (2016). Down Syndrome Developmental Brain Transcriptome Reveals Defective Oligodendrocyte Differentiation and Myelination. *Neuron*.
- Oluich, L.J., Stratton, J.A., Xing, Y.L., Ng, S.W., Cate, H.S., Sah, P., Windels, F., Kilpatrick, T.J., and Merson, T.D. (2012). Targeted ablation of oligodendrocytes induces axonal pathology independent of overt demyelination. *J Neurosci* *32*, 8317-8330.
- Onyango, I.G., and Khan, S.M. (2006). Oxidative stress, mitochondrial dysfunction, and stress signaling in Alzheimer's disease. *Current Alzheimer research* *3*, 339-349.
- Papa, S. (2002). The NDUFS4 nuclear gene of complex I of mitochondria and the cAMP cascade. *Biochim Biophys Acta* *1555*, 147-153.
- Papadopoulou, L.C., Sue, C.M., Davidson, M.M., Tanji, K., Nishino, I., Sadlock, J.E., Krishna, S., Walker, W., Selby, J., Glerum, D.M., *et al.* (1999). Fatal infantile cardioencephalomyopathy with COX deficiency and mutations in SCO2, a COX assembly gene. *Nat Genet* *23*, 333-337.
- Patzig, J., Jahn, O., Tenzer, S., Wichert, S.P., de Monasterio-Schrader, P., Rosfà, S., Kuharev, J., Yan, K., Bormuth, I., Bremer, J., *et al.* (2011). Quantitative and integrative proteome analysis of peripheral nerve myelin identifies novel myelin proteins and candidate neuropathy loci. *J Neurosci* *31*, 16369-16386.
- Pellerin, L., and Magistretti, P.J. (1994). Glutamate Uptake into Astrocytes Stimulates Aerobic Glycolysis - a Mechanism Coupling Neuronal-Activity to Glucose-Utilization. *Proc Natl Acad Sci U S A* *91*, 10625-10629.
- Pierson, T.M., Adams, D., Bonn, F., Martinelli, P., Cherukuri, P.F., Teer, J.K., Hansen, N.F., Cruz, P., Mullikin For The Nisc Comparative Sequencing Program, J.C., Blakesley, R.W., *et al.* (2011). Whole-exome sequencing identifies homozygous AFG3L2 mutations in a spastic ataxia-neuropathy syndrome linked to mitochondrial m-AAA proteases. *PLoS Genet* *7*, e1002325.
- Pistorio, A.L., Hendry, S.H., and Wang, X. (2006). A modified technique for high-resolution staining of myelin. *J Neurosci Methods* *153*, 135-146.
- Pohl, H.B., Porcheri, C., Mueggler, T., Bachmann, L.C., Martino, G., Riethmacher, D., Franklin, R.J., Rudin, M., and Suter, U. (2011). Genetically induced adult oligodendrocyte cell death is associated with poor myelin clearance, reduced remyelination, and axonal damage. *J Neurosci* *31*, 1069-1080.
- Polydefkis, M., Hauer, P., Sheth, S., Sirdofsky, M., Griffin, J.W., and McArthur, J.C. (2004). The time course of epidermal nerve fibre regeneration: studies in normal controls and in people with diabetes, with and without neuropathy. *Brain : a journal of neurology* *127*, 1606-1615.

- Popescu, B.F., and Lucchinetti, C.F. (2012). Pathology of demyelinating diseases. *Annu Rev Pathol* 7, 185-217.
- Qi, Y., Liu, H., Daniels, M.P., Zhang, G., and Xu, H. (2016). Loss of *Drosophila* i-AAA protease, dYME1L, causes abnormal mitochondria and apoptotic degeneration. *Cell Death Differ* 23, 291-302.
- Quiros, P.M., Langer, T., and Lopez-Otin, C. (2015). New roles for mitochondrial proteases in health, ageing and disease. *Nat Rev Mol Cell Biol* 16, 345-359.
- Quiros, P.M., Mottis, A., and Auwerx, J. (2016). Mitonuclear communication in homeostasis and stress. *Nat Rev Mol Cell Biol* 17, 213-226.
- Rawles, M.E. (1947). Origin of pigment cells from the neural crest in the mouse embryo. *Physiol Zool* 20, 248-266.
- Rinholm, J.E., Hamilton, N.B., Kessar, N., Richardson, W.D., Bergersen, L.H., and Attwell, D. (2011). Regulation of oligodendrocyte development and myelination by glucose and lactate. *J Neurosci* 31, 538-548.
- Rugarli, E.I., and Langer, T. (2012). Mitochondrial quality control: a matter of life and death for neurons. *Embo J* 31, 1336-1349.
- Sacco, T., Boda, E., Hoxha, E., Pizzo, R., Cagnoli, C., Brusco, A., and Tempia, F. (2010). Mouse brain expression patterns of Spg7, Afg3l1, and Afg3l2 transcripts, encoding for the mitochondrial m-AAA protease. *BMC Neurosci* 11, 55.
- Salinas, S., Proukakis, C., Crosby, A., and Warner, T.T. (2008). Hereditary spastic paraplegia: clinical features and pathogenetic mechanisms. *Lancet Neurol* 7, 1127-1138.
- Sánchez-Ferrero, E., Coto, E., Beetz, C., Gámez, J., Corao, A.I., Díaz, M., Esteban, J., del Castillo, E., Moris, G., Infante, J., *et al.* (2013). SPG7 mutational screening in spastic paraplegia patients supports a dominant effect for some mutations and a pathogenic role for p.A510V. *Clinical Genetics* 83, 257-262.
- Schoenfeld, R., Wong, A., Silva, J., Li, M., Itoh, A., Horiuchi, M., Itoh, T., Pleasure, D., and Cortopassi, G. (2010). Oligodendroglial differentiation induces mitochondrial genes and inhibition of mitochondrial function represses oligodendroglial differentiation. *Mitochondrion* 10, 143-150.
- Schols, L., Bauer, P., Schmidt, T., Schulte, T., and Riess, O. (2004). Autosomal dominant cerebellar ataxias: clinical features, genetics, and pathogenesis. *Lancet Neurol* 3, 291-304.
- Shin, R.W., Iwaki, T., Kitamoto, T., and Tateishi, J. (1991). Hydrated autoclave pretreatment enhances tau immunoreactivity in formalin-fixed normal and Alzheimer's disease brain tissues. *Lab Invest* 64, 693-702.
- Simons, M., and Trajkovic, K. (2006). Neuron-glia communication in the control of oligodendrocyte function and myelin biogenesis. *J Cell Sci* 119, 4381-4389.
- Simons, M., and Trotter, J. (2007). Wrapping it up: the cell biology of myelination. *Current opinion in neurobiology* 17, 533-540.
- Skipuletz, T., Hackstette, D., Bauer, K., Gudi, V., Pul, R., Voss, E., Berger, K., Kipp, M., Baumgartner, W., and Stangel, M. (2013). Astrocytes regulate myelin clearance through recruitment of microglia during cuprizone-induced demyelination. *Brain : a journal of neurology* 136, 147-167.

- Smets, K., Deconinck, T., Baets, J., Sieben, A., Martin, J.J., Smouts, I., Wang, S., Taroni, F., Di Bella, D., Van Hecke, W., *et al.* (2014). Partial deletion of AFG3L2 causing spinocerebellar ataxia type 28. *Neurology* 82, 2092-2100.
- Smirnova, E., Griparic, L., Shurland, D.L., and van der Blik, A.M. (2001). Dynamin-related protein Drp1 is required for mitochondrial division in mammalian cells. *Mol Biol Cell* 12, 2245-2256.
- Snaidero, N., Mobius, W., Czopka, T., Hekking, L.H., Mathisen, C., Verkleij, D., Goebbels, S., Edgar, J., Merkler, D., Lyons, D.A., *et al.* (2014). Myelin membrane wrapping of CNS axons by PI(3,4,5)P3-dependent polarized growth at the inner tongue. *Cell* 156, 277-290.
- Sommer, C., and Lauria, G. (2007). Skin biopsy in the management of peripheral neuropathy. *Lancet Neurol* 6, 632-642.
- Sorensen, L., Ekstrand, M., Silva, J.P., Lindqvist, E., Xu, B., Rustin, P., Olson, L., and Larsson, N.G. (2001). Late-onset corticohippocampal neurodepletion attributable to catastrophic failure of oxidative phosphorylation in MILON mice. *J Neurosci* 21, 8082-8090.
- Stanley, J.L., Lincoln, R.J., Brown, T.A., McDonald, L.M., Dawson, G.R., and Reynolds, D.S. (2005). The mouse beam walking assay offers improved sensitivity over the mouse rotarod in determining motor coordination deficits induced by benzodiazepines. *J Psychopharmacol* 19, 221-227.
- Steglich, G., Neupert, W., and Langer, T. (1999). Prohibitins regulate membrane protein degradation by the m-AAA protease in mitochondria. *Mol Cell Biol* 19, 3435-3442.
- Sterky, F.H., Lee, S., Wibom, R., Olson, L., and Larsson, N.G. (2011). Impaired mitochondrial transport and Parkin-independent degeneration of respiratory chain-deficient dopamine neurons in vivo. *Proc Natl Acad Sci U S A* 108, 12937-12942.
- Stiburek, L., Cesnekova, J., Kostkova, O., Fornuskova, D., Vinsova, K., Wenchich, L., Houstek, J., and Zeman, J. (2012). YME1L controls the accumulation of respiratory chain subunits and is required for apoptotic resistance, cristae morphogenesis, and cell proliferation. *Mol Biol Cell* 23, 1010-1023.
- Stoothoff, W.H., and Johnson, G.V. (2005). Tau phosphorylation: physiological and pathological consequences. *Biochim Biophys Acta* 1739, 280-297.
- Sugiura, A., McLelland, G.L., Fon, E.A., and McBride, H.M. (2014). A new pathway for mitochondrial quality control: mitochondrial-derived vesicles. *Embo J* 33, 2142-2156.
- Svenstrup, K., Nielsen, T.T., Aidt, F., Rostgaard, N., Duno, M., Wibrand, F., Vinther-Jensen, T., Law, I., Vissing, J., Roos, P., *et al.* (2016). SCA28: Novel Mutation in the AFG3L2 Proteolytic Domain Causes a Mild Cerebellar Syndrome with Selective Type-1 Muscle Fiber Atrophy. *Cerebellum*.
- Taguchi, N., Ishihara, N., Jofuku, A., Oka, T., and Mihara, K. (2007). Mitotic phosphorylation of dynamin-related GTPase Drp1 participates in mitochondrial fission. *J Biol Chem* 282, 11521-11529.
- Tatsuta, T., and Langer, T. (2008). Quality control of mitochondria: protection against neurodegeneration and ageing. *Embo J* 27, 306-314.
- Taveggia, C., Zanazzi, G., Petrylak, A., Yano, H., Rosenbluth, J., Einheber, S., Xu, X., Esper, R.M., Loeb, J.A., Shrager, P., *et al.* (2005). Neuregulin-1 type III determines the ensheathment fate of axons. *Neuron* 47, 681-694.
- Thorburne, S.K., and Juurlink, B.H. (1996). Low glutathione and high iron govern the susceptibility of oligodendroglial precursors to oxidative stress. *J Neurochem* 67, 1014-1022.

- Timsit, S., Martinez, S., Allinquant, B., Peyron, F., Puelles, L., and Zalc, B. (1995). Oligodendrocytes originate in a restricted zone of the embryonic ventral neural tube defined by DM-20 mRNA expression. *J Neurosci* *15*, 1012-1024.
- Traka, M., Arasi, K., Avila, R.L., Podojil, J.R., Christakos, A., Miller, S.D., Soliven, B., and Popko, B. (2010). A genetic mouse model of adult-onset, pervasive central nervous system demyelination with robust remyelination. *Brain : a journal of neurology* *133*, 3017-3029.
- Traka, M., Podojil, J.R., McCarthy, D.P., Miller, S.D., and Popko, B. (2016). Oligodendrocyte death results in immune-mediated CNS demyelination. *Nature neuroscience* *19*, 65-74.
- Trapp, B.D., and Nave, K.A. (2008). Multiple sclerosis: an immune or neurodegenerative disorder? *Annual review of neuroscience* *31*, 247-269.
- Twig, G., Hyde, B., and Shirihai, O.S. (2008). Mitochondrial fusion, fission and autophagy as a quality control axis: The bioenergetic view. *Biochimica et Biophysica Acta (BBA) - Bioenergetics* *1777*, 1092-1097.
- Uschkureit, T., Sporkel, O., Stracke, J., Bussow, H., and Stoffel, W. (2000). Early onset of axonal degeneration in double (plp-/-mag-/-) and hypomyelinoses in triple (plp-/-mbp-/-mag-/-) mutant mice. *J Neurosci* *20*, 5225-5233.
- Vallstedt, A., Klos, J.M., and Ericson, J. (2005). Multiple dorsoventral origins of oligodendrocyte generation in the spinal cord and hindbrain. *Neuron* *45*, 55-67.
- Van Raamsdonk, C.D., and Deo, M. (2013). Links between Schwann cells and melanocytes in development and disease. *Pigment Cell Melanoma Res* *26*, 634-645.
- Vega, C., Martiel, J.L., Drouhault, D., Burckhart, M.F., and Coles, J.A. (2003). Uptake of locally applied deoxyglucose, glucose and lactate by axons and Schwann cells of rat vagus nerve. *J Physiol-London* *546*, 551-564.
- Viader, A., Golden, J.P., Baloh, R.H., Schmidt, R.E., Hunter, D.A., and Milbrandt, J. (2011). Schwann cell mitochondrial metabolism supports long-term axonal survival and peripheral nerve function. *J Neurosci* *31*, 10128-10140.
- Viader, A., Sasaki, Y., Kim, S., Strickland, A., Workman, C.S., Yang, K., Gross, R.W., and Milbrandt, J. (2013). Aberrant Schwann cell lipid metabolism linked to mitochondrial deficits leads to axon degeneration and neuropathy. *Neuron* *77*, 886-898.
- Viscomi, C., Bottani, E., Civiletto, G., Cerutti, R., Moggio, M., Fagiolari, G., Schon, E.A., Lamperti, C., and Zeviani, M. (2011). In vivo correction of COX deficiency by activation of the AMPK/PGC-1alpha axis. *Cell metabolism* *14*, 80-90.
- Vossel, K.A., Zhang, K., Brodbeck, J., Daub, A.C., Sharma, P., Finkbeiner, S., Cui, B., and Mucke, L. (2010). Tau reduction prevents Abeta-induced defects in axonal transport. *Science* *330*, 198.
- Wai, T., Garcia-Prieto, J., Baker, M.J., Merkwirth, C., Benit, P., Rustin, P., Ruperez, F.J., Barbas, C., Ibanez, B., and Langer, T. (2015). Imbalanced OPA1 processing and mitochondrial fragmentation cause heart failure in mice. *Science* *350*, aad0116.
- Wallace, D.C. (2005). A mitochondrial paradigm of metabolic and degenerative diseases, aging, and cancer: a dawn for evolutionary medicine. *Annu Rev Genet* *39*, 359-407.

- Warnecke, T., Duning, T., Schwan, A., Lohmann, H., Epplen, J.T., and Young, P. (2007). A novel form of autosomal recessive hereditary spastic paraplegia caused by a new SPG7 mutation. *Neurology* *69*, 368-375.
- Waxman, S.G., and Sims, T.J. (1984). Specificity in central myelination: evidence for local regulation of myelin thickness. *Brain research* *292*, 179-185.
- Wedding, I.M., Koht, J., Tran, G.T., Misceo, D., Selmer, K.K., Holmgren, A., Frengen, E., Bindoff, L., Tallaksen, C.M.E., and Tzoulis, C. (2014). Spastic Paraplegia Type 7 Is Associated with Multiple Mitochondrial DNA Deletions. *PLoS One* *9*.
- Wieckowski, M.R., Giorgi, C., Lebedzinska, M., Duszynski, J., and Pinton, P. (2009). Isolation of mitochondria-associated membranes and mitochondria from animal tissues and cells. *Nat Protoc* *4*, 1582-1590.
- Wikstrom, J.D., Mahdavian, K., Liesa, M., Sereda, S.B., Si, Y.G., Las, G., Twig, G., Petrovic, N., Zingaretti, C., Graham, A., *et al.* (2014). Hormone-induced mitochondrial fission is utilized by brown adipocytes as an amplification pathway for energy expenditure. *Embo Journal* *33*, 418-436.
- Wilkinson, P.A., Crosby, A.H., Turner, C., Bradley, L.J., Ginsberg, L., Wood, N.W., Schapira, A.H., and Warner, T.T. (2004). A clinical, genetic and biochemical study of SPG7 mutations in hereditary spastic paraplegia. *Brain : a journal of neurology* *127*, 973-980.
- Williams, A., Piaton, G., and Lubetzki, C. (2007). Astrocytes--friends or foes in multiple sclerosis? *Glia* *55*, 1300-1312.
- Williamson, T.L., Marszalek, J.R., Vechio, J.D., Bruijn, L.I., Lee, M.K., Xu, Z., Brown, R.H., Jr., and Cleveland, D.W. (1996). Neurofilaments, radial growth of axons, and mechanisms of motor neuron disease. *Cold Spring Harb Symp Quant Biol* *61*, 709-723.
- Witte, M.E., Mahad, D.J., Lassmann, H., and van Horssen, J. (2014). Mitochondrial dysfunction contributes to neurodegeneration in multiple sclerosis. *Trends Mol Med* *20*, 179-187.
- Woodhoo, A., and Sommer, L. (2008). Development of the Schwann cell lineage: from the neural crest to the myelinated nerve. *Glia* *56*, 1481-1490.
- Yamazaki, S., Ema, H., Karlsson, G., Yamaguchi, T., Miyoshi, H., Shioda, S., Taketo, M.M., Karlsson, S., Iwama, A., and Nakauchi, H. (2011). Nonmyelinating Schwann cells maintain hematopoietic stem cell hibernation in the bone marrow niche. *Cell* *147*, 1146-1158.
- Yang, H., Brose, S., Acin-Perez, R., Slavkovich, V., Nishino, I., Khan, R., Goldberg, I.J., Graziano, J., Manfredi, G., and Schon, E.A. (2010). Analysis of mouse models of cytochrome c oxidase deficiency owing to mutations in *Sco2*. *Hum Mol Genet* *19*, 170-180.
- Youle, R.J., and van der Bliek, A.M. (2012). Mitochondrial Fission, Fusion, and Stress. *Science* *337*, 1062-1065.
- Yu, Y., Run, X., Liang, Z., Li, Y., Liu, F., Liu, Y., Iqbal, K., Grundke-Iqbal, I., and Gong, C.X. (2009). Developmental regulation of tau phosphorylation, tau kinases, and tau phosphatases. *J Neurochem* *108*, 1480-1494.
- Zafrilla, P., Mulero, J., Xandri, J.M., Santo, E., Caravaca, G., and Morillas, J.M. (2006). Oxidative stress in Alzheimer patients in different stages of the disease. *Current medicinal chemistry* *13*, 1075-1083.

- Zambonin, J.L., Zhao, C., Ohno, N., Campbell, G.R., Engeham, S., Ziabreva, I., Schwarz, N., Lee, S.E., Frischer, J.M., Turnbull, D.M., *et al.* (2011). Increased mitochondrial content in remyelinated axons: implications for multiple sclerosis. *Brain : a journal of neurology* *134*, 1901-1913.
- Zhu, X., Raina, A.K., Lee, H.G., Casadesus, G., Smith, M.A., and Perry, G. (2004). Oxidative stress signalling in Alzheimer's disease. *Brain research* *1000*, 32-39.
- Zhu, Z., Yao, J., Johns, T., Fu, K., De Bie, I., Macmillan, C., Cuthbert, A.P., Newbold, R.F., Wang, J., Chevrette, M., *et al.* (1998). SURF1, encoding a factor involved in the biogenesis of cytochrome c oxidase, is mutated in Leigh syndrome. *Nat Genet* *20*, 337-343.
- Ziabreva, I., Campbell, G., Rist, J., Zambonin, J., Rorbach, J., Wydro, M.M., Lassmann, H., Franklin, R.J., and Mahad, D. (2010). Injury and differentiation following inhibition of mitochondrial respiratory chain complex IV in rat oligodendrocytes. *Glia* *58*, 1827-1837.
- Zuchner, S., Mersyanova, I.V., Muglia, M., Bissar-Tadmouri, N., Rochelle, J., Dadali, E.L., Zappia, M., Nelis, E., Patitucci, A., Senderek, J., *et al.* (2004). Mutations in the mitochondrial GTPase mitofusin 2 cause Charcot-Marie-Tooth neuropathy type 2A. *Nat Genet* *36*, 449-451.
- Zuhlke, C., Mikat, B., Timmann, D., Wieczorek, D., Gillessen-Kaesbach, G., and Burk, K. (2015). Spinocerebellar ataxia 28: a novel AFG3L2 mutation in a German family with young onset, slow progression and saccadic slowing. *Cerebellum Ataxias* *2*, 19.

Acknowledgements

This experience of 5-year Ph.D is the most important and unforgettable part of my life. I would like to take this opportunity to thank people who have helped and supported me over the years. First of all, I am tremendously grateful to my advisor, Prof. Elena I. Rugarli, for providing this interesting project and giving extended support to me. I have learnt from her not only how to do research, but also how to be a good scientist, which is invaluable for me. I also would like to express my gratitude to Prof. Aleksandra Trifunovic and Prof. Jan Riemer for accepting to be on my thesis committee.

Next, I would like to thank my dear lab mates, with whom I work, have lunch, eat cakes, play games, have barbecue, watch movies and go out together. Without you, my project could not go so far, my English would not be so improved and my life would not be so enriched. Many thanks to Julie Jacquemyn, a very talented girl, who did her master thesis under my supervision and provided excellent assistance in the skin studies. To Esther Barth, who introduced the skills of EM to me without any reservation and also helped me to cut when there was a need. To my former lab mates, Arun Kumar Kondadi, Eva R. Almajan, David Herholz, Paola Martinelli and Sara Montagner, who also worked on the *m*-AAA protease project and established a good platform for me. A special thanks goes to Eva for teaching me everything during my first year and inviting me to celebrate Christmas for my first time. I am deeply indebted to Nimesha Tadepalle and Jie Gao (Jane), who are always there to support me. We used to go home together almost everyday sharing ups and downs with each other, and I always felt that time was passing too fast when I was with you. During the writing period, I like to thank Jane for giving me strength and Nimesha for coming to refresh me when I am alone in the writing room. I am very grateful to Desiree Schatton (Desi) for supporting me all the time and giving me warm hugs. A big thanks to Simon Schumacher, I have learnt from him to have an attitude of positive thinking even during difficult situations. I appreciate David Pla-Martin for sharing his expertise with me and hosting me for my last a few months in Cologne. Thanks to Sara Murru for being willing to help me and encouraging me whenever I am stressed. To Chrisovalantis Papadopoulos (Valentin), a young superman with a good sense of humour. I would like to acknowledge all past and current lab mates including Anja Gruszczyk, Antonella Di Domenico, Giuseppe Mancuso, Henriette Hansen, Kristina Braunöhler, Marie-Charlotte Marx and Tsukasa

Hara, for being part of my journey and broadening my knowledge about sciences, food, culture as well as other aspects. Thanks to all my German lab mates, graduate school for biological sciences coordinator Isabell Witt and Kathy Jörgens, and Johannes Winkler for helping me with German documents.

Furthermore, I also would like to expand my thanks to CECAD in vivo facility for mouse care and management, and CECAD imaging facility for microscopy assistance. I am very grateful to Prof. Nils-Göran Larsson, Prof. Thomas Langer and Prof. Massimo Zeviani for sharing mouse lines or providing tissues. I sincerely thank Prof. Carien Niessen and Prof. Wilhelm Stoffel for fruitful discussions, Helga Bank for genotyping and Steffen Hermans for the Rotarod test. Many thanks to members of Langer lab, Trifunovic lab, Bergami lab, Brüning lab, Niessen lab and Pasparakis lab for sharing antibodies and protocols. Also thanks to Anne Korwitz, Marijana Aradjanski and Marie-Lune Simard for their technical support.

Coming to the end, I have to thank my parents Chunhua Wang and Aifan Xiao for their forever love and concerns. Thanks to my husband, Hongbo Zhang, who also motivates and supports me throughout my Ph.D stage. Even though I Skype with him everyday and with my parents every week, I know I am living so far away from them, and I really hope that the day when all of us are living close comes as soon as possible. Moreover, I am very much obliged to other members of my families, Hongbo's families, all of our relatives, teachers, friends and colleagues for everything.

Finally, I would like to express my deepest gratitude and best wishes to all of you!

Eidesstattliche Erklärung

Ich versichere, dass ich die von mir vorgelegte Dissertation selbständig angefertigt, die benutzen Quellen und Hilfsmittel vollständig angegeben und die Stellen der Arbeit – einschließlich der Tabellen, Karten und Abbildungen –, die anderen Werken im Wortlaut oder dem Sinn nach entnommen sind, in jedem Einzelfall als Entlehnung kenntlich gemacht habe; dass diese Dissertation noch keiner anderen Fakultät oder Universität zur Prüfung vorgelegen hat; dass sie – abgesehen von unten angegebenen Teilpublikationen – noch nicht veröffentlicht worden ist sowie, dass ich eine solche Veröffentlichung vor Abschluss des Promotionsverfahrens nicht vornehmen werde. Die Bestimmungen der Promotionsordnung sind mir bekannt. Die von mir vorgelegte Dissertation ist von Professorin Dr. Elena I. Rugarli betreut worden.

Ort, Datum

Shuaiyu Wang

Curriculum Vitae

PERSÖNLICHE DATEN

Name Shuaiyu Wang
Geburtsdatum / – ort 06.11.1983 / Hunan, China
Staatsangehörigkeit Chinesisch

AUSBILDUNG UND BERUFLICHER WERDEGANG

2011 - 2016 Ph.D
Prof. Dr. Elena I. Rugarli laboratory, Institute for Genetics,
University of Cologne, Germany

2009 - 2011 Research Assistant
Prof. Dr. Jiansheng Kang laboratory, Institute for nutritional
sciences, Shanghai Institute for Biological sciences, Chinese
Academic of Sciences, China

2006 - 2009 M.Sc. Biochemistry and molecular biology
Prof. Dr. Yaozhou Zhang laboratory, College of life sciences,
Zhejiang Sci-Tech University, China

2002 - 2006 B.Sc. Biotechnology
College of Bioscience and Biotechnology, Hunan Agricultural
University, China

PUBLIKATIONEN

1. Kondadi AK, **Wang S**, Montagner S, Kladt N, Korwitz A, Martinelli P, Herholz D, Baker MJ, Schauss AC, Langer T, Rugarli EI. Loss of the m-AAA protease subunit AFG3L2 causes mitochondrial transport defects and tau hyperphosphorylation. *EMBO Journal*. 2014 May 2; 33 (9): 1011-1026.
2. Dogan SA, Pujol C, Maiti P, Kukat A, **Wang S**, Hermans S, Senft K, Wibom R, Rugarli EI, Trifunovic A. Tissue-specific loss of DARS2 activates stress responses independently of respiratory chain deficiency in the heart. *Cell Metabolism*. 2014 Mar 4; 19 (3): 458-469.
3. Smets K, Deconinck T, Baets J, Sieben A, Martin JJ, Smouts I, **Wang S**, Taroni F, Di Bella D, Van Hecke W, Parizel PM, Jadoul C, De Potter R, Couvreur F, Rugarli E, De Jonghe P. Partial deletion of AFG3L2 causing spinocerebellar ataxia type 28. *Neurology*. 2014 Jun 10; 82 (23): 2092-2100.

KONFERENZEN

Oral presentation

- Mitochondrial DNA and neurodegeneration (EMBO workshop). Sitges, Spain. September 23-25, 2015.

Poster presentation

- International meeting on mitochondrial pathology (EUROMIT 2014). Tampere, Finland. June 15-19, 2014.
- Mitochondria: from signaling to diseases (Cell symposia). Lisbon, Portugal. May 5-7, 2013.

Attendee

- 2nd Cologne Ageing Conference. Cologne, Germany. April 4-6, 2016.
- International Meeting of the German Society for Cell Biology (DGZ meeting). Cologne, Germany. March 14-16, 2015.
- Hot Topics in Intracellular Communication (SFB635 International symposium). Cologne, Germany. November 6-7, 2014.
- Neural circuits: development, function, and degeneration (Cologne Spring Meeting). Cologne, Germany. February 27 - March 01, 2013.
- Degenerative diseases with particular reference to the HSP (Tom Wahlig foundation symposium). Cologne, Germany. March 16, 2012.